Polyacrylamide-based Hydrogel Electrolyte for Zinc-ion Batteries and Capacitors

by

Rujiao Ma

A thesis submitted in partial fulfillment of the requirements for the degree of

Master of Science

in

Chemical Engineering

Department of Chemical and Materials Engineering
University of Alberta

Abstract

Aqueous Zn-ion batteries (ZIBs) and Zn-ion hybrid capacitors (ZICs) have recently attracted tremendous research interest due to promising electrochemical performances, mild assembly conditions, intrinsic safety, and low-cost potential for grid-level energy storage. However, both ZIBs and ZICs are challenged with issues such as dendrite growth and side reactions on the anode side and metal dissolution and low capacity on the cathode side. While anode issues can jeopardize the cycling stability and cycle life, cathode issues lower the cell-level energy density. As such, it is urgently needed to address those issues and levitate its competitiveness among other energy storage devices. The use of hydrogel electrolytes, e.g., polyacrylamide (PAM), can tackle the above problems due to their uniform and controllable 3D polymer network for ion homogenizing, proper water absorption for ion transferring, superior adhesiveness for electrolyte-electrode interface stability, and high strength for mechanically resisting dendrites.

Chapter 1 is a literature review on hydrogels for functional ZIBs, in which backgrounds of ZIBs and hydrogel electrolytes were introduced, followed by a summary of different hydrogel electrolytes applied in ZIBs, including working principles behind their suppression on dendrite growth and side reactions. Moreover, hydrogel electrolytes have shown great potential for wearable and environmental-adaptive ZIBs given their good flexibility, elasticity, and high mechanical strength. As

such, more hydrogel electrolytes were introduced in the literature review based on the colorful functions they bring to ZIBs, including self-healing behavior, super toughness, tailorability, anti-freezing property, and thermo-protection behavior, etc. Also, the mechanisms behind those functions, summary, and perspectives were detailly described.

In Chapter 2, hydrogel electrolytes were demonstrated to endow ZICs with decent electrochemical performance and high flexibility. Activated carbon was used as the cathode for the assembly of ZICs (Zn//AC supercapacitors). Single-network PAM hydrogel electrolyte was firstly prepared and optimized for ZICs. Then, alginate was introduced to this hydrogel electrolyte to make Alginate/PAM hydrogel electrolyte with double-crosslinked network and further improve the performance of ZICs. FTIR spectra structurally confirmed these hydrogels, and their water-absorbing ability and stretchability were tested. Zn//AC supercapacitors based on both single PAM and Zn-Alginate/PAM hydrogel electrolyte showed stable cycling life of over 5000 cycles for electrochemical performances. More importantly, hydrogels also endowed ZICs with high flexibility while maintaining good performance. The assembled flexible soft-packaged Zn//AC supercapacitor based on Zn-Alginate/PAM hydrogel electrolyte exhibited a high specific capacity of 194 mAh g^{-1} at 0.1 A g^{-1} and stable cycling performance with 77.0 % capacity retention after 1900 cycles at 1.0 A g^{-1}. Moreover, good flexibility is demonstrated as only 5 % capacity loss under different bending angles and long resting stability of low self-discharge rate of 9.45 mV h^{-1}.

In Chapter 3, hydrogel electrolytes were further applied in ZIBs to demonstrate the

capability to inhibit metal dissolution and improve cycling performance. Rather than using Zn as the anode, molybdenum oxide with hexagonal structure (h-MoO$_3$) was synthesized, characterized, and applied as zinc-free anode materials for ZIBs. As a result, the involved battery in aqueous 3 M ZnSO$_4$ electrolytes shows high capacities of 128 mAh g^{-1} and 107 mAh g^{-1} at 0.1 A g^{-1} in Zn//h-MoO$_3$ half-cell test and h-MoO$_3$//ZnMn$_2$O$_4$/Carbon (ZMC) full cell test, respectively. However, its cyclability was poor, in which after 150 cycles zero capacity is maintained for Zn//h-MoO$_3$ half-cell and only 43 cycles for h-MoO$_3$//ZMC full cell. By contrast, using Zn-Alginate/PAM hydrogel electrolyte containing 3 M ZnSO$_4$ primarily enhanced cycling performances of both Zn//h-MoO$_3$ half-cell (63.6 % after 220 cycles) and h-MoO$_3$//ZMC full cell (91.2 % after 200 cycles) were achieved. At the same time, high capacities of 129 mAh g^{-1} and 102 mAh g^{-1} were maintained in both half-cell and full-cell, further confirming the advantage of hydrogel electrolytes for elongating cycle life in rocking-chair type ZIBs.

Chapter 4 briefly summarizes recent research progress and experimental results in previous chapters, as well as the challenges and future perspectives toward hydrogel electrolytes.

Preface

Chapter 1 of this thesis has been written as a manuscript and already be submitted, and I was the first author. For contributions, I competed the original manuscript, arranged Figures, summarized Tables and managed references, PhD candidate Mr. Zhixiao Xu helped to review and polish it. Dr. Xiaolei Wang contributed in conceptualization, supervision, and review and editing of the manuscript.

The work in second part of Chapter 2 (the flexible Zn//Ac supercapacitor based on Zn-Alginate/PAM hydrogel electrolyte) has been involved as one section in a published paper as Xu, Z., Ma, R., Wang, X., Ultrafast, long-life, high-loading, and wide-temperature zinc ion supercapacitors. Energy Storage Mater. (2022). https://doi.org/10.1016/j.ensm.2022.01.011. As the second author, I was responsible for methodology, validation, formal analysis, data curation, writing original draft for the flexible Zn//Ac supercapacitor part, while the conceptualization, methodology, validation, formal analysis, investigation, data curation, writing original draft of all other parts were completed by PhD candidate Mr. Zhixiao Xu. Dr. Xiaolei Wang contributed in conceptualization, resources, writing review & editing, supervision, project administration, funding acquisition.

Acknowledgements

Table of Contents

List of Tables

List of Figures

List of Schemes

List of abbreviations

Abstract

ZIBs	Zn-ion batteries
ZICs	Zn-ion hybrid capacitors
HEs	Hydrogel electrolytes
PAM	Polyacrylamide
AC	Activated carbon
FTIR	Fourier transform infrared spectra
h-MoO$_3$	Hexagonal molybdenum oxide
ZMC	ZnMn$_2$O$_4$/Carbon composite

Chapter 1

AZIBs	Aqueous zinc-ion batteries
OLED	Organic light-emitting diode
LIBs	Lithium-ion batteries
SHE	Standard hydrogen electrode
HER	Hydrogen evolution reaction
OER	Oxygen evolution reaction
PVA	Polyvinyl alcohol
PAA	Polyacrylic acid
PANa	Sodium polyacrylate
CMC	Carboxymethyl cellulose sodium
XG	Xanthan gum
PAMPZn	Zinc 2-acrylamido-2-methyl-1-propane sulfonate
AMPS	2-acrylamido-2-methyl-1-propanesulfonic acid
MBAA	N,N'-methylenebis(acrylamide)

α-KGA	*α*-ketoglutaric acid
MIHE	Multi-ion conducting hydrogel electrolyte
SIHE	Single-ion conducting hydrogel electrolyte
IC	Iota carrageenan
P(ICZn-AAM)	Hydrogel of ic and polyacrylamide electrolyte
WIS	Water-in-salt
WIG	Water-in-gel
SA	Sodium alginate
ASZIB	Aqueous Na-Zn hybrid battery
CLMS	Confocal laser microscopy
Poly-ZIS	Polyzwitterionic salt
Zn//PANI	Zn//polyaniline
ZnHCF	Zinc hexacyanoferrate
PBA	Prussian blue analogs
LED	Light-emitting diode
PANI/CFs	Polyaniline/carbon felts
D-MoS$_2$-O	In-situ structure defects manufacturing and o-doping within mos$_2$ lattice
NCHO	Nickel cobalt hydroxide
eG/P-Zn@SFB	Elastic graphene/polyaniline-zn@silver fiber-based battery
PU	Polyurethane
AM	Acrylamide
APS	Ammonium persulfate
KPS	Potassium persulfate
CC	Carbon cloth
CNT	Carbon nanotube

CV	Cyclic voltammogram
LiTFSI	Lithium bis(trifluoromethanesulfonyl)imide
$Zn(OTf)_2$	Zinc trifluoromethanesulfonate
MSA:	Methanesulfonic acid
AMP	Adenosine 5′-monophosphate
GA	Glutaraldehyde
GCD	Galvanostatic charging/discharging
PVA-PAA	Poly(vinyl alcohol)-poly(acrylate acid)
CMC	Carboxymethyl cellulose sodium
KCR	Kynol Novoloid carbonized yarn
GAME	Gelatin and alginate based membrane electrolyte
GE	Gelatin
SA	Sodium alginate
ChNFs	Chitin nanofibers
ssZIB	Solid-state ZIB
LCD	Liquid crystal display
κ-CG	κ-carrageenan
PAM-co-PAA	Poly(acrylamide-acrylic acid)
SL	Sodium lignosulfonate
SL-PAM	Sodium lignosulfonate–polyacrylamide
PE^+	Polycation hydrogel
PE^-	Polyanion hydrogel
G-GE	GE cross-link with glutaraldehyde
Caalginate	SA cross-link with $CaCl_2$
FESEM	Field-emission scanning electron microscope
NiCo//Zn battery	NiCo hydroxide//Zn battery
SPI	Soybean protein isolate nanoparticles

MPS	3-methacryloxypropyltrimethoxysilane
M-HNTs:	3-methacryloxypropyltrimethoxysilane modified halloysite nanotubes
PVA/Zn(CF3SO$_3$)$_2$	Polyvinyl alcohol /zinc trifluoromethanesulfonate
PVA-Zn/Mn	Polyvinyl alcohol /Zn(CH$_3$COO)$_2$/Mn(CH$_3$COO)$_2$
B-PVA/NFC hydrogel	Borax-assisted crosslinking polyvinyl alcohol/nanofibrillated cellulose hydrogel
NFC-PAM	Nanofibrillated cellulose/polyacrylamide
ZSC-gel	Zwitterionic sulfobetaine/cellulose gel
EG	Ethylene glycol
EG-waPUA	Ethylene glycol (EG) based waterborne anionic polyurethane acrylates
IPDI	Isophorone diisocyanate
DMPA	Dimethylol propionic acid
HEMA	Hydroxyethyl methacrylate
GG	Guar gum
CNF-PAM hidrogel	Cellulose nanofiber-polyacrylamide hydrogel
ZL-PAM	PAM-based hydrogel electrolyte containing 2 mol L^{-1} ZnSO$_4$ and 4 mol L^{-1} LiCl
CNCs	Cellulose nanocrystals
TCs	Tannic acid-encapsulated CNCs
PZHE	Polyzwitterionic hydrogel electrolyte
DES	Deep eutectic solvent
PNIPAM	Poly(N-isopropylacrylamide)
VPTT	Volume phase transition temperature

PNIPAM-AM-5	Poly(N-isopropylacrylamide)/acrylamide -5 (mA/N=5%)
EA battery	Environmental-adaptive battery
OHE	Organohydrogel electrolyte
PAMPS/PAAM	Poly(2-acrylamido-2-methylpropanesulfonic acid)/polyacrylamide
Alg-Zn	Zinc alginate
XG-PAM	Xanthan gum- polyacrylamide
CNF	Cotton cellulose nanofiber
TEOS	Tetraethyl orthosilicate
CT3G30	C, T, 3, G, and 30 represent cellulose, tetraethyl orthosilicate (TEOS), the milliliters of TEOS added, glycerol, and the milliliters of glycerol added, respectively.
CNF-PAM	Cellulose nanofiber-polyacrylamide
MVO//Zn	$Mg_{0.23}V_2O_5 \cdot 1.0H_2O$
QSS	Quasi-solid-state
PVA/LiCl-ZnCl$_2$-MnSO$_4$	PVA gel electrolyte containing LiCl, $ZnCl_2$, $MnSO_4$
PAN	Polyacrylonitrile
Micro-AZBs	Zn micro-battery
PEO-PPO-PEO	Poly(ethylene oxide)-poly(propylene oxide)-poly(ethylene oxide)
PHE	Polymer hydrogel electrolyte
PZHE	Polyzwitterionic hydrogel electrolyte
PSBMA	Poly [2-(methacryloyloxy) ethyl] dimethyl-(3-sulfopropyl)

SBMA	[2-(methacryloyloxy)ethyl]dimethyl-(3-sulfopropyl)
DMAPS	[2-methylacryloxy) ethyl]dimethyl-(3-sulfonic acid propyl) ammonium hydroxide
AMPSZn	2-acrylamido-2-methyl-1-propane sulfonate zinc
AAZn	Zinc acrylate
P(AMPSZn-AAZn)/ZnCl$_2$	Poly[(2-acrylamido-2-methyl-1-propane sulfonate zinc)-(zinc acrylate)]/ZnCl$_2$
ILs	Ionic liquids
DFT	Density functional theory

Chapter 2

Petri	Julius Richard Petri
PAM	PAM synthesized directly in 2M ZnSO$_4$
PAM-soaking	Making of PAM first followed by soaking in 2M ZnSO$_4$
A	Mean value
S	Standard deviation
DN	Double-network
DN Zn-Alginate/PAM	Double-network Zn-Alginate/polyacrylamide
GCD	Galvanostatic charging/discharging
EIS	Electrochemical impedance spectroscopy
LSV	Linear sweep voltammetry
ATR	Attenuated total reflection
Zn-Alg/PAM-2M ZnSO$_4$	Zn-Alginate/polyacrylamide hydrogel containing 2M ZnSO$_4$

PAM-2M ZnSO4	Pure PAM synthesized directly in 2 M ZnSO$_4$
Soaking PAM-2M ZnSO$_4$	Making of PAM first followed by soaking in 2 M ZnSO$_4$

Chapter 3

ZMO	ZnMn$_2$O$_4$
PVDF-NMP	Polyvinyl difluoride- N-methyl-2-pyrrolidone
SSM	Stainless steel mesh
N/P ratio	Ratio of negative electrode and positive electrode
XRD	X-ray diffraction
Zn-Alg/PAM-3M ZnSO$_4$	Zn-Alginate/PAM hydrogel electrolyte containing 3 M ZnSO$_4$

Chapter 1. Literature review

Polymer hydrogel electrolytes for flexible and multifunctional zinc-ion batteries

1.1 Abstract

Flexibility and multifunctionality are now becoming inevitable worldwide tendencies for electronic devices to meet modern life's convenience, efficiency, and quality demand. To that end, developing flexible and wearable energy storage devices is a must. Among energy storage systems, aqueous zinc-ion batteries (AZIBs) stand out as one of the most potent candidates for wearable electronics due to their high capacity, intrinsic safety, low cost, and functional controllability. Simultaneously, polymer electrolytes' introduction and rational design, especially various hydrogels, have endowed conventional ZIBs with colorful functions, which has been regarded as a perfect answer for energy suppliers integrated into those advanced wearable electronic devices. This review concentrates on the functional hydrogel electrolytes (HEs) and their application for multifunctional AZIBs. Previously reported HEs for AZIBs were classified and analyzed, from the most basic flexibility to other specific functions, such as mechanical endurance, temperature adaptability, electrochemical stability, and finally cell-level AZIBs based on multifunctional HEs. Besides introducing the diverse and exciting functions of HEs, inside working principles were also analyzed. Ultimately, all the details of these examples were summarized, and the related challenges, constructive solutions, futural prospects of functional AZIBs were also dedicatedly evaluated.

1.2 Introduction

To catch up with the faster pace and higher quality demand in modern life, flexible, wearable, and multifunctional electronic devices are gaining increasing attention and have become a hot spot in the market of digital devices.[1-6] For example, smartwatches,[7, 8] bendable smartphones,[9] flexible and foldable OLED panels,[10, 11] smart fibers,[12-16] e-textiles,[17-20] and electronic skin,[21] etc. These electronics rely on power sources, such as batteries and supercapacitors.[22-26] Thus, it is inevitable to develop next-generation energy storage devices with corresponding flexibility, wearability, environmental adaptability, reliable electrochemical performance, together with reasonable safety and biocompatibility at the same time.[27-30] Among energy storage devices, lithium-ion batteries (LIBs) with lightweight, high energy, and power density seem promising for flexible electronics yet are challenged with safety issues and high cost .[23, 24, 28, 31-33]

Alternatively, aqueous zinc-ion batteries (AZIBs) hold great potential as the energy suppliers for flexible electronics, thanks to the following advantages: first, high safety due to the use of nontoxic and air-moisture-stable Zn metal electrodes as well as mildly acidic aqueous electrolytes;[34, 35] second, low cost due to the abundance of Zn element on Earth as well as simple cell fabrication conditions in no need of gloveboxes;[36, 37] third. high theoretical capacity (820 mAh/g and 5855 mAh/cm^3) and proper redox potential (-0.763 V vs. SHE)[34, 38-40] compatible with aqueous electrolytes. Despite these advantages, the practical applications of AZIBs are still faced with challenges, including (1) dendrite growth due to uneven Zn deposition at the anode;[41-43] (2) side reactions due to water splitting reactions, including hydrogen evolution reaction (HER) and oxygen evolution reaction (OER); (3) dissolution of electrode materials in salty electrolyte to some extent, shortening cycling life;[44-46] (4) extra cost due to the need of separator;[47] (5) possibility of liquid leakage, etc.[48]

These challenges push forward the development of novel electrolyte systems. Among them, hydrogel electrolytes have received tremendous research interest. Hydrogels hold three-dimensional networks of water and hydrophilic polymers, which can be

derived from natural biomass or synthetic chemicals.[49-51] With many hydrophilic groups (such as -OH, -COOH, -NH$_2$, etc.) in the polymer chains, a massive amount of water molecules can be absorbed in the hydrogels while showing both liquid and solid material properties.[52, 53] With good hygroscopic, adhesion, and water-retaining properties, together with certain elasticity, long lifespan, excellent biocompatibility, and relatively low preparation cost, hydrogels have been regarded as one of the most attractive soft materials for tissue engineering scaffolds,[54, 55] wound dressings,[56-58] drug delivery,[59, 60] water purification,[61, 62] and energy storage systems.[63, 64]

Hydrogel electrolytes (HEs) possess the following advantages compared to aqueous electrolytes when applied to energy storage systems: (1). Hydrogels can accommodate a large number of aqueous electrolytes and maintain them for a long cycle life with the existence of countless hydrophilic groups, three-dimensional network structure and large internal pores, guaranteeing its decent ionic conductivity up to 12.6 S cm^{-1}.[65] (2). Zn^{2+} deposition can be effectively regulated via interactions between Zn^{2+} and functional groups anchored along with their 3D networks holding evenly distributed three-dimensional ion transfer channels inside. Besides, due to their excellent adhesion effect from abundant polar groups, interfacial stability between electrodes and electrolytes is largely enhanced.[66-68] Moreover, their quasi-solid state and mechanical elasticity can achieve close contact with active materials on electrodes. Hence, based on these above factors, dendrite growth and side reactions represented by HER will be greatly ameliorated, greatly elongating the cyclability and service life of the involved battery.[68, 69] (3). Moreover, with less content of water solution and mild acid electrolyte stored in hydrogels' crosslink network, water leakage, water splitting side reactions, and cathode material dissolution can be prevented. (4). Due to certain controllable thickness, HEs can also act as separators with simpler assemble steps and lower costs.[48] (5) Raw materials to prepare HEs can be derived from biomass, standing in line with current advocates for environmental sustainability.[70] (6). As one of the most popular soft materials applied in biomedical fields, most hydrogels possess superior biocompatibility and can be directly attached to a human's skin or implanted into a human's body.[71] (7). HEs can achieve

flexibility, mechanical endurance, and more special functions simultaneously due to their soft water-containing quasi-solid state, robust polymer network, and further modification of their functional groups, which make HEs powerful candidates for flexible energy storage and wearable electronic devices.[49, 72, 73]

There have been several kinds of hydrogels successfully applied in functional ZIBs, such as polyvinyl alcohol (PVA),[74, 75] polyacrylamide (PAM),[76, 77] polyacrylic acid (PAA),[66, 78] sodium polyacrylate (PANa),[79] carboxymethyl cellulose sodium (CMC),[80, 81] xanthan gum (XG),[82] etc. All of them will be mentioned in the following literature review with a detailed analysis of their structures, preparations, and functions on both electrolyte and battery levels with the involved mechanisms. From **Table 1**, we summarized the most widely applied HEs for ZIBs, together with their molecule structure, crosslinking type, and highlighted features when acting as electrolytes for ZIBs.

Therefore, this review summarizes different hydrogel electrolytes with different functions that improve environmental adaptivity to ZIBs, including stabilized cyclability, outstanding flexibility, mechanical endurance, and temperature adaptivity. It further provides a valuable reference to future development for hydrogel electrolytes in ZIBs toward more expansive application fields. At the same time, their working mechanisms can inspire more insightful ideas for advanced hydrogel electrolytes design. For starters stepping into this field, this work can be a reliable knowledge resource for gaining a transparent understanding of hydrogel electrolytes. Based on those goals, firstly, we started from the urgent need for HEs to address dendrite growth and side effects of conventional aqueous electrolytes, which were notorious causes of unsatisfied cyclability and unstable interfacial conditions ZIBs. Then, focusing on additional functions that benefited from HEs, those HEs with intrinsic flexibility with single polymer networks were introduced first. They acted as a vital component for assembling flexible pouch cell and yarn-shape ZIBs, enabling those batteries to work normally under various harsh external deformations, including bending, folding, twisting, stretching, etc. Afterward, HEs obtained from natural biomass (e.g., cellulose, alginate, gelatin, etc.) were introduced with decent

performance to indicate their environmental friendliness and sustainability.

Furthermore, besides improved cyclability and flexibility, HEs were classified into two categories by their different functions at the device level, including mechanical endurance and temperature adaptability. Finally, multi-functional HEs and those involved with batteries possessing two or more functions were discussed. For those mentioned above HEs, the related electrochemical data and highlighted functions were carefully summarized and listed in **Table 2**. Ultimately, existing challenges with HEs for ZIBs were presented and discussed, along with rational solutions and prospects for HEs-based ZIBs.
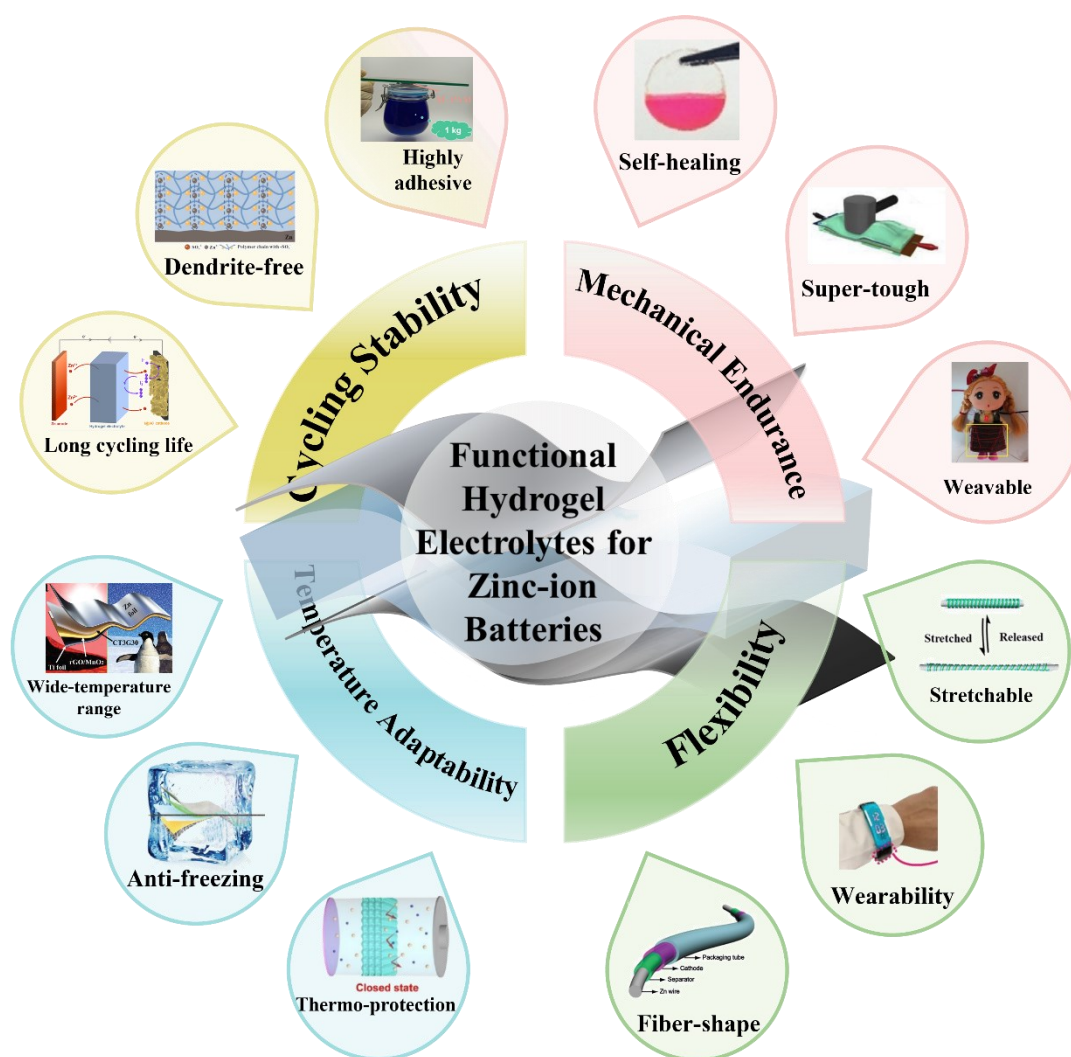
Scheme 1. Overview of functional hydrogel electrolytes for zinc-ion batteries. The

picture attached to "Long cycling life" was reproduced with permission.[83] Copyright 2021, American Chemical Society. The picture attached to "Dendrite-free" was reproduced with permission.[68] Copyright 2021, Elsevier B.V. The picture attached to "Highly adhesive" was reproduced with permission.[84] Copyright 2021, Elsevier Inc. The picture attached to "Self-healing" was reproducedwith permission.[65] Copyright 2019, Wiley-VCH Verlag GmbH &Co. KGaA, Weinheim. The picture attached to "Super-tough" was reproduced with permission.[85] Copyright 2019, Elsevier B.V. bThe picture attached to "Weavable" was reproduced with permission.[86] Copyright 2019, WILEY-VCH Verlag GmbH & Co. KGaA, Weinheim. The picture attached to "Stretchable" was reproduced with permission.[87] Copyright 2021, American Chemical Society. The picture attached to "Wearability" was reproduced with permission.[11] Copyright 2019, WILEY-VCH Verlag GmbH & Co. KGaA, Weinheim. The picture attached to "Fiber-shape" was reproduced with permission.[88] Copyright 2018, WILEY-VCH Verlag GmbH & Co. KGaA, Weinheim. The picture attached to "Thermo-protection" was reproduced with permission.[89] Copyright 2020, Wiley-VCH Verlag GmbH & Co. KGaA, Weinheim. The picture attached to "Anti-freezing" was reproduced with permission.[90] Copyright 2019, The Royal Society of Chemistry. The picture attached to "Wide-temperature range" was reproduced with permission.[91] Copyright 2021, Wiley-VCH GmbH.

1.3 Hydrogel electrolytes for stable and long-life zinc-ion batteries

Dendrite growth on Zn anode has become one of the most significant barriers to developing ZIBs because of uneven electrochemical reaction and interfacial contact using acidic aqueous electrolytes.[92] For traditional aqueous electrolytes widely applied in AZIBs, some severe shortcomings have been getting in the way of further application of AZIBs, including: (1). Dendrite growth due to uneven Zn deposition at the anode:[41-43]

$$4Zn^{2+} + 6OH^- + SO_4^{2-} + 5H_2O \rightarrow Zn_4(OH)_6SO_4 \cdot 5H_2O$$
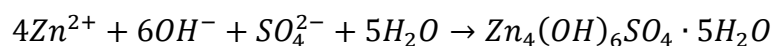
(2) Side reactions represented by water splitting reactions are easy to happen due to the utilization of aqueous electrolytes, including hydrogen evolution reaction (HER) and oxygen evolution reaction (OER), which can be expressed as (in the neutral or mild acid electrolyte):[48, 93, 94]

$$2H^+ + 2e^- \rightarrow H_2 \quad (0 \; V \; vs \; SHE)$$
$$2H_2O \rightarrow 4H^+ + O_2 + 4e^- \quad (1.23 \; V \; vs \; SHE)$$
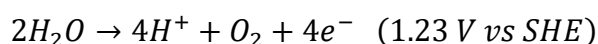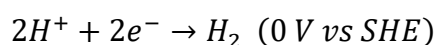
However, to address the above problems, the rational design of hydrogel electrolytes can effectively alleviate this phenomenon due to their dense and uniform 3D porous structure and certain function groups along polymer chains.

As **Figure 1a** suggests, a zinc 2-acrylamido-2-methyl-1-propane sulfonate (PAMPSZn) hydrogel electrolyte was synthesized by ion exchange between 2-acrylamido-2-methyl-1-propanesulfonic acid (AMPS, monomer) and 3Zn(OH)2•2ZnCO3, together with N,N'-Methylenebis(acrylamide) (MBAA, cross-linker) and α-Ketoglutaric acid (α-KGA, initiator).[68] Detailly, from **Figure 1b** and **1c**, comparing with severe dendrites growth in aqueous solution, due to partial interaction between SO_3^- group fixed along polyanionic chains and Zn^{2+}, side reactions at anode-electrolyte interface were efficiently suppressed. At the same time, zinc ion transport was confined within hydrogel's porous channels, achieving deposition/stripping of Zn^{2+} on the anode (**Figure 1e**) evenly and ultra-stable cycling life. With the hydrogel's ionic conductivity enhanced to 2.01×10^{-2} S cm^{-1}, the resulting Zn/Zn symmetric cell operated for over 4500 hours at 1.0 mA cm^{-2} (**Figure 1d**). From **Figure 1f**, the assembled Zn-V2O5 cell presented admirable reversibility and ultra-long cycle life of 80.2 % after 400 cycles at 0.5 A g^{-1} and negligible coulombic efficiency decay after 2000 cycles with PAMPSZn hydrogel electrolyte.

Compared with multi-ion conducting hydrogel electrolyte (MIHE), single-ion

conducting hydrogel electrolyte (SIHE) removes unwanted anions to guarantee the expected homogeneous Zn^{2+} plating/stripping and outstanding interfacial stability. Thus, a dual-crosslink SIHE electrolyte composed of iota carrageenan (IC) and PAM, denoted as P(ICZn-AAM), was conducted.[69] When the above hydrogel was soaked in $ZnSO_4$ solution, Zn^{2+} replaced the original Ca^{2+} and generated more robust ionic networks with IC due to abundant sulfate groups on IC's skeleton. Simultaneously, $CaSO_4$ precipitate was formed via the above ion exchange process, so the SO_4^{2-} anions were immobilized and removed from the ion transfer channel, allowing Zn^{2+} to be the major mobile ion in the electrolyte. Therefore, highly efficient ionic transport of Zn^{2+} with a transference number of 0.93 and ionic conductivity of 2.15 mS cm^{-1} were achieved. The assembled Zn-V_2O_5 battery showed excellent rate capacity and 81.9 % capacity retention after 500 cycles at 5 C, suggesting the merits of the above SIHE. An alginate-based hydrogel electrolyte was constructed for zinc-iodine batteries by applying glycerol as a plasticizer.[83] Firstly, crosslinked polyanionic alginate chain efficiently depressed uncontrolled I_3^- shuttling and facilitated cation transportation, thus protecting electrodes from unwanted side reactions (**Figure 1g and 1h**). Secondly, with ample cationic coordinating positions provided by rich carboxyl and hydroxyl groups alongside the alginate network, Zn^{2+} flux was rectified to become homogeneous; thus, the dendrite growth on anode was significantly avoided. Next, the free water-involved corrosive side reactions and surface passivation were effectively mitigated by confining most of the free water away from electrolyte/anode interfaces through its dense and robust polymer network and excellent water storage capability during the swollen process in Zn^{2+} solution. Combined with its decent ionic conductivity (32.8 mS cm^{-1}), admirable cycling endurance was realized within the above hydrogel. Therefore, the assembled Zn/I_2 battery showed decent average Coulombic efficiency of 99.5 % and capacity retention after 2000 cycles at 2.0 A g^{-1}.

Both the performance and application potential of conventional aqueous electrolytes suffered a lot from its narrow electrochemical stability window due to the activity of

water and its related side reactions. As a solution, electrolyte applying water-in-salt electrolyte (WIS) strategy was proposed, in which the amount of salt exceeds the solvent in both weight and volume. Thus, water activity was well inhibited, and the electrochemical window was much broadened.[95] Inspired by the above, the "water-in-gel" (WIG) method, which means the weights of salt and polymer surpass the weight of water, was adopted, followed by the preparation of a "water-in-gel" NaCl/ZnSO4/sodium alginate (SA) with mass ratios of 1:1:0.3:0.8 of NaCl, $ZnSO_4 \cdot 7H_2O$, SA and DI water.[96] When applied in an aqueous Na-Zn hybrid battery (ASZIB), it exhibited broadened electrochemical window of 2.72 V and a high discharge voltage of 2.10 V. Besides, many polar groups along SA chains interacted with water molecules via H-bonds, protecting direct contact between water and electrodes, improving the electrochemical window, and stabilizing the electrode-electrolyte interface. From **Figure 1i**, by coordinating among Na/Zn ions with its carboxylate groups, a 3D coil, and a uniform porous network were formed, so considerable dendrite growth on the anode was effectively suppressed. Therefore, even at 10 A g^{-1}, the fabricated ASZIB exhibited admirable stability with 94 % capacity retention and over 95 % Coulombic efficiency after 1000 cycles.
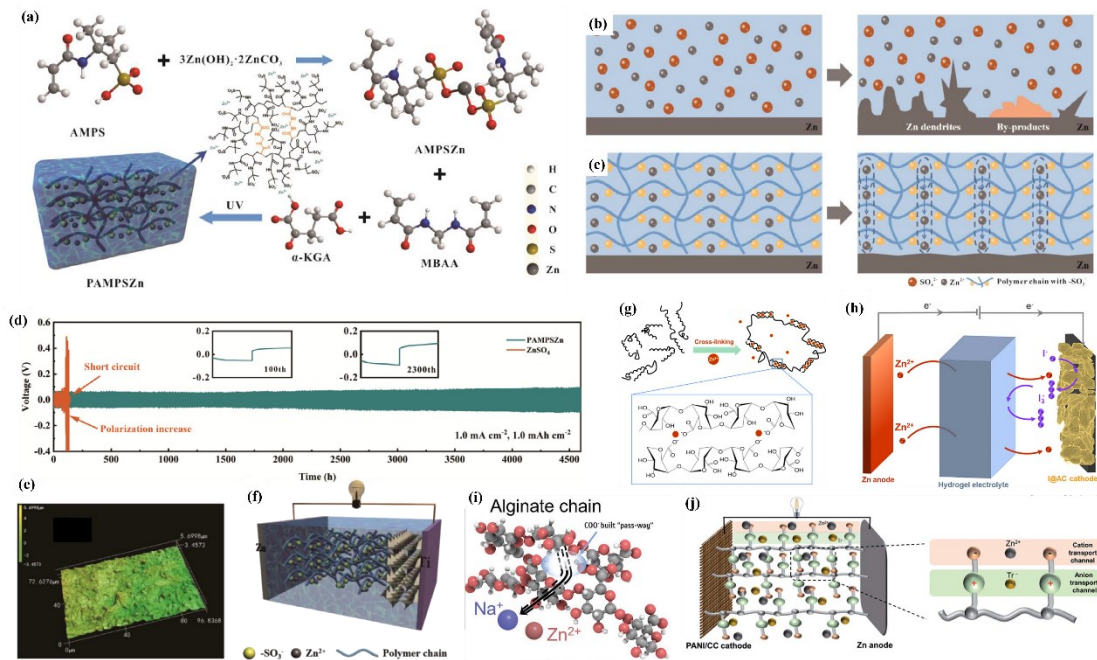
Figure 1. a) Schematic synthesis of PAMPSZn hydrogel electrolyte. b) Voltage profile of Zn/Zn symmetric cells with different electrolytes. The insets are the voltage profile of 100th and 2300th cycle, respectively. c) 3D models of Zn/V_2O_5 cells with PAMPSZn hydrogel electrolyte. (d) CLMS images of Zn anodes in the Zn/Zn symmetric cell after several cycles with PAMPSZn hydrogel electrolyte at 1.0 mA cm^{-2} and 1.0 mAh cm^{-2} after 50 cycles. e)- f) The mechanism of Zn deposition/stripping with e) $ZnSO_4$ aqueous electrolyte and f) PAMPSZn hydrogel electrolyte. Reproduced with permission.[68] Copyright 2021, Elsevier. g) Schematic diagram of Zn^{2+}-cross-linked alginate-based hydrogels and h) working principle of the Zn/I_2 battery with an alginate-based hydrogel electrolyte. Reproduced with permission.[83] Copyright 2021, American Chemical Society. i) Schematic Figure of ion transportation in water-in-gel electrolyte. Reproduced with permission.[96] Copyright 2021, WILEY-VCH Verlag GmbH. j) Schematic of the ZIS–PVA hydrogel electrolytes in dual-ion Zn/PANI batteries. Reproduced with permission.[97] Copyright 2021, The Royal Society of Chemistry.

Since polyzwitterionic HE regulates both anion and cation transfer by electrostatic interactions among their zwitterion units, which contain both positive and negative groups, ionic transport pathways within the hydrogel network are uniformly separated, further achieving their high-efficient transfer and homogeneous deposition. Therefore, Li and coworkers.[97] prepared a PVA-based hydrogel electrolyte containing polyzwitterionic salt (poly-ZIS) (denoted as ZIS-PVA hydrogel). As shown in **Figure 1j**, the cation transfer pathway was constructed along the negatively charged groups of the ZIS-PVA hydrogel chains, and the anion transfer pathway was built along the positively charged groups. Thus, the transport channels of cations and anions were successfully regulated and separated, ensuring promoted rate capacity and cycling performances. Moreover, SO_3^- groups in ZIS-PVA networks rectified Zn^{2+} diffusion and realized uniform dendrite-free Zn plating/stripping, preventing the Zn anode from dendrite growth. Hence, the above hydrogel reached a high ionic conductivity of 10.3 mS cm^{-1}, and the related Zn//PANI battery exhibited 87.5% capacity retention after

600 cycles.

1.4 Hydrogel electrolytes for flexible zinc-ion batteries

Commonly used batteries were rigid in both outer shell and inner components. Moreover, the conventional glassy fiber membrane separator is highly fragile and could be broken under harsh distortions.[98] As a result, the cylinder, coin cell configuration, and flimsy separator are unsuitable for future flexible and wearable use.[99] Worse, those energy storage systems based on flammable Li^+ (or Na^+) and organic electrolytes exhibited apparent safety concerns that can not be ignored when applied in wearable and close-fitting scenarios. By contrast, ZIBs based on HEs showed much reliable safety with applications of non-flammable Zn^{2+} and water-contained quasi-solid electrolytes. Moreover, with the intrinsic flexibility of HEs, they can work under repeated external deformations and be designed for highly bendable pouch cells or fiber-shaped batteries for future daily uses.[100, 101]

This section will focus on the flexibility of novel ZIBs with hydrogel electrolytes, which is the most fundamental feature for future application in wearable and multifunctional devices. For better demonstration, some significant parameters that must be considered when designing flexible systems were introduced and analyzed, including physical (e.g., water storage capability, porosity, surface morphology, interfacial contact, etc.) and mechanical (e.g., fracture strength, tensile modulus, hysteresis under external forces, endurance under external force treatments, etc.) properties in electrolyte's level, along with flexibility (mechanical endurance and electrochemical performance reservation under various external force treatments) and electrochemical performance (ionic conductivity, specific capacity, working voltage window, rate performance, cycling stability, etc.) in battery level. Furthermore, the mechanisms of how hydrogel electrolytes work for ZIBs, how hydrogel electrolytes can result in such desired functions, and the fabrication and modification of those batteries are also analyzed. Finally, the electrochemical performances and the related

flexibility were presented together, from which the highlights and potential applications can be evaluated.

With its wide applications in daily life, polyvinyl alcohol (PVA) has become one of the most popular hydrogels applied as electrolytes toward flexible ZIBs owing to its high water retention, nontoxicity, good ionic conductivity, easy preparation, and low cost.[102] Mostly, PVA is a typical hydrophilic polymer with abundant hydroxyl groups alongside its backbone, resulting in intricate reversible hydrogen bonds and physical-crosslinked 3D porous structure.[103] Thus, highly flexible, self-healing, super-adhesive, and other special functions can be obtained through further modification of PVA.[87] Besides, to gain better mechanical property, PVA can also be crosslinked to generate highly durable networks with crosslinkers.[74, 104]

A flexible quasi-solid ZIB with $ZnSO_4$/PVA hydrogel was reported.[105] The resulted Zn/ZnHCF@MnO_2 battery delivered comparable electrochemical performance to other ZIBs with Prussian blue analogs (PBA) derivative cathode. It maintained its CV curve under different bending angles (**Figure 2a**), powering an LED bulb under bending or folding, or even cutting out of a corner (**Figure 2b**), suggesting its practical potential for flexible and wearable applications. By sandwiching PVA hydrogel electrolyte containing 1 M $Zn(CF_3SO_3)_2$ between PANI/Carbon Felts (PANI/CFs) cathode and Zn foil (or Zn wire) anode, a soft-packaged and a cable-type Zn/PANI batteries were respectively fabricated (**Figure 2c, 2d**).[88] From **Figure 2e-2h**, there was no obvious capacity decay under their bending states, and the soft-package ZIB in series can power a wristwatch, while the cable-shaped ZIB can enlighten a series of LED lights under their bending states. After absorbing 3M $Zn(CF_3SO_3)_2$, PVA was also applied as hydrogel electrolyte for the Zn//D-MoS2-O battery,[106] as shown in **Figure 2i**. PVA enabled the corresponding battery with decent flexibility and good electrochemical performance. The assembled quasi-solid flexible battery with PVA-based electrolyte showed high ionic conductivity of 9.76 mS cm^{-1} and voltage of 2.2 V, while its specific capacity reached 215.0 mAh g^{-1} at 0.1 A g^{-1}. Also, the flexible battery worked well under 0° to 180° bending with slight capacity loss (**Figure 2j**), which successfully enlightened an LED panel when bent as a

wristband (**Figure 2k**).
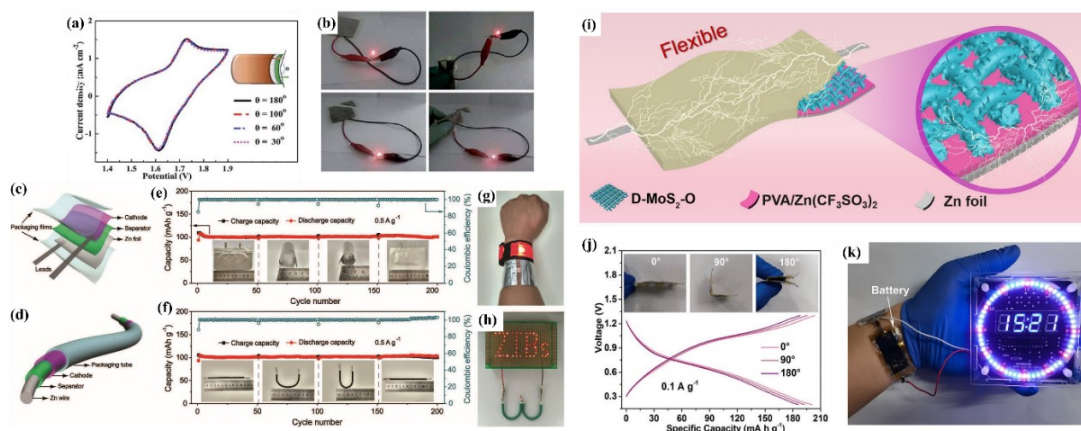
Figure 2. Flexible solid-state Zn-ion battery with a ZnHCF@MnO2 coating on Ni foil acting as cathode. a) CV curves (1 mV s^{-1}) at different bending conditions. b) The cell continued to power an LED bulb even after being horizontally cut. Reproduced with permission.[105] Copyright 2017, The Royal Society of Chemistry. Schematic diagrams of c) flexible soft-packaged and d) cable-type quasi-solid-state batteries. Cycling performance of e) soft-packaged and f) cable-type quasi-solid-state batteries under different bending states at 0.5 A g^{-1}. The insets show the optical images of soft-packaged and cable-type batteries under different bending states. Optical images of g) a wrist strap and h) an LED array powered by two soft-packaged quasi-solid-state batteries in series and two cable-type quasi-solid-state batteries in series, respectively. Reproduced with permission.[88] Copyright 2018, WILEY-VCH Verlag GmbH & Co. KGaA, Weinheim. i) Diagram of the flexible quasi-solid-state Zn-ion battery. j) typical voltage curves under 0°, 90°, and 180° bending states of the quasi-solid-state D-MoS2-O//Zn battery. k) Optical image of a LED array powered by five wearable series batteries. Reproduced with permission.[106] Copyright 2021, WILEY-VCH Verlag GmbH.

Recently, a yarn-shaped Zn/nickel-cobalt hydroxide (denoted as Zn/NCHO) battery was fabricated, as demonstrated in **Figure 3a and 3b**, in which the prepared parallel

electrodes yarns were coated with PVA hydrogel electrolyte containing KOH and Zn(Ac)$_2$.[107] A nonplanar deformation cycle was applied to test the flexibility of the PVA hydrogel electrolyte for the assembled yarn-shape battery, including initially straight, 95° bending, 360° twisting, and finally recovered straight. As expected, high capacity retention of 78% of the above yarn battery was achieved. Furthermore, over 80% and 70% of the initial capacity were respectively kept after 1000 cycles of individually 95° bending and 360° twisting. From **Figure 3c**, it successfully powered an electrical watch, LED bulb set, and a pulse sensor in series.

Likewise, inspired by the unique helix structure of luffa tendrils, as demonstrated in **Figure 3d**, a fiber-based all-solid and ultra elastic graphene/polyaniline-Zn@silver fiber-based battery (denoted as eG/P-Zn@SFB) was reported.[87] PVA hydrogel electrolyte containing 1M ZnSO$_4$ was coated onto electrodes and encapsulated with polyurethane (PU) film. Due to the superior flexibility and elasticity of the PVA electrolyte, the eG/P-Zn@SFB maintained 99.0 %, 93.6 %, and 91.5 % capacity after knotting, bending, and twisting treatment, respectively. Even after several 900% stretching cycles, it preserved 70% of its initial capacity and successfully powered a LED bulb. Toward real-life applications, after being woven into a textile (**Figure 3e** and **3f**) or integrated with a stretch band (**Figure 3g**), it was able to power LED devices, showing great power for flexible and elastic power supply, wearable electronics, and intelligent textiles.

By applying the flexible PVA-KOH hydrogel, a wind-charged, ultra-endurance, fiber-shaped quasi-solid Zn-Ag$_2$O battery can be bent from 0° to 180°, retaining its capacity of more than 95.6 % after 100 cycles under 180° bending state.[108] For application in micro-batteries, utilizing PVA/LiCl-ZnCl$_2$-MnSO$_4$ hydrogel as a solid electrolyte guaranteed the Ni@MnO$_2$//Zn micro-battery with 95.4 % capacity retention after 1000 repeated 90° bending cycles, and it can be further integrated into wearable pressure sensor system.[109]

Polyacrylamide (PAM) is a chemical-crosslinked polymer, which is usually prepared by using acrylamide (AM) as the monomer, N, N'-methylenebisacrylamide (MBAA) as the crosslinker, and ammonium persulfate (APS) or potassium persulfate (KPS) as

the initiator through free radical polymerization.[110, 111] PAM contains ample amide groups, imparting itself with the outstanding hydrophilic property. Moreover, PAM possesses higher mechanical strength with robust and irreversible chemical cross-linked covalent bonds, resulting in a much stronger network than PVA.[77] Therefore, with only a limited electrochemical output sacrifice, PAM-based flexible ZIBs can withstand more severe outer strength. It has become one of the most widely used hydrogels in daily life and electrolyte application.[41]

As shown in **Figure 3h**, polyacrylamide (PAM) hydrogel electrolyte film containing 1 M $ZnSO_4$ solution was sandwiched between Zn@CC anode PANI@CNT cathode to construct a solid-state ZIB.[112] With ionic conductivity of 5.56 mS cm^{-1}, the assembled battery showed a capacity of 144.0 mAh g^{-1} at 0.2 A g^{-1} and maintained 91.0 % capacity after 150 cycles. Due to the intrinsic flexibility of the PAM electrolyte, from **Figure 3i** and **3j**, the battery worked normally without prominent CV or capacity loss under different bending angles and consecutive bending cycles.
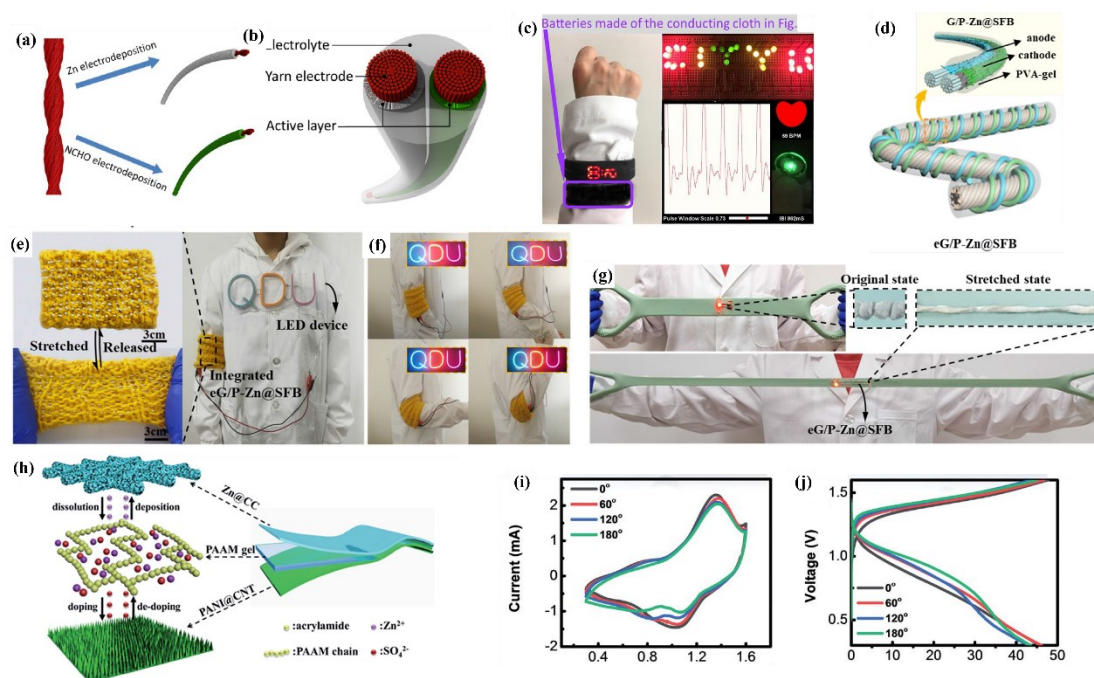
Figure 3. Demonstration and schematics of conductive yarns. a) Yarns electrodeposited with Zn and NCHO. b) Schematics of a free-standing solid-state yarn

battery. c) Energy wrist band made of a woven cloth powers a watch (left), a set of LEDs (upper right), and a pulse sensor (bottom right). Reproduced with permission. [107] Copyright 2017, American Chemical Society. d) Schematic diagram of eG/P-Zn@SFB. e) Photographs of integrated eG/P-Zn@SFB and wearable applications. f) Luminance of "QDU" with various bending angles from 0° to 180° of the elbow. g) Luminance of the LED before and after stretching of the elastic belt. Reproduced with permission.[87] Copyright 2021, American Chemical Society. h) Illustration of the structure and mechanism of a flexible solid-state Zn battery. Flexibility tests of the solid-state Zn battery. i) CV curves at a scan rate of 0.2 mV s^{-1} and j) galvanostatic charge–discharge profiles at a current density of 0.5 A g^{-1} of the solid-state Zn battery in different bending states. Reproduced with permission.[112] Copyright 2020, The Royal Society of Chemistry.

Besides, polyacrylamide (PAM) hydrogel containing $ZnSO_4$ and $CoSO_4$ was applied for a solid-state Zn/Co(III)rich-Co_3O_4 battery.[113] With high ionic conductivity of 0.12 S cm^{-1}, the corresponding battery achieved decent capacity and cyclability in **Figure 4a**. From **Figure 4b**, its capacity stayed almost the same under different distortion angles and 1000 cycles of 90° bending at 1 A g^{-1}. Also, as shown in **Figure 4c**, this battery successfully powered an electronic watch and flexible electroluminescent panel. Lately, a PAM hydrogel electrolyte and its corresponded flexible solid-state Zn hybrid battery were reported. With "water-in-salt" solutions of 21 M LiTFSI and 2 M Zn(OTf)$_2$ inside, due to water absence, side reactions and dendrite growth were well suppressed by the above hydrogel.[11] Simultaneously, such a highly concentrated solution hosted within the hydrogel network lasted for much longer by absorbing moisture from the surrounding, achieving admirable water-retaining properties and durability. Thus, the flexible battery shown in **Figure 4d** exhibited no apparent electrochemical performance injury under different bending angles (**Figure 4e**), with more than 92% capacity preserved over 1000 bending cycles. It can be attached to and power electroluminescent ribbon and panel and serves as an energy belt to power an electronic bracelet watch (**Figure 4f** and **4g**).

Compared with pure hydrogel electrolytes, reasonable modifications include introducing inorganic salts or fillers, ionic liquids, and high-concentrate electrolyte solution into the HEs system to better ionic conductivity have been proposed and developed so far.[11, 94, 114, 115] Among all the engineering strategies, utilizing crosslinked hydrogel composed of two or more hydrogels to enhance the mechanical strength of HEs structures is now becoming an inevitable trend to overcome the existing challenges, optimize performance, explore more functionalities of HEs. Thus, large-scale fabrication, commercial distribution, and practical applications of HEs can be finally achieved.[49, 116]

For example, methanesulfonic acid (MSA) with two hydrogen bond acceptors and one donor can form many multidirectional hydrogen bonds with the PVA chain.[114] Hence, it was introduced to PVA hydrogel electrolyte as an additive to facilitate low-energy-barrier cation migration with its additional hopping sites. The hydrogel's ionic conductivity was enhanced by 30.6 mS cm^{-1}. Therefore, the involved yarn battery can tolerate a bending curvature radius of 2.5 mm with 92.7% capacity retention after 500 cycles and can be fabricated into a curved bracelet shape wearing on the wrist and power a calculator simultaneously. Herein, a double-network AMP-Mn/PVA hydrogel electrolyte was reported.[117] As shown in **Figure 4h**, adenosine 5′-monophosphate (AMP) was applied to form a supramolecular network with Mn^{2+} by noncovalent interactions, while PVA crosslinked by glutaraldehyde (GA) appeared as a chemical crosslinked network. H-bonds intertwined the above two networks, forming the AMP-Mn/PVA hydrogel. With its high ionic conductivity of 34.1 mS cm^{-1}, the assembled flexible $Zn-MnO_2$ battery shown in **Figure 4i** delivered decent and stable capacity under different bending angles (**Figure 4j**).
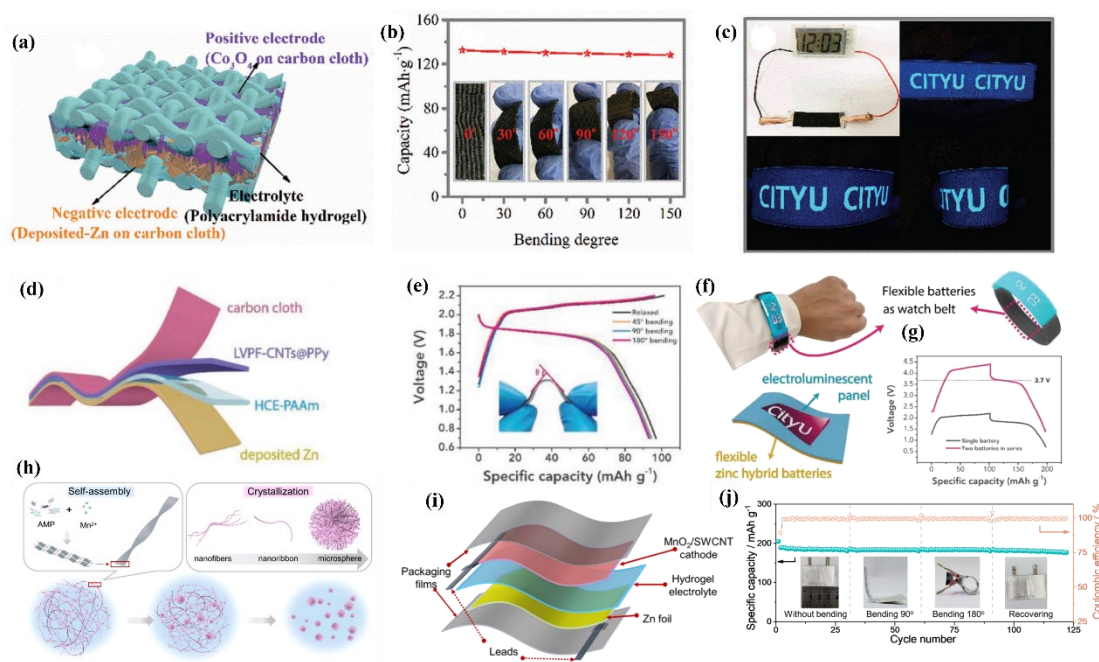
Figure 4. a) schematic illustration of the structure of solid-state Zn/Co(III) rich-Co₃O₄ batteries. b) electrochemical performance at different bending degrees. c) a single battery to power a digital watch and two batteries connected in series to power an electroluminescent panel (size: 12*3 cm) under different bending conditions. Reproduced with permission.[113] Copyright 2018, The Royal Society of Chemistry. d) Schematics of the configuration of the as assembled flexible hybrid battery. e) GCD curves of the hybrid battery at various bending angles. Bending radius R = 8 mm, device length L = 45. f) A wearable electronic watch powered by the flexible hybrid batteries serving as watch belt. g) GCD curves of single zinc hybrid battery and the two zinc hybrid batteries connected in series at the current density of 0.8 A g⁻¹. The latter serving as watch belt yielded a stable output voltage of 3.7 V, corresponding to the working voltage of traditional LIBs. Reproduced with permission.[11] Copyright 2019, WILEY-VCH Verlag GmbH & Co. KGaA, Weinheim. h) Illustration of the hierarchical self-assembly of forming AMP−Mn hydrogel and the structural changes of the AMP−Mn hydrogel during the further crystallization process. i) Schematic illustration of the flexible battery. j) LED array containing 66 bulbs powered by two flexible batteries. k) Cycle performance of the battery under different bending states at

a current density of 0.5 A g^{-1}. Reproduced with permission.[117] Copyright 2020, American Chemical Society.

With abundant hydrophilic groups existing within the porous structure of poly(vinyl alcohol) (PVA)-poly(acrylate acid) (PAA) copolymer hydrogel, the ion diffusion was greatly enhanced, so the resulted Zn//Co$_3$O$_4$ battery showed a high capacity of 162 mAh g^{-1} and 80% retention after 2000 cycles at 1 A g^{-1}.[78] Besides, the resulting hydrogel and battery's mechanical strength were significantly elevated with the stable PVA-PAA copolymer network, so it successfully worked under bending, twisting, and folding states.

Due to increased pressure on limited oil resources, synthetic polymers, including PVA, PAM, PEO, etc., which have been widely applied as polymer electrolytes, are produced from non-sustainable petroleum resources and could worsen the concerns about the environment energy resource issues.[70, 118] In sharp contrast to synthetic polymers, natural polymers such as cellulose,[91, 119] alginate,[96, 120] Chitosan,[81] kappa-carrageenan,[71, 121] chitin,[122] agarose,[123] xanthan gum,[124] protein,[72] , etc., were better choices for polymer electrolyte materials from the aspect of sustainability and processing cost. Thus, more and more natural-based hydrogels were introduced and utilized as electrolytes in the following parts.

First of all, a ZnSO$_4$/CMC hydrogel electrolyte (Carboxymethyl cellulose sodium, mZnSO$_4$: mCMC =1.9:1) was prepared for a flexible Zn/V$_2$O$_5$ battery.[125] The corresponding solid-state ZIB displayed a specific capacity of 481mAh g^{-1} at 0.1 A g^{-1}, and its capacity decreased from 335 mAh g^{-1} to 243 mAh g^{-1} when bent from 0° to 180°, respectively. Moreover, kappa-carrageenan can also facilitate ionic conductivity by coordinating with Zn^{2+} owing to its abundant hydroxyl groups, thus was regarded as an ideal HE for ZIBs. Huang et al.[121] reported a bio-polymer electrolyte denoted as KCR by dissolving kappa-carrageenan in ZnSO$_4$/MnSO$_4$ solution. KCR showed decent ionic conductivity of 33.2 mS cm^{-1}, and the assembled Zn/MnO$_2$ battery demonstrated an excellent specific capacity of 291.5 mAh g^{-1} at 0.15 A g^{-1} with 95% capacity retention after 300 times 180° bending cycles. Furthermore, a Starch/PAM

composite hydrogel electrolyte with high ionic conductivity of 2.65×10^{-2} S cm^{-1} was introduced to a flexible and high-performance ZIB.[118] The involved Zn-MoS$_2$ battery exhibited a specific capacity of 161.7 mAh g^{-1} and maintained nearly the same capacity as its initial state under several repeated bending cycles of 30°, 60°, 90°, and 180°.

Recently, a gelatin and alginate based membrane electrolyte (GAME) was reported.[116] From **Figure 5a** and **5b**, the hydrogel electrolyte possessed 3D double-crosslinked network, in which solid covalent bonding between GE and glutaraldehyde resulted in decent mechanical strength. In contrast, reversible ionic bonds between SA and Ca^{2+}, together with H-bonds among Ca-alginate and GE, result in excellent flexibility. With good compatibility between GE and SA with abundant hydrophilic groups, highly amorphous and interconnected porous channels were formed, achieving ionic conductivity of 3.7×10^{-2} S cm^{-1}. Therefore, as presented in **Figure 5c**, the resulting Zn/V$_2$O$_5$ battery showed 251 mAh g^{-1} at 2.0 A g^{-1} and maintained its capacity well at different bending diameters and 55 folding cycles under 1470 times loading of its weight. The SEM images proved the well-preserved interfacial area after bending (**Figure 5d**), suggesting alleviated electrode volume change due to the existence of the above hydrogel electrolyte..

Lately, a novel PAM–chitin nanofibers (ChNFs) hydrogel electrolyte was assembled into a self-charging Zn//VO$_2$ solid-state ZIB (ssZIB).[122] Specifically, as an eco-friendly raw material, ChNFs come from the waste lobster shell, showing an entangled and coil network. Thus, as presented in **Figure 5e**, the above PAM–ChNF hydrogel was prepared with ChNFs intertwining through PAM pores via physical interlacing and H-bonds interaction, generating a highly interconnected porous structure and robust double-cross network (as supported in **Figure 5f**), resulting in decent ionic conductivity of 15.2 mS cm^{-1}. When connected in series, the assembled battery successfully powered a liquid crystal display (LCD) even under a 90° bending angle, benefiting from the excellent flexibility of the hydrogel electrolyte.

Except for ZIBs, the flexibility of zinc-ion hybrid supercapacitor (ZICs) can also be improved by nature-derived HEs. Recently, a high-performance and cost-friendly

zinc-ion hybrid supercapacitor based on Zn-Alginate/PAM hydrogel was proposed by our group, exhibiting attractive flexibility and low self-discharge rate under various bending angles with a negligible sacrifice of electrochemical performance.[126] Cui et al.[66] designed a double crosslinked PAM-co-PAA/κ-CG hybrid hydrogel, in which the double helix κ-carrageenan (κ-CG) generated an ionic crosslink network with KCl. At the same time, the second network was formed by a covalent crosslink of poly(acrylamide-acrylic acid) (PAM-co-PAA) copolymer network. PAM-co-PAA and κ-CG chains also interacted via inter-molecular hydrogen bonds among their functional groups. Hence, excellent flexibility was ensured, and high ionic conductivity of 17.6 mS cm^{-1} was achieved, further guaranteeing the admirable performance of the involved ZIC.

Nevertheless, till this chapter ends, there are still some challenges existing those hydrogel electrolytes-based flexible zinc-ion storage systems, which can be summarized as follows: 1) the mechanical strength of some HEs is still insufficient to be applied in extreme practical conditions. 2) the operating temperature range of those systems is still too narrow to meet the demands in various regions and seasons. 3) compared to the conventional aqueous electrolyte, the ionic conductivity of HEs still have ample space to improve. 4) the research on their working mechanism is still in its infancy stage, which means more quantitative investigations need to be developed.

1.5 Hydrogel electrolytes for mechanically endurable zinc-ion batteries

1.5.1 Highly adhesive hydrogel electrolytes

When facing tremendous external deformation and harsh conditions, conventional HEs without excellent adhesion properties could be exfoliated from electrodes, deconstructing the battery integration and resulting in the battery failure.[67] Moreover, on the other hand, dendrites grown on electrodes can be suppressed by the stabilized

interface, intimate contact among each battery component with the application of highly adhesive HEs.[127] Thus, those HEs with great adhesion functions can bring ZIBs with better stability and durability in mechanics and electrochemistry.

Based on the strong interaction between catechol groups with two electrodes and improved ionic conductivity brought by sulfonate groups, sodium lignosulfonate (SL) was applied to the PAM network to enhance the adhesion for flexible ZIB.[84] As a result, the super-adhesive sodium lignosulfonate–polyacrylamide (SL-PAM) hydrogel electrolyte showed an enhanced shear strength from Zn foil to 3.7 J m^{-2} and ionic conductivity to 31.1 mS cm^{-1}. Furthermore, the HE involved flexible MnO$_2$|SL-PAM|Zn battery exhibited reasonable capacity even at 180° bending angle and maintained well under different bending angles, resulting from superior interfacial adhesion of SL-PAM hydrogel electrolyte.

As shown in **Figure 5g**, a novel diode-like hydrogel electrolyte was proposed. Polycation hydrogel (denoted as PE$^+$) acted as n-type hydrogel with mobile Cl$^-$ while polyanion hydrogel (denoted as PE$^-$) acted as p-type hydrogel with Na$^+$ as the movable counterion.[67] Like semiconductor diodes, the above hydrogel exhibited an assertive ionic rectification behavior. Owing to strong Coulombic interaction between PE$^+$ and PE$^-$ at the depletion zone and the double network structure generated from neutral agarose hydrogel matrix and opposite charged two hydrogels, the diode-like hydrogel can tolerate high loading and peeling forces, which can be demonstrated by the peeling force curves, optimal photos and SEM image in **Figure 5h-5k**). The assembled Cu-Zn battery delivered a capacity of 160 mAh g^{-1} and ran over 2000 cycles of stretching (50%) and bending (60°).
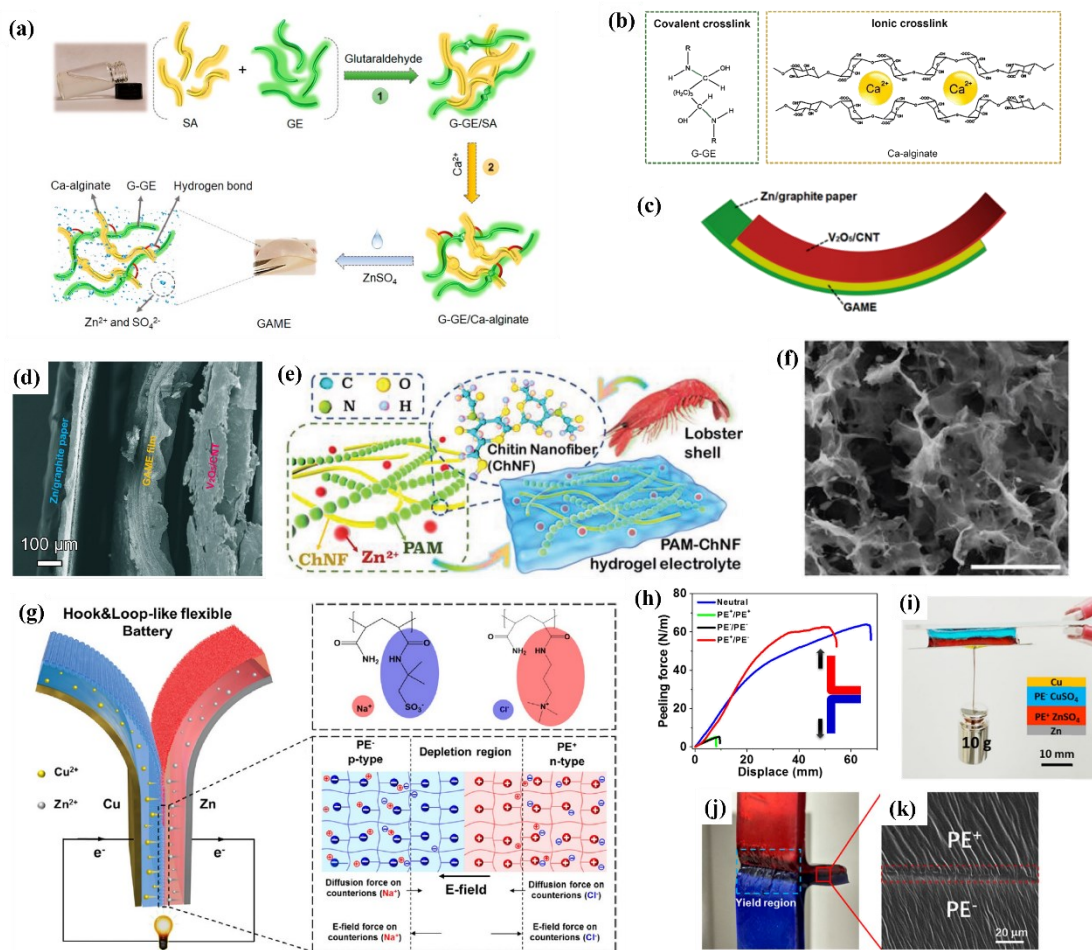
Figure 5. a) Schematic of the overall process to make GAME. b) Cross-linked polymers of G-GE (GE cross-link with glutaraldehyde) and Caalginate (SA cross-link with CaCl₂). c) Schematic diagram of a flexible semisolid Zn/V₂O₅ battery. d) Cross-sectional SEM image of the flexible semi-solid Zn/V₂O₅ battery. Reproduced with permission.[116] Copyright 2019, American Chemical Society. e) Preparation procedure of PAM–ChNF hydrogel. f) FESEM images of PAM–ChNF hydrogel. Reproduced with permission.[122] Copyright 2021, Wiley-VCH GmbH. g) A schematic Hook&Loop-like Cu-Zn flexible battery based on hydrogel diodes. h) The peeling force curves of two as-contacted hydrogel sheets. The blue curve represented tearing force curve (destroying the covalent bonds) of a single neutral hydrogel. i) a battery loading 10 g of weight. j) The picture of a hydrogel diode during peeling process. The yield region was marked in the dashed box. k) The cross-section SEM image of the hydrogel diode interface. Reproduced with permission.[67] Copyright 2018, Elsevier

Ltd..

1.5.2 Super-tough hydrogel electrolytes

Tough hydrogels have been widely explored with their intrinsic mechanical endurance towards harsh external treatments. Their crosslink network strengthened by inside strong covalent bonds or synergistic inter (intra) molecular interactions allows the tremendous outer force to be effectively dissipated upon their robust hydrogel matrix instead of causing severe breakage on a concentrated area.[85, 128]

Sodium polyacrylate (PANa) is a powerful candidate, endowing ZIBs with admirable mechanical durability against external compression and stretch. With outstanding ionic conductivity of 0.2 S cm^{-1}, a tough PANa hydrogel containing KOH and Zn(CH3COO)$_2$ was applied in a flexible NiCo//Zn battery.[79] The involved battery successfully maintained its capacity and even increased 9% under 0-50% compressive strain and still delivered 87% and 97% of its initial capacity after 500 stretching cycles and 1500 compressing cycles, respectively.

Polyacrylamide (PAM) hydrogel electrolyte appeared as a perfect candidate for elastic and compressive ZIBs due to its superior mechanical strength from strong covalent bonds and decent flexibility from reversible H-bonds, together with proper ionic conductivity from significant water absorption and hierarchical porous structure. After being soaked in 1 M ZnSO$_4$ and 0.1 M MnSO$_4$, the PAM hydrogel electrolyte was equipped with a Zn-MnO$_2$ battery.[129] Under high compression, its capacity was slightly boosted due to tighter contact between electrode and electrolyte and shorter ionic transport distance. The battery successfully enlightened a luminescent panel under a 3kg load for its wearable applications.

A PAM-based HE was prepared by introducing soybean protein isolate nanoparticles (SPI) into the PAM network.[127] Due to electrostatic interactions, negative charged SPI gathered around positive PAM chains, working as buffer clusters to disperse the outer force, thus improving its mechanical strength. Simultaneously, the SPI/PAM

hydrogel also achieved a high conductivity of 58 mS cm^{-1}. The related Zn//MnO$_2$ battery showed decent specific capacity and slightly increased stable capacity under 96% compression and strain contributed by the solid mechanical property of the HE.

Moreover, another ultra-strength PAM-based hydrogel was adjusted for flexible ZIBs.[130] Here, 3-methacryloxypropyltrimethoxysilane (MPS) modified HNTs (M-HNTs) was applied as both crosslinker and inorganic framework of the whole hydrogel 3D network. With abundant exposed polar groups interacting among surrounding acrylamide monomers and water molecules, the obtained hydrogel exhibited high mechanical strength of 1200% strain. Based on high ionic conductivity of 26 mS cm^{-1}, the fabricated ZIB exhibited negligible performance decay after bending, hammering, compressing and tailoring several times without packaging.

As presented in **Figure 6a** and **6b**, Liu et al.[85] developed a dual-crosslinked Zn-alginate/PAM hydrogel electrolyte, applying irreversible covalently crosslinked polyacrylamide (PAM) as the first network and reversible ionically crosslinked Zn-alginate chains as the second network. The above hydrogel was regarded as the vital component used in a super-tough Zn-MnO$_2$ battery, showing a specific capacity of 300.4 mAh g^{-1} at 0.11 A g^{-1} and 82 % capacity retention after 500 cycles at 0.88 A g^{-1}. At the same time, the ionic conductivity of 43.2 mS cm^{-2} was reached as well. When encountering external strengths, Zn-alginate ionic network will break to alleviate local strength and dissipate the energy to the extended zone by reversibly unzipping its egg-box configuration. In contrast, the robust covalent-linked PAM network maintained its basic framework from damage. Its original shape can be recovered by rebuilding the ionic Zn-alginate crosslink after removing external strength. Therefore, the battery maintained its stable electrochemical performance well under severe outer force, including cutting (**Figure 6c** and **6d**), folding and pressing (**Figure 6e**), squeezing (**Figure 6f**), hammering (**Figure 6g**), even being trodden under feet for two days (**Figure 6h** and **6j**) or even been grinding for 20 times random run-over by a car (**Figure 6i** and **6k**).
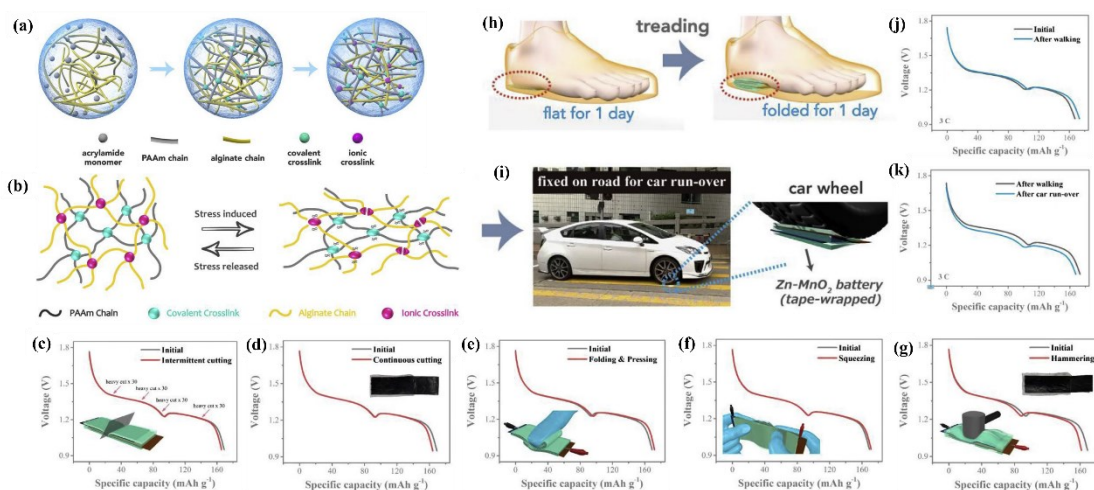
Figure 6. a) Schematics of the evolution of hydrogel structure. Grey lines and yellow lines represent PAM chains and alginate chains, respectively. Cyan and rosy dots represent covalent crosslinks and ionic crosslinks, respectively. b) Energy dissipation mechanism of the hydrogel. Upon stress loading, ionic crosslinks break to dissipate energy; upon unloading, ionic crosslinks rebuild to recover. c) Discharge curve of the battery recorded when being intermittently cut (30 times of cutting as a set, the cutting force was around 10–20 N). d) Discharge curve of the battery recorded when being continuously cut. Inset in the upper right corner is the optical image showing the intact electrode surface after cutting. e) Discharge curve of the battery recorded when being dynamically folded & pressed. f) Discharge curve of the battery recorded when being dynamically squeezed. g) Discharge curve of the battery recorded when being dynamically hammered. Inset in the upper right corner is the optical image showing the intact electrode after hammering. All the discharge curves were measured at the current density of 0.924 A g^{-1} (3C rate). Illustrations of the Zn-MnO$_2$ battery h) being placed under foot and i) going through car run-over. j) Discharge curve of the battery after 2 days' everyday treading. k) Discharge curve of the battery after 20 times of random run-over by cars on road. All the discharge curves were recorded at 0.924 A g^{-1} (3 C rate). Reproduced with permission.[85] Copyright 2019, Elsevier B.V.

1.5.3 Self-Healing hydrogel electrolytes

Owing to the existence of ample hydroxy side groups in each chain segment and O-H···O hydrogen bonds inside its network, PVA has an outstanding self-healing property. When it is cut into two segments, the two parts can automatically attract each other, stick to each other, become integrity again, and finish the self-healing process by re-establishing the reversible hydrogen bonds at the fracture surface without any external stimulus or other additives.[65, 131] Therefore, PVA has become a powerful candidate electrolyte in self-healing batteries.

Typically, a PVA/zinc trifluoromethanesulfonate (PVA/Zn(CF$_3$SO$_3$)$_2$) hydrogel electrolyte with self-healing function was developed, showing an incredibly high ionic conductivity up of 12.6 S cm^{-1} (**Figure 7a**).[65] Besides good flexibility under bending and folding states, **Figure 7b** demonstrated the self-healing capability brought by PVA hydrogel. The electrochemical performance of the related battery was re-established spontaneously and recovered to the same level as the initial even after several cutting/self-healing cycles (**Figure 7c**), which can also be demonstrated by the brightness recovering of LED bulbs powered by the connected batteries (**Figure 7d**). Furthermore, the self-healing behavior also happens when the battery pieces are reconnected in different directions, resulting in good tailorability. Another self-healing hydrogel electrolyte was composed of PVA/Zn(CH$_3$COO)$_2$/Mn(CH$_3$COO)$_2$ (denoted as PVA–Zn/Mn).[132] Resulting from easy re-formation of hydrogen bonds among free-moving PVA chain segments exposed on each fracture surface, the self-healing Zn/VS$_2$ battery exhibited 89.9% and 70.9% capacity retention after the first and second self-healing process, respectively. After four cutting/healing cycles, it can also continuously power a LED bulb. Even been cut into six pieces, the battery still preserved high potential retention.

Similarly, PVA-based self-healing hydrogel electrolyte can also be applied to zinc-ion hybrid supercapacitors (ZICs). A PVA/nanofibrillated cellulose hydrogel was developed through borax-assisted crosslinking (B-PVA/NFC hydrogel).[74] Due to the strongly crosslinked network and reversible H-bonds formed among abundant

hydroxyl groups, the B-PVA/NFC hydrogel reached high ionic conductivity of 18.1 mS cm^{-1}. The related ZIC also worked well under harsh conditions, including cutting/self-healing.

1.5.4 Weavable hydrogel electrolytes

With ample functional groups (such as hydroxy and carbonate bonds) on backbones, hydrogen bonds and other reversible interactions exist in some HEs, bringing high flexibility and elasticity to hydrogels. Thus, these HEs were facilitated to preserve their properties and functionalities well, even been stitched and sewed with electrodes to fabricate ultra-tough all-in-one batteries.[86] The integrated sewable and tailorable batteries show comparable flexibility and durability as cloth and human skin when facing various daily motions. When attached to humans' bodies, they freely work perfectly to meet the demand for next-generation wearable energy storage devices.[77]

From **Figure 7e**, a novel nanofibrillated cellulose/polyacrylamide (NFC/PAM) hydrogel electrolyte was synthesized by grafting PAM chains within the NFC framework through free radical polymerization, in which NFC was responsible for maintaining a 3D porous network with its robust nature, and PAM can enlarge the pore size with its excellent water-storage capability.[86] Thus, the composite hydrogel simultaneously exhibited decent mechanical property and ionic conductivity (22.8 mS cm^{-1}). To demonstrate its sewability and shearing resistance of assembled solid Zn-MnO$_2$ battery, as shown in **Figure 7f** and **7g**, the electrodes and electrolyte were sewed together, showing 88.5 % capacity retention after 120 stitches and bearing a high shear force of more than 43 N without exfoliating, together with 54 % original capacity retained as well. For practical applications, the sewed battery was used as a skirt for a toy doll while enlightened a LED at the same time.

Zwitterionic polymers possess both cationic and anionic functional groups, generating strong electrostatic interactions among those charged groups and water molecules (or other charged groups or ions), resulting in excellent water-absorption capability,

favored ion transport, better interfacial adhesion, substantial mechanical property, and superior stability.[133, 134] Inspired by this, a novel hydrogel electrolyte based on zwitterionic sulfobetaine/cellulose semi-interpenetrating networks (ZSC-gel) was prepared, in which the zwitterionic monomer was polymerized in cellulose nanofibrils backbone.[135] Based on the above factors, the ZSC-gel reached both high stretchability (920 %) and ionic conductivity (24.6 mS cm^{-1}). As shown in **Figure 7h**, the involved and twisted Zn/MnO$_2$ fiber-shape battery ran with 77.5 % capacity retention after 300 cycles. Four of them were then woven into a cloth, continuing to enlighten LED bulbs under different bending states (**Figure 7i**).
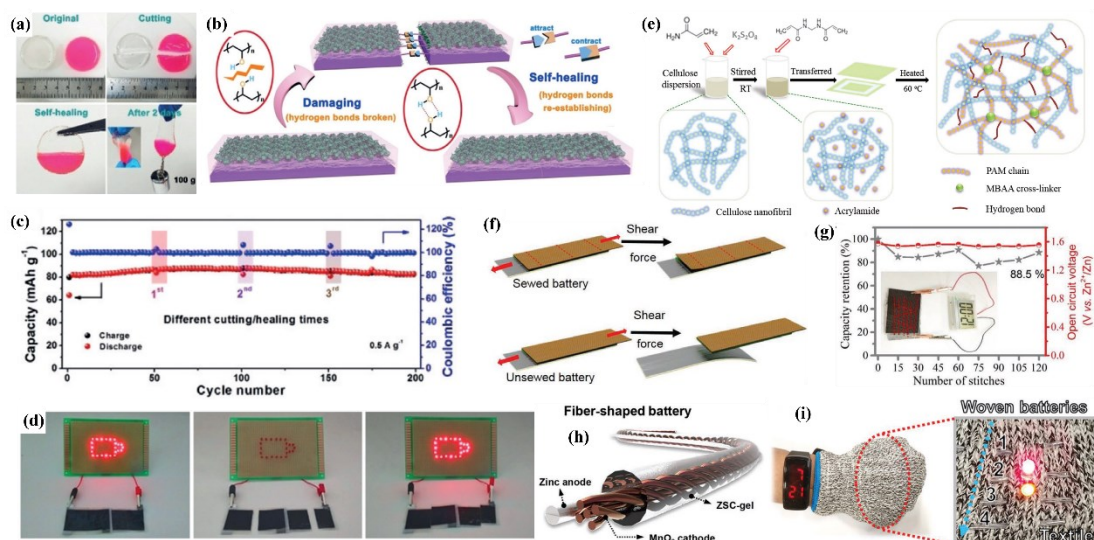
Figure 7. a) the self-healing behavior of the hydrogel electrolyte with and without rhodamine B for coloration. b) Illustration of the structure of self-healing integrated all-in one ZIBs. c) Cycle performance of the self-healing ZIBs at original state and after multiple cutting/self-healing times. d) Photographs of the two self-healing ZIBs in series powering an LED array containing 23 bulbs before cutting (light on), after cutting (light off), and after self-healing with dislocation in the direction parallel to the surface of devices (light on again). Reproduced with permission.[65] Copyright 2019, Wiley-VCH Verlag GmbH &Co. KGaA, Weinheim. e) Schematic of the synthesis route of the cellulose/PAM hydrogel through a facile free radical

polymerization approach. f) Schematic illustration of the process under shear force for sewed battery and unsewed battery. g) open-circuit voltage and capacity retention under sewing test; discharge curves of the solid-state rechargeable Zn–MnO2 battery under shear force. Reproduced with permission.[86] Copyright 2018, WILEY-VCH Verlag GmbH & Co. KGaA, Weinheim. h) Schematic of the fiber-shaped polyzwitterion-battery. i) Fabric integrated with four fiber-shaped batteries in series. Reproduced with permission.[135] Copyright 2020, WILEY-VCH Verlag GmbH & Co. KGaA, Weinheim.

1.6 Hydrogel electrolytes for temperature-adaptive zinc-ion batteries

1.6.1 Anti-freezing HEs

It has been widely considered that batteries, especially aqueous batteries, cannot normally work under minus temperature due to aqueous electrolyte frozen, resulting in sluggish ion transfer and performance decay. As a result, applying aqueous batteries in cold regions has been seriously restricted.[136] By engineering toward hydrogel electrolytes, the assembled quasi-solid battery can work well under sub-zero temperatures, and its flexibility can also be well-preserved with the nature of HEs.

Ethylene glycol (glycol) served as a commonly added anti-freezing agent. Due to abundant hydroxyl groups existing in glycerol, stable molecular clusters were formed with H_2O molecules via hydrogen bonds, which can compete with hydrogen bond formation among water molecules, resulting in a decrease in the saturated vapor pressure of water.[90] Therefore, ice crystallization is effectively disrupted with a much-lowered freezing point, which is the most applied mechanism in anti-freezing HEs.[137]

In **Figure 8a**, Mo et al.[90] synthesized an ethylene glycol (EG) based waterborne anionic polyurethane acrylates (EG-waPUA) hydrogel electrolyte possessing

excellent flexibility and anti-freezing property. They applied EG as the anti-freezing agent, isophorone diisocyanate (IPDI) as the monomer, dimethylol propionic acid (DMPA) as the chain extender, and hydroxyethyl methacrylate (HEMA) as the end-capping reagent. From **Figure 8b**, with abundant water molecules being trapped and locked as bridges among EG-waPUA and PAM chains, their crystallization and binding energy were inhibited and boosted by those hydrophilic groups alongside the network. Therefore, after copolymerized with acrylamide monomer, the dual-crosslinked EG-waPUA/PAM hydrogel electrolyte retained good anti-freezing capability with 14.6 mS cm^{-1} ionic conductivity at -20 °C. As shown in **Figure 8c**, the prepared Zn-MnO$_2$ battery maintained both its capacity and cyclability well, with the temperature falling to -20 °C (**Figure 8d** and **8e**). Its excellent flexibility and mechanical strength were also maintained when the integrated device was sealed in an ice cube (**Figure 8f**), which was inseparable from the outstanding property of the EG-waPUA/PAM hydrogel electrolyte. Another anti-freezing PAM-based hydrogel electrolyte was proposed with ethylene glycol as an anti-freezing agent.[138] Thus outstanding anti-freezing property and ionic conductivity were achieved to 14.9 mS cm^{-1} at -20 °C. The corresponding Zn-MnO$_2$ battery exhibited extraordinary capacity and anti-freeze function of 183.2 mAh g^{-1} and 61.0% capacity retention after 1000 cycles at −20 °C. By combining sodium alginate (SA) and guar gum (GG) and introducing ethylene glycol (EG) as an anti-freezing agent, a composite hydrogel electrolyte (denoted as GG/SA/EG) was designed.[139] Due to rich hydrophilic hydroxyl and carboxylate groups within SA, a decent ionic conductivity of 6.19 mS cm^{-1} was realized at −20 °C, and the related Zn-MnO$_2$ battery exhibited a capacity of 114.6 mAh g^{-1} at 0.3 A g^{-1} with working well with 97.58% capacity retention under bending at −20 °C.

Methanol, a simple polar molecule with a hydroxyl group, was also a compelling anti-freezing agent. It can interact with water molecules and form strong hydrogen bonds among them, significantly suppressing ice growth and lowering the freezing temperature. Based on the above, a cellulose nanofiber-polyacrylamide hydrogel (CNF-PAM hydrogel) with a 56% methanol molar ratio was reported, in which the

CNF network acted as the polymer backbone with high mechanical strength.[119] Furthermore, based on the above, the involved ZIB ran well under several repeated deformations in -20 °C (**Figure 8g**), together with admirable cycling performance (**Figure 8h**) and capacity (**Figure 8i**) even at -60 °C.
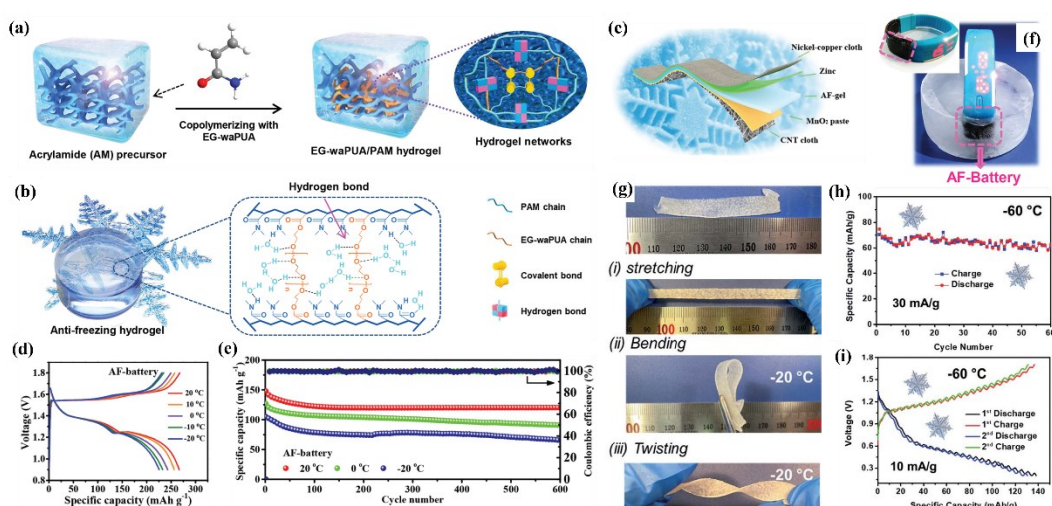
Figure 8. a) Polymerization of EG-waPUA and AM monomers to form the EG-waPUA/PAM hydrogel. The covalent/hydrogen bond hybrid crosslinked networks synergistically contributed to the excellent mechanical performance. b) Schematic illustration of the strong hydrogen bonds between EG-waPUA, water and PAM in the AF-gel. c) Schematic illustration of the structure of the AF-battery. d) AF-battery at a current density of 0.2 A g^{-1}. e) Extended cycling performance at 2.4 A g^{-1} of the AF-battery at different temperatures. f) Two AF-batteries were connected in series to operate a wristband electrical watch while being sealed in solid ice. Reproduced with permission.[90] Copyright 2019, The Royal Society of Chemistry. g) the optical photos of the prepared CNF–PAM hydrogel membrane under (i) stretching, (ii) bending and (iii) twisting after freezing at -20 °C for two days. h) cycling performance at 30 mA g^{-1} at -60 °C. i) charge–discharge profiles at 10 mA g-1 at -60 °C. Reproduced with permission.[119] Copyright 2021, The Royal Society of Chemistry.

Since additional Li$^+$ can cooperate with Zn^{2+} to enhance the hydration level by

forming highly hydrated cations, suppressing the formation of intermolecular hydrogen bonding among water molecules, and reducing the hydrogel's freezing point. Therefore, a PAM-based hydrogel electrolyte containing 2 mol L^{-1} ZnSO$_4$ and 4 mol L^{-1} LiCl (denoted as ZL-PAM) was assembled into a Zn/LiFePO$_4$ hybrid battery, showing 98% capacity retention at −20 °C and running over 500 cycles with negligible capacity decay.[140] Moreover, Li$^+$ lessened H-bonding among hydrogel chains through the doping effect and mitigated chains distortion by pairing with SO$_4^{2-}$, guaranteeing good mechanical property and durability of the hydrogel electrolyte. Thus, after being stored at −20 °C for 24 h, the flexible battery can still preserve >80% capacity retention after 400 bending cycles.

Increased salt concentration can effectively confine H-bonds formation by decreasing water content and breaking existing H-bonds by ionic interactions.[94] Thus, Wang et al.[124] utilized xanthan gum containing 4 M ZnCl$_2$ as a high-concentrated hydrogel electrolyte. The optimized concentration of ZnCl$_2$ realized a low freezing point and high ionic conductivity of 2.54 mS cm^{-1} at -20 °C, so the corresponding Zn/NH$_4$V$_3$O$_8$ flexible battery showed a good specific capacity of 201 mAh g^{-1} at 0.2 A g^{-1} in -20 °C. Even at -40 °C, the battery still exhibited 115 mAh g^{-1} at 0.1 A g^{-1}, suggesting its superior anti-freezing property..

For ZICs, with tannic acid-encapsulated CNCs (TCs) activating the initiator during polymerization, the hierarchically porous structure of PZHE was greatly enhanced, realizing outstanding ion transfer efficiency at low temperature.[141] Moreover, they adopt the "water-in-salt" strategy by filling 7.5 M ZnCl$_2$ in the above hydrogel. Therefore, excellent electrochemical performance was ensured even at -60 °C. Meanwhile, another anti-freezing hydrogel electrolyte was reported based on the "water-in-salt" strategy.[142] By dissolving cotton cellulose in a high-concentrated 1.75 g/g ZnCl$_2$/H$_2$O solution, the cellulose-based hydrogel maintained a high ionic conductivity of 47.7 mS cm^{-1} at -20 °C, and the involved ZIC showed only a limited capacity decay and stably worked when sealed in an ice package.

As a novel ionic liquid, deep eutectic solvent (DES) formed by eutectic mixtures of anionic Lewis acid and cationic base substances possess high stability and negligible

vapor pressure.[143, 144] In a recent report, DES was applied to the ZIC system and combined with HE to prepare flexible and anti-freeze ZIC.[145] Through one-step polymerization triggered by ClO_4^-, the Zn-PAM-H_2O eutectogel was prepared based on Zn(ClO_4)$_2$-acrylamide-H_2O ternary DES. Besides the suppressed activity of free water molecules by their interaction with PAM chains, the hydrogen bonds among water molecules were weakened due to competitive Zn^{2+}-O interactions and weak ClO_4^--H_2O hydrogen bonds.[146-148] Thus, the eutectogel achieved excellent anti-freezing property with a high voltage window of 2.2 V, and the involved flexible ZIC worked stably at a low temperature of -20 °C.

1.6.2 Thermo-responsible hydrogel electrolytes

It has already been known that high temperature is full of risk for batteries since the heat accumulation can cause active material degradation and even fire or explosion.[89] Therefore, an intelligent battery with thermal self-protection behavior achieved by HEs can be a powerful and attractive candidate for realizing safe and stable operation. As demonstrated in **Figure 9a**, a PAM hydrogel containing $ZnCl_2$ as highly thermal-responsible and reversible self-lock was introduced.[149] When the inner battery temperature reached 50 °C, water inside the hydrogel's porous structure gradually evaporated, bringing heat away and cooling down the whole battery. Simultaneously, the ionic conductivity decreased dramatically with insufficient water. Finally, the hydrogel shrank and shut down inside ion migration, which was the so-called hydrogel's self-protection behavior. Reversibly, when the battery was cooled down, abundant hydrophilic groups of PAM hydrogel would automatically absorb water from the outer environment, with mechanical and electrochemical performance recovering. For the corresponding ZIB, when the temperature increased to 50 °C, its ionic conductivity significantly decreased from 43 to 11 mS cm^{-1} with almost disappeared capacity output. After 3h cooling at room temperature, both capacity and water content regained to initial state, and the whole change process of capacity was

demonstrated in **Figure 9b**. Furthermore, other hydrogels (e.g., PVA) and metal ions can also be developed using the same method to realize thermal self-protection behavior, which can be applied to other battery systems.

Zhu et al.[89] prepared a poly(N-isopropylacrylamide) (PNIPAM) hydrogel with acrylamide (AM) added to form more hydrogen bonds, further elevating its volume phase transition temperature (VPTT). For the obtained thermal-gated PNIPAM/AM-5 (mA/N = 5 %) hydrogel, as illustrated in **Figure 9c** and **9d**, when the temperature reaches VPTT, intermolecular H-bonds among H_2O molecules and PNIPAM/AM-5 chains dissociated, while intramolecular H-bonds formed within PNIPAM/AM-5 instead, causing its porous network shrinkage and finally disappearance (supported by **Figure 9e - 9g**), shutting down ion transfer. Simultaneously, hydrophobic isopropyl groups were exposed to the PNIPAM chain, promoting polymer crystallization and hydrophobic association, leading the polymer to transit from hydrophilic to hydrophobic, further suppressing ion migration, achieving the smart thermal-gate function. After cooling down, its porous structure and hydrophilic property recovered to the original state. With $Zn(CF_3SO_3)_2$ contained, PNIPAM/AM-5 (mA/N =5 %) hydrogel was then coated onto a glassy fiber separator (denoted as PNIPAM/AM-5@GF) as an integrated separator. The involved Zn-PANI battery showed high reversibility for multiple heating/cooling cycles (**Figure 9h**), which can be visualized by the fast turning off and turning on of the connected LED (**Figure 9i**).
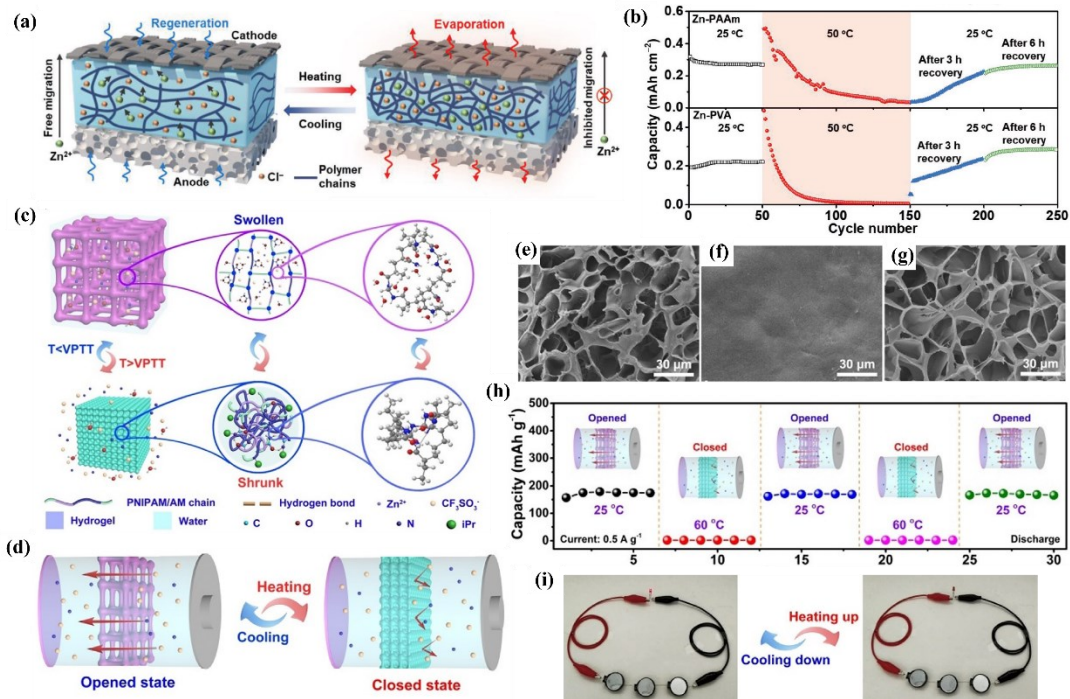
Figure 9. a) Working principle of the thermal self-protective zinc-ion batteries based on hygroscopic hydrogel electrolyte. b) The thermal-responsive reversibility of the zinc-ion batteries based on two types of hydrogel electrolytes: Zn-PAAm hydrogel (top panel) and Zn-PVA hydrogel (bottom panel). The capacity is derived from galvanostatic discharge measurement with a current density of 12 mA cm^{-2}. Reproduced with permission.[149] Copyright 2020, Wiley-VCH GmbH. c) Working mechanism of the thermal-gated PNIPAM/AM electrolytes with VPTT. d) Schematic illustration of smart ZIBs with thermal-gated PNIPAM/AM electrolytes. The SEM images of PNIPAM/AM-5@GF separators at different temperatures: e) 25 °C, g) 60 °C, and g) after cooling to 25 °C. h) The thermal-responsive reversibility of the aqueous ZIBs with thermal-gated separators at different cycles. i) The optical images of the three ZIBs in series to power a LED at heating and cooling states. Reproduced with permission.[89] Copyright 2020, Wiley-VCH Verlag GmbH & Co. KGaA, Weinheim.

1.7 Multi-functional HEs for flexible and environmental-adaptive ZIBs

More and more HEs have been prepared with three or even more functions to make the corresponding ZIBs adapt to drastic environmental change and severe external force with little electrochemical performance compromise, thus bettering their potential to serve as ideal next-generation devices in wearable electronics. During this part, highlight functions of those mentioned HEs-based environmental-adaptive ZIBs were listed in **Table 3**.

A Zn-alginate/polyacrylamide (PAM) hydrogel was proposed by applying ethylene glycol (EG) as an anti-freezing agent. Functional groups along the alginate chain further suppressed the crystallization of water molecules.[150] Inspired by epidermal tissue, the hydrogel was coated with a silane elastomer layer with coupling agents and surfactant, which acted as a shield to alleviate water evaporation at high temperatures and deferred solution exchange during the long-term performance. With good ionic conductivity of 14.1 mS cm^{-1} (-20 °C) to 18.2 mS cm^{-1} (80 °C), the assembled Zn/MnO$_2$ environmental-adaptive battery (EA battery) performed well from -20 °C to 80 °C. It still worked well under several extreme conditions, including mechanical deformations, ice packaging, boil water immersion, etc. A flexible, temperature-adaptive, mechanically durable and ultra-stable organohydrogel electrolyte (OHE) based on poly(2-acrylamido-2-methylpropanesulfonic acid)/polyacrylamide (PAMPS/PAAm) double-crosslink network was introduced, in which contained ZnCl$_2$/NH$_4$Cl in EG/H$_2$O binary solution system.[151] Besides being applied as an anti-freezing agent, EG intimately contacted with Zn anode, mitigating water-related side reactions, favoring dense and uniform Zn^{2+} deposition onto the electrode surface. Moreover, OHE possessed excellent mechanical properties and water content owing to ample hydrophilic functional groups, so the ionic conductivity still reached 1.62 mS cm^{-1} at -30 °C. The fabricated Zn/PANI battery showed stable cyclability of 81.5% capacity retention after 4000 cycles, outstanding mechanical strength under bending,

pressure, hammering, soaking, together with a wide working temperature range from -30 °C to 80 °C, which was contributed from the OHE.

Recently, zinc alginate (Alg-Zn) hydrogel electrolyte was synthesized, in which Zn^{2+} transfer was regulated within the hydrogel's network by interaction among Zn^{2+} and carboxylate groups.[152] Therefore, side reactions and dendrite growth were repressed with high ionic conductivity of 18.3 mS cm^{-1} and admirable endurance. The relevant battery showed excellent capacity and stability and retained its performance from 0 °C – 50 °C with improved environmental adaptability.

Based on PAM hydrogel electrolyte with high ionic conductivity of 17.3 mS cm^{-1}, a tailorable elastic yarn ZIB with decent mechanical property and electrochemical output was fabricated.[77] The prepared Zn/MnO_2 yarn-shaped battery lost negligible capacity after bending, knotting, and twisting. Reliable waterproof ability was confirmed with 96.5 % capacity retention after immersing in water for 12 h. Notably, this yarn ZIB can be cut to any desired length. After being cut into eight parts, each segment can power an electronic watch, and they can be woven together to enlighten a LED belt of 100 bulbs. A solid-state zinc hybrid battery with superior waterproof ability and washability was designed with highly absorbent and ionic conductive PAM hydrogel electrolyte.[153] Noteworthily, the above battery showed a specific air-triggered self-charging behavior by switching between Zn-air mode and $Zn-Co_3O_{4-x}$ battery mode. It delivered decent discharge capacity and cyclability and successfully powered an electronic watch under different bending conditions after being designed into a wristband.

By grafting acrylamide (AM) onto the xanthan gum (XG) backbone and incorporating XG-PAM copolymer with cotton cellulose nanofiber (CNF), the XG-PAM/CNF hydrogel electrolyte was synthesized with the homogeneous inter-penetrating dual cross-linking network.[82] With ionic conductivity to 28.8 mS cm^{-1}, the above hydrogel electrolyte ensured the associated $Zn-MnO_2$ battery with a good capacity of 237 mAh g^{-1} at 1 C and capacity retention of 86.2 % after 1000 cycles at 4 C. Moreover, benefiting from its good flexibility, mechanical strength, excellent hygroscopicity, interfacial adhesiveness, and suppressed dendrite growth, the above ZIB retained its

capacity well underwater without packaging, being bent, harshly poking, freely attached to human cloth for submarine situations. From **Figure 10a**, by adopting cellulose as the framework, tetraethyl orthosilicate (TEOS) as the crosslinker, and glycerol as the anti-freezing agent, a multifunctional hydrogel electrolyte (denoted as CT3G30 with optimized property) was highlighted for its outstanding flexibility, self-healing behavior, suppressed dendrite growth, intimate adhesion, and the combination of anti-freezing and heat-resistance property.[91] With a 3D porous network and extra-low freezing point of -64.6 ℃, it showed admirable ionic conductivity of 32.3 mS cm^{-1} (60.1 % maintained at –40 °C). As illustrated in **Figure 10b**, the fabricated Zn-MnO$_2$ battery exhibited a high specific capacity (**Figure 10c**) and ultra-stable cyclability after 2000 cycles from 60 to -40 ℃ (**Figure 10d**). It can freely work under massive deformation at –40 °C (**Figure 10e**), sealed in an ice cube, and immersed in boiling water. Moreover, with plenty of reversible H-bonds and Si-O-Si bonds inside, the battery showed 96.7% capacity retention after three cutting/self-healing cycles (**Figure 10f**).
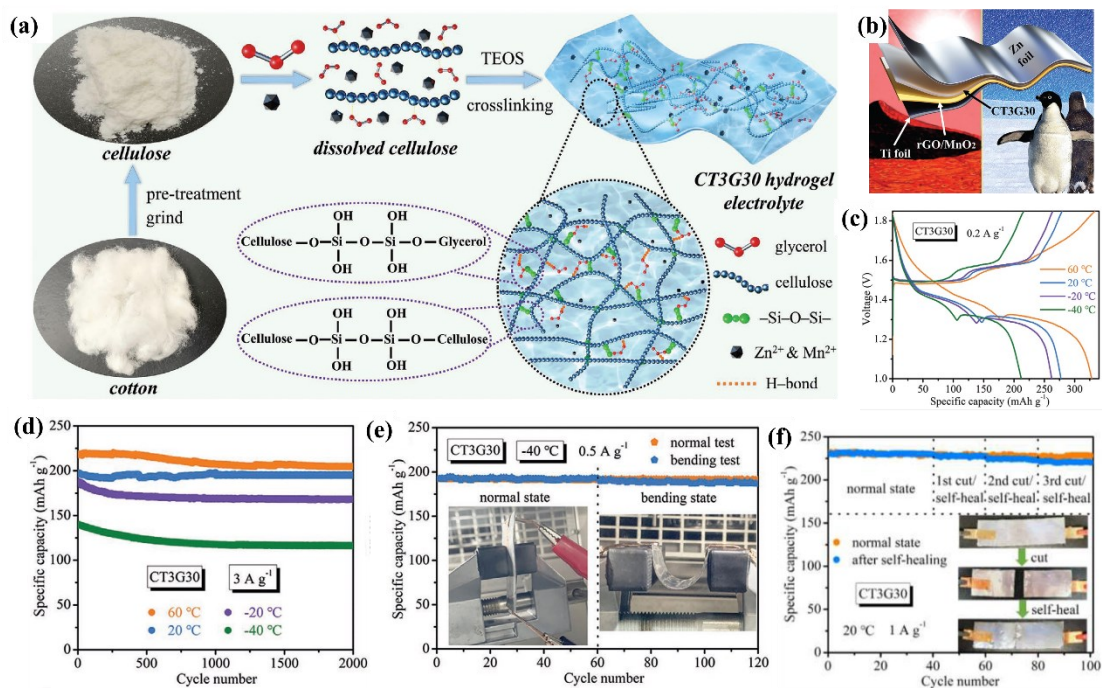
Figure 10. a) Synthesis schematic of the CT3G30 hydrogel electrolyte. b) Graphic

illustration of the environmentally adaptive flexible Zn–MnO$_2$ battery with CT3G30. c) GCD curves at 0.2 A g^{-1}. d) Cyclic performance of the Zn–MnO$_2$ batteries with CT3G30 at 3 A g^{-1} and different temperatures. e) Capacity evolution of the Zn–MnO2 batteries with CT3G30 at −40 °C and 0.5 A g^{-1}: in the normal state and under bending. f) The capacity evolution of our Zn-MnO$_2$ batteries with CT3G30 in normal state and after 1−3 cutting/self-healing rounds (the inset shows photographs of a Zn-MnO2 battery with CT3G30 during the 1st cutting/self-healing round). Reproduced with permission.[91] Copyright 2021, Wiley-VCH GmbH.

A multifunctional crosslinked cellulose nanofiber-polyacrylamide (CNF-PAM) hydrogel electrolyte was reported by grafting PAM onto the CNF surface, as shown in **Figure 11a**.[154] From **Figure 11b** and **11c**, because the CNF network formed a 3D backbone with PAM affixed on its surface and linkages among their hydroxide and carboxyl groups, the obtained hydrogel film possessed ultra-stable honeycomb-like porous morphology with high ionic conductivity of 6.8 mS cm^{-1}. The assembled Mg$_{0.23}$V$_2$O$_5$ • 1.0H$_2$O (MVO)/Zn battery showed a high capacity and cycling performance after 2000 cycles (**Figure 11d**). Even at an ultra-high current density of 20 A g^{-1}, it still exhibited decent capacity retention after 20000 cycles (**Figure 11e**). Moreover, the battery worked well under external strain (**Figure 11f** and **11g**, with sealed in a spring-type plastic tube), bending (**Figure 11h**), cutting (**Figure 11i**), freezing (**Figure 11j**), and heating (**Figure 11k**), suggesting its environmental-adaptive nature from the merits of CNF-PAM hydrogel electrolyte..
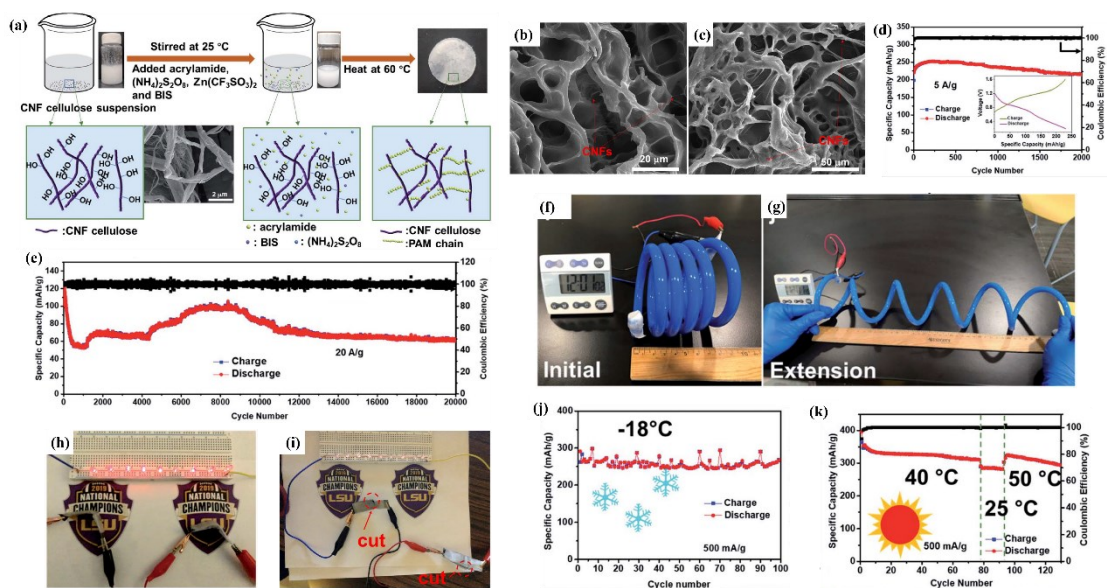
Figure 11. a) Schematic illustration of the synthesis route to form the solid-state electrolyte by grafting PAM on CNFs via a facile free radical polymerization approach. b) and c) SEM images of freeze-dried CNF-PAM films. Long-term cycling performance at high current densities of d) 5 and e) 20 A g^{-1}. f) and g) The optical photos of a designed spring battery powering a watch. h) An optical photo of nine LED lights powered by two MVO/Zn ssBs with a bending degree of 90 °. i) Optical photos of cutting on CNF-PAM films. Cycling performance at a current density of 500 mA g^{-1} at temperatures of j) -18 °C, k) 40 °C and 50 °C. Reproduced with permission.[154] Copyright 2020, The Royal Society of Chemistry.

Lately, a high-performance and flexible quasi-solid-state (QSS) ZIBs with PVA gel electrolyte containing LiCl, ZnCl$_2$, MnSO$_4$ (denoted as PVA/LiCl-ZnCl$_2$-MnSO$_4$) was reported.[103] It showed high specific capacity and excellent stability with a wide temperature range from -20 °C (capacity of 0.52 mAh cm^{-2}) to 80 °C (capacity of 3.26 mAh cm^{-2}). With the above hydrogel electrolyte, the battery preserved 103.4 % capacity after 1000 bending cycles under a 90° bending angle and worked stably under harsh conditions, including puncturing, cutting, cropping, hammering, soaking in water, and heating by a lighter. It was also integrated into a self-powered bracelet with a health monitoring function. Moreover, a hierarchical hydrogel electrolyte for

one ultra-safe and wearable ZIB was obtained through grafting polyacrylamide (PAM) onto gelatin chains and then injecting the above mixture into the pores of the polyacrylonitrile (PAN) electrospun fiber membrane.[76] With high ionic conductivity of 17.6 mS cm^{-1} and strength of 7.76 MPa, the assembled Zn-MnO$_2$ battery provided excellent specific capacity and cyclability. It maintained its performance well under bending, loading, hammer striking, exposure to fire, soaking and stirring in water, punching, and sewing, showing admirable stability and safety. Likewise, it can be tailored to other shapes and power an electronic watch. It can further be integrated into a smartwatch, health monitoring pulse sensor, and smart insoles, revealing its extraordinary potential in wearable electronics applications.

Zn batteries can even be designed into textile micro batteries with aesthetic patterns. Combined with the resist dyeing method, an in-plane battery was fabricated into stylish patterns. Therefore, Liu et al.[102] assembled an in-plane solid-state alkaline Zn micro-battery (micro-AZBs) on a textile substrate with a particular aesthetic pattern by taking advantage of the decent flexibility and transparency of PVA hydrogel, as demonstrated in **Figure 12a**. After coating PVA on integrated textile electrodes, the assembled micro Zn battery delivered excellent capacity and cycle performance (**Figure 12b** and **12c**) and only 9.4 % capacity loss after 1600 bending cycles (**Figure 12d**). The in-plane battery successfully enlightened a LED bulb under deformation and continued powering it after being cut four times (**Figure 12e**) with slight open-circuit voltage loss (**Figure 12f**). Furthermore, the letter-shaped micro-battery can be easily sewed onto cloth and power an LED bulb under repeated bending and casual motion (**Figure 12g**, **12h**, **12i**), keeping outstanding tailorability, sewability, and specific ornamental value at the same time.
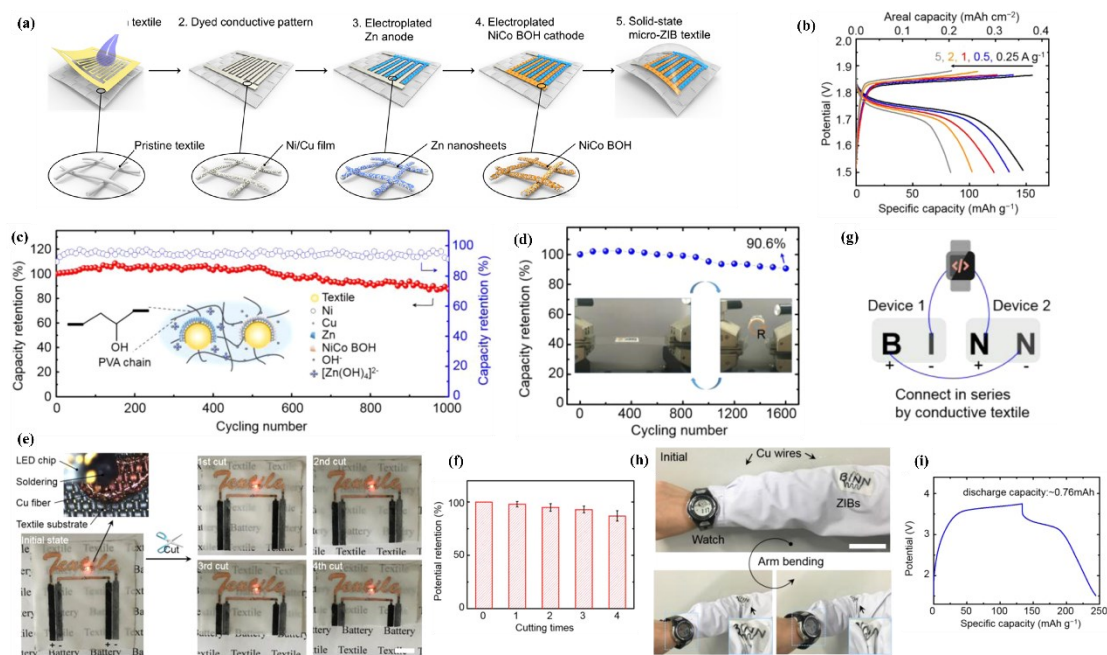
Figure 12. a) Schematic illustration of the fabrication procedures of textile micro-AZB. b) GCD curves of the device at various current densities. c) Cycling performance of the micro-AZB at a current density of 2.5 A g^{-1}. d) Capacity retention as a function of bending cycles. The radius of curvature R = 4.1 mm. e) Cutting test of the textile AZBs. The LED cells can still be powered through the letter ("textile")-shaped Cu textile circuit after the first, second, third, and fourth cuts of AZBs. f) Potential retention of the AZB at different cutting statuses. g) and h) AZBs in the shape of four letters, that is, "BINN". The letter-shaped AZBs sewed on a garment power a commercial watch under bending condition. i) GCD curves of the BINN AZBs. Scale bar, 1 cm (e) and 5 cm (h). Reproduced with permission.[102] Copyright 2019, American Chemical Society.

Pluronic polymer hydrogel composed of poly(ethylene oxide)-poly(propylene oxide)-poly(ethylene oxide) (denoted as PEO-PPO-PEO) was applied as a cooling-recovery electrolyte for flexible Zn-based batteries.[155] At low temperatures, hydrated PEO generated H-bonds among water molecules, turning to a liquid state. The PEO-PPO interface was dehydrated with hydrophobic packing when the temperature rises, regaining the gel phase. Moreover, when turning to the liquid state, it can re-wet

43

electrodes, refreshing and repairing wounded interface, realizing cooling-recovery behavior. The above hydrogel exhibited ionic conductivity of 6.33 mS cm^{-1}. For the involved battery, even after the PHE layer was exfoliated from the electrode under intense folding, it quickly returned to the liquid phase when the temperature dropped to -5 °C, and the tandem battery unit successfully powered LED bulbs under various bending states. Newly, a polyzwitterionic hydrogel electrolyte (PZHE) called poly [2-(methacryloyloxy) ethyl] dimethyl-(3-sulfopropyl) (PSBMA) was reported.[156] The hydrogel containing both physical and chemical crosslinks was synthesized from a zwitterionic monomer called [2-(methacryloyloxy)ethyl]dimethyl-(3-sulfopropyl) (SBMA), which contained C–N$^+$ as the cationic group and SO$_3^-$ acted as the anionic group. From **Figure 13a**, water molecules were locked inside by the interactions with countless polar and hydrophilic groups; functional groups also immobilized unneeded anions and steric hindrance of PSBMA. Thus, simultaneously, reversible and synergistic electrostatic interactions and hydrogen bonds among charged groups and water molecules were formed. Therefore, the mechanical strength, interfacial adhesion, and uniform Zn^{2+} deposition were further ensured, resulting in high ionic conductivity of 32.0 mS cm^{-1}, alleviated dendrite growth, self-healing behavior, and anti-freezing property. The corresponding VS$_2$/PZHE/Zn quasi-solid ZIB delivered reasonable electrochemical properties (**Figure 13b**, **13c**). It also powered an electronic device after hammering (**Figure 13d**), being cutting and self-healing (**Figure 13e**), washing and soaking (**Figure 13f**) and cutting in water (**Figure 13g**), heating on an alcohol lamp (**Figure 13h**), and keeping at -20 °C (**Figure 13i**), which were inseparable from the benefits of PZHE.
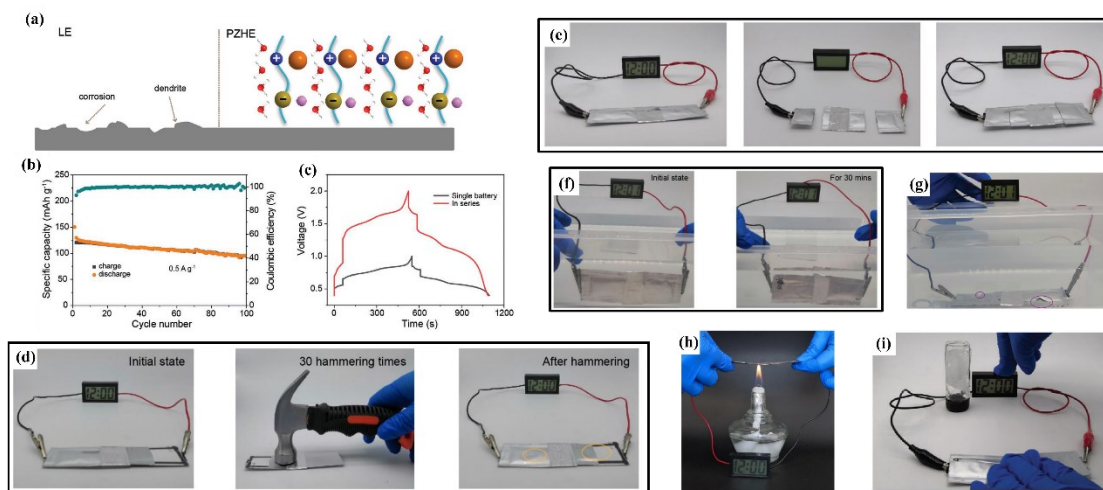
Figure 13. a) Schematic illustration of the morphologies of Zn metal anode with LE/PZHE during Zn plating. b) Cycling performance of the quasi-solid state ZMBs at 0.5 A g^{-1}. c) Galvanostatic charge/discharge curves of the two quasi-solid state ZMBs connected in series. Optical images of d) hammering test of the quasi-solid state rechargeable ZMBs, e) cutting and soaking test of the quasi-solid state ZMBs, f) soaking test of the quasi-solid state rechargeable ZMBs in DI water. g) cutting and soaking test of the quasi-solid state ZMBs, h) burning test of the quasi-solid state rechargeable ZMBs, i) low temperature anti-icing test of quasi-solid state ZMBs at −20 °C. Reproduced with permission.[156] Copyright 2020, WILEY-VCH Verlag GmbH & Co. KGaA, Weinheim.

Besides dual-crosslink network HEs, a triple-network HE named polyacrylamide/gelatin/[2-methylacryloxy) ethyl]dimethyl-(3-sulfonic acid propyl) ammonium hydroxide (DMAPS) was reported recently.[133] Specifically, PAM was applied as the hydrogel matrix, gelatin was used as the enhancer toward mechanical strength and self-healing property, and the usage of DMAPS can greatly promote Zn^{2+} kinetics, regulating Zn^{2+} transfer and thus improving the battery cyclability by its rich zwitterionic groups along the polymer chain. Therefore, the high ionic conductivity of 35.1 mS cm^{-1} was achieved, and the involved Zn//MnO$_2$ battery showed both high capacity and stable work under any bending angels and heavy pressure.

In the field of Zn-ion hybrid capacitors (ZICs), a multi-functional and ionic-

crosslinked copolymer hydrogel based on anionic P(AMPSZn-AAZn)/ZnCl$_2$ polymer chain was presented, in which FeCl$_3$ formed ionic bond crosslink with carboxylate groups, and SO$_3^-$ anchored on the chain regulated Zn^{2+} transport.[157] Hence, the ionic conductivity of 0.66 mS cm^{-1} was achieved, and the involved ZIC showed decent electrochemical performance and flexibility. Moreover, owing to non-covalent reversible interactions between Fe^{3+} and -COO$^-$, it exhibited self-healing properties after being cut and re-put together, and the ZIC still worked well under low temperatures to -18 °C. With water molecules trapped inside concentrated salt and function groups along PAM chains, side reactions were disallowed, and the anode's stability was enhanced.[158] Thus, the PAM hydrogel electrolyte containing 7.5 M ZnCl$_2$ further enlarged its voltage window from 0-1.8 V and exhibited high ionic conductivity of 71.4 mS cm^{-1}. Furthermore, the assembled ZIC showed an excellent capacitance retention rate of 95.1 % after 100 000 cycles at 5 A g^{-1}. Since its freezing point got lower with higher ZnCl$_2$ concentration, at -20 °C, it maintained its ionic conductivity of 17.9 mS cm^{-1} and 92.9% capacitance retention over 40000 cycles at 5 A g^{-1}. Also, the flexible ZIC worked well under bending and twisting at -25 °C. Recently, a PVA-CMC hydrogel electrolyte was developed for a highly environmental-adaptive ZIC.[159] Specifically, the PVA matrix guaranteed its excellent hygroscopic and adhesion property. Furthermore, the application of EG improved its frost resistance and promoted its mechanical reinforcement by facilitating PVA crystalline domain formation via hydrogen-bonds interactions. Also, CMC further enhanced its mechanical strength through hydrogen bonds. Meanwhile, −COO$^-$ groups on CMC chains regulated Zn^{2+} diffusion and homogenized Zn^{2+} stripping and deposition and prevented dendrite growth. Based on those combined benefits, the hydrogel exhibited impressive mechanical robustness and an admirable ionic capacity of 1.73/0.75 S m^{-1} at 20/-20 °C. The assembled ZIC also showed reliable cycling stability at 20 and -20 °C.

1.8 Summary of challenges and perspectives

In summary, HEs, with their enchanting potential, have been regarded as alluring candidates for next-generation batteries for the following reasons: 1. Their robust polymer backbones and admirable flexibility are qualified to maintain their chemical and physical stability under harsh external treatments. 2. Their controllable and homogeneous 3D porous structure generates fast and uniform ion diffusion channels to achieve decent ionic conductivity and evenly ion deposition on the electrode. 3. Their mechanical property and adhesive nature produce a stable and intimate interfacial contact, guaranteeing the involved batteries cycling stability with efficiently suppressed dendrite growth, side reactions, and exfoliation among each battery component, further bettering batteries' steadiness and safety. 4. With plenty of functional groups, complicated intermolecular and intramolecular interactions were created, exhibiting more valuable functions both at electrolyte level and battery level, shining as highlights for aqueous ZIBs to catch the tendency in the application of flexible, wearable, and multifunctional devices.

Nevertheless, while deepening the research and exploration of various HEs, existing challenges below were inevitably found and further got in the way of their large-scale application and commercialization.

Firstly, the ionic conductivity of HEs still possesses much space to improve. Compared to the aqueous electrolyte, considering intertwined 3D porous structure with larger thickness, discontinuous quasi-solid-solid electrolyte-electrode interface, and unavoidable water evaporation during operation, the resistance of HEs is inevitably heightened, resulting in lower ionic conductivity, sluggish ion transfer, and poor electrochemical performance. Therefore, some novel fabrication methods of HEs should be considered to lower the thickness, such as adopting electrospun technology to make it as thin as a film. For the interfacial barrier, super adhesive hydrogels were proposed and utilized to increase the interface stability with the existence of those numerous polar groups. Furthermore, more hydrophilic groups and intermolecular interactions should be introduced into the hydrogel network to alleviate water

evaporation. For example, by co-polymerizing with or grafting to other hydrogel networks, the number of hydrophilic groups alongside the polymer backbone can be doubled or even more, thus realizing a much-improved water storage capability. Besides, applying the "water-in-salt" strategy or ionic liquids (ILs) are also wise to decrease or even avoid the usage of problematic aqueous electrolyte from the start. However, the much higher cost of using ILs still needed to be noted.
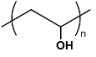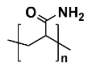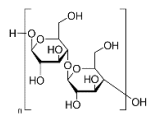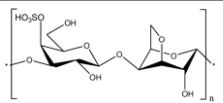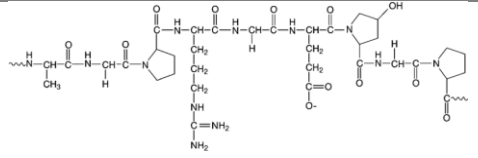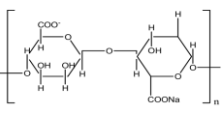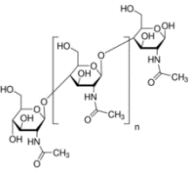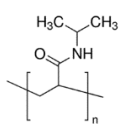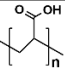
Second, the mechanical strength of HEs still cannot be comparable to those of all-solid-state electrolytes, such as thermoset polymers. Especially those HEs do not have chemically covalent bonds-based crosslinks, like PVA, alginate, etc. Those reversible and weak interactions serve as the vital force to construct the hydrogel network. The corresponding HEs exhibit better compliance and self-healing property but sanctify their mechanical robustness. In order to realize HEs with both flexibility and mechanical stability, preparing dual-crosslink HE should be a rational method by introducing a second polymer crosslink via blocking, grafting, crosslinking, in which the first network acts as a strong covalently crosslink backbone, and the second with reversible crosslink serve to realize better flexibility or other functions. The above strategy has been widely used, especially by grafting PAM onto gelatin, alginate, xanthan gum, CMC, chitin, PVA, etc., to achieve significantly improved mechanical without ionic conductivity sacrifice. Therefore, it is reasonable to utilize HEs with dual or trial crosslinks in the future. Furthermore, hydrogels from natural resources should also become hot candidates as hydrogel substrates or components to meet the demands of environmental sustainability.
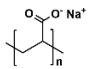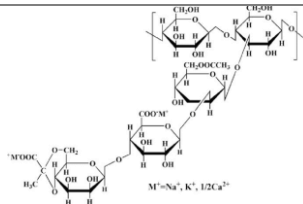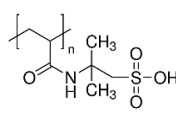
Thirdly, to be competitive among environmental adaptive batteries based on other electrolytes, the anti-freezing property and thermal-protection behavior of HEs still need to be emphasized, and the working temperature window also needs to be widened. The popular methods include modifying the polymer chain or introducing other functional agents to the original system. For example, glycerol can be used as an anti-freezing agent to decrease the freezing point of water inside HEs through competition with the hydrogen bonds between water molecules to prevent the crystallization of water molecules. Similarly, other polymers with plenty of O or N

containing groups can also form abundant hydrogen bonds with water molecules. Therefore, they can be introduced by grafting or co-polymerization into the initial HEs network and lower the freezing point in the same way. Moreover, for most hydrogel electrolytes, the voltage window of the battery is still relatively narrow, and the cycling stability is still not as good as expected. Therefore, hydrogel electrolytes' selection, preparation, and modification strategies still have ample space to improve.

The research toward HEs and ZIBs is still in the infancy stage. Exploring their mechanisms is urgently needed since it is the prerequisite to further optimizing and commercializing both HPEs and next-generation ZIBs. Therefore, mechanism-related research, such as operando characterizations, DFT calculation, model construction, computer simulation, etc., will become critical in future research. Based on deeper mechanism understanding and further performance optimization, we believe HEs, as essential components for ZIBs with unique and irreplaceable advantages, can make ZIBs and other battery technologies serve as a more reliable power supply in every aspect of human life in the future.

Table 1 Structures and features of widely used hydrogel substrates

Name	Molecule structure	Crosslinking	Highlight features	Ref.
PVA		Physical Chemical	Flexible Self-healing Ultra-stable	[65, 97]
PAM		Chemical	Flexible Super-tough Anti-freeze Thermo-protection	[129, 138, 149]
Cellulose		Physical Chemical	Flexible Mechanical property Anti-freeze Self-healing Natural Resource	[86, 91, 125, 154]
kappa-carrageenan		Physical	Flexible Natural Resource	[66, 121]
Gelatin		Physical	Flexible Natural Resource	[76, 116]
SA		Physical	Flexible Mechanical property Ultra-stable Natural Resource	[85, 96, 116, 150, 152]
Chitin		Physical	Flexible Mechanical property Natural Resource	[122]
Poly(N-isopropylacrylamide) (PNiPAM)		Chemical	Flexible Mechanical property Thermo-protection	[70, 89]
PAA		Physical Chemical	Flexible	[66, 78]

50

PANa		Physical Chemical	Flexible Mechanical property	[79]
Xanthan Gum		Physical	Flexible Anti-freeze Ultra-stable Natural Resource	[82, 124]
Poly 2-Acrylamido-2-methyl-1-propanesulfonic acid (PAMPS)		Chemical	Flexible Mechanical property Ultra-stable	[67, 68, 151]

Table 2 Summary of electrochemical performance of HEs and the related ZIBs

Hydrogel matrix	Electrolyte solution	Ionic conductivity	Battery performance		Highlight function	Ref.
			Capacity	Cycling performance		
PVA	0.35 M $ZnSO_4$	-	89 mAh g^{-1} (0.1 A g^{-1})	71 % / 500 cycles (0.4 A g^{-1})	Flexibility	[105]
PVA	1 M $Zn(CF_3SO_3)_2$	-	109 mAh g^{-1} (0.5 A g^{-1})	91.7 % / 200 cycles (0.5 A g^{-1})	Flexibility	[88]
PVA	3 M $Zn(CF_3SO_3)_2$	9.76 mS cm^{-1}	215 mAh g^{-1} (0.1 A g^{-1})	-	Flexibility	[106]
PVA	1.5 M KOH 0.05 M $Zn(Ac)_2$	-	18.7 mAh cm^{-3} (1.45 C)	> 80 % / 1000 cycles (under 95° bending)	Flexibility	[107]
PVA	1 M $ZnSO_4$	-	32.56 mAh cm^{-3} (10 mA cm^{-3})	76.5 % / 1000 cycles (50 mA cm^{-3})	Flexibility	[87]
PVA	10 M KOH	-	1.03 mAh cm^{-2} (0.5 mA cm^{-2})	79.5 % / 200 cycles (0.5 mA cm^{-2})	Flexibility	[108]
PVA	3 M LiCl 2 M $ZnCl_2$ 0.4 M $MnSO_4$	-	0.718 mAh cm^{-2} (0.1 mA cm^{-2})	82.5 % / 500 cycles (0.1 mA cm^{-2})	Flexibility	[109]
PAM	1 M $ZnSO_4$	5.56 mS cm^{-1}	144 mAh g^{-1} (0.2 A g^{-1})	91.1 % / 150 cycles (0.5 A g^{-1})	Flexibility	[112]
PAM	2 M $ZnSO_4$ 0.2 M $CoSO_4$	0.12 mS cm^{-1}	180.6 mAh g^{-1} (0.5 A g^{-1})	94.6 % / 2000 cycles (2 A g^{-1})	Flexibility	[113]

PAM	21 M LiTFSI 2M Zn(OTF)$_2$	6 mS cm^{-1}	141.2 mAh g^{-1} (0.2 A g^{-1})	~ 100 % / 300 cycles (1 A g^{-1})	Flexibility	[11]
CMC	ZnSO$_4$ (m $_{ZnSO4}$: m$_{CMC}$ =1.9:1)	-	481 mAh g^{-1} (0.1 A g^{-1})	28.5 % / 100 cycles (0.1 A g^{-1})	Flexibility	[125]
kappa-carrageenan	2 M ZnSO$_4$ 0.1 M MnSO$_4$	33.2 mS cm^{-1}	291.5 mAh g^{-1} (0.15 A g^{-1})	80 % / 450 cycles (6 A g^{-1})	Flexibility	[121]
PVA-MSA	0.5 M ZnCl$_2$ 1 M NH$_4$Cl	30.6 mS cm^{-1}	100.3 mAh g^{-1} (5 A g^{-1})	88 % / 2000 cycles (2 A g^{-1})	Flexibility	[114]
AMP-Mn/PVA	1 M ZnSO$_4$	34.1 mS cm^{-1}	230 mAh g^{-1} (0.2 A g^{-1})	99.97 % / 600 cycles (2 A g^{-1})	Flexibility	[117]
PVA/PAA	1 M KOH 0.001 M Zn(Ac)$_2$	-	162 mAh g^{-1} (1 A g^{-1})	80 % / 2000 cycles (1 A g^{-1})	Flexibility	[78]
Gelatin-Sodium Alginate	2 M ZnSO$_4$	37 mS cm^{-1}	251 mAh g^{-1} (2 A g^{-1})	75 % / 200 cycles (2 A g^{-1})	Flexibility	[116]
Starch-PAM	2 M ZnSO$_4$	26.5 mS cm^{-1}	161.7 mAh g^{-1} (1 A g^{-1})	97.7 % / 500 cycles (1 A g^{-1})	Flexibility	[118]
SPI/PAM	1 M ZnSO$_4$ 0.1 M MnSO$_4$	58 mS cm^{-1}	299.3 mAh g^{-1} (0.4 C)	78 % / 500 cycles (0.4 C)	Flexibility	[127]
PAM-ChNF	10 mM Zn(CF$_3$SO$_3$)$_2$	15.2 mS cm^{-1}	343.9 mAh g^{-1} (0.2 A g^{-1})	90.7 % / 1000 cycles (10 A g^{-1})	Flexibility	[122]
PAM/Gelatin/DMAPS	2 M ZnSO$_4$	35.1 mS cm^{-1}	175 mAh g^{-1} (0.5 A g^{-1})	~ 100 % / 100 cycles (0.5 A g^{-1})	Flexibility	[133]
PAM-co-PAA/κ-CG	2 M ZnSO$_4$	17.6 mS cm^{-1}	72.5 mAh g^{-1} (0.1 A g^{-1})	96.4 % / 10000 cycles (3 A g^{-1})	Flexibility	[66]
SL-PAM	2 M ZnSO$_4$	31.1 mS	109 mAh	~ 350 % /	Highly adhesive	[84]

	0.1 M MnSO$_4$	cm^{-1}	g^{-1} (0.5 A g^{-1})	600 cycles (0.1 A g^{-1})		
PAPTQ/PAM/PAMPS	1 M ZnSO$_4$ 1 M CuSO4	-	160 mAh g^{-1} (2 mA cm^{-2})	-	Highly adhesive	[67]
PANa	6 M KOH 0.2 M Zn(Ac)$_2$	200 mS cm^{-1}	96 mAh g^{-1} (2.3 A g^{-1})	86 % / 340 cycles (56.5 C)	Super-tough	[79]
PAM	1 M ZnSO$_4$ 0.1 M MnSO$_4$	-	136.2 mAh g^{-1} (4 C)	69.02 % / 1000 cycles (4 C)	Super-tough	[129]
M-HNTs/PAM	2 M ZnSO$_4$ 0.1 M MnSO$_4$	26 mS cm^{-1}	209.8 mAh g^{-1} (1 C)	92.7 % / 1000 cycles (10 C)	Super-tough	[130]
Zn-Alginate/PAM	2 M ZnSO$_4$ 0.1 M MnSO$_4$	43.2 mS cm^{-1}	300.4 mAh g^{-1} (0.11 A g^{-1})	82 % / 500 cycles (0.88 A g^{-1})	Super-tough	[85]
PVA	2 M Zn(CF$_3$SO$_3$)$_2$	12.6 S cm^{-1}	123 mAh g^{-1} (0.1 A g^{-1})	97.1 % / 1000 cycles (1 A g^{-1})	Self-healing	[65]
PVA	1.1 M Zn(Ac)$_2$ 0.1 M Mn(Ac)$_2$	-	123 mAh g^{-1} (0.2 A g^{-1})	-	Self-healing	[132]
B-PVA/NFC	2 M ZnSO$_4$	18.1 mS cm^{-1}	56.1 mAh g^{-1} (0.5 mA cm^{-2})	95.3 % / 5000 cycles (2 mA cm^{-2})	Self-healing	[74]
NFC/PAM	2 M ZnSO$_4$ 0.2 M MnSO$_4$	22.8 mS cm^{-1}	210 mAh g^{-1} (4 C)	88.3 % / 1000 cycles (4 C)	Sewable & Tailorable	[86]
ZSC-gel (Containing cellulose)	2 M ZnSO$_4$ 0.2 M MnSO$_4$	24.6 mS cm^{-1}	158 mAh g^{-1} (6.5 C)	94.9 % / 500 cycles (6.5 C)	Sewable & Tailorable	[135]
EG-waPUA/PAM	2 M ZnSO$_4$ 0.1 M MnSO$_4$	14.6 mS cm^{-1} (-20 °C)	226 mAh g^{-1} (0.2 A g^{-1}, -20 °C)	72.54 % / 600 cycles (2.4 A g^{-1}, -20 °C)	Anti-freezing	[90]

			183.2 mAh g^{-1} (0.2 A g^{-1}, -20 °C)	61 % / 1000 cycles (1 A g^{-1}, -20 °C)	Anti-freezing	[138]
PAM/GO/EG	2 M ZnSO$_4$ 0.2 M MnSO$_4$	14.9 mS cm^{-1} (-20 °C)	183.2 mAh g^{-1} (0.2 A g^{-1}, -20 °C)	61 % / 1000 cycles (1 A g^{-1}, -20 °C)	Anti-freezing	[138]
GG/SA/EG	2 M ZnSO$_4$ 0.1 M MnSO$_4$	6.19 mS cm^{-1} (-20 °C)	114.61 mAh g^{-1} (0.3 A g^{-1}, -20 °C)	80.39 % / 100 cycles (0.3 A g^{-1}, -20 °C)	Anti-freezing	[139]
CNF/PAM	Zn(CF$_3$SO$_3$)$_2$	-	140 mAh g^{-1} (1 A g^{-1}, -60 °C)	79.3 % / 60 cycles (30 mA g^{-1}, -60 °C)	Anti-freezing	[119]
PAM	2 M ZnSO$_4$ 4 M LiCl	-	104 mAh g^{-1} (0.1 A g^{-1}, -20 °C)	~ 100 % / 500 cycles (0.5 A g^{-1}, -20 °C)	Anti-freezing	[140]
Xanthan gum	4 M ZnCl$_2$	2.54 mS cm^{-1} (-20 °C)	201 mAh g^{-1} (0.2 A g^{-1}, -20 °C)	77 % / 1500 cycles (1 A g^{-1}, -20 °C)	Anti-freezing	[124]
PZHE	7.5 M ZnCl$_2$	15.6 mS cm^{-1} (-60 °C)	81.5 mAh g^{-1} (0.5 A g^{-1}, -40 °C)	84.6 % / 100000 cycles (5 A g^{-1}, -40 °C)	Anti-freezing	[141]
PAM	5.5 M ZnCl$_2$	43 mS cm^{-1}	370 mAh g^{-1} (2 mA cm^{-2})	~ 100 % / 500 cycles (10 mA cm^{-2})	Thermo-protection	[149]
PNIPAM/AM-5	0.25 M Zn(CF$_3$SO$_3$)$_2$	78 mS cm^{-1}	168.7 mAh g^{-1} (0.1 A g^{-1})	80 % / 1000 cycles (1 A g^{-1})	Thermo-protection	[89]
PAMPSZn	-	20.1 mS cm^{-1}	438.9 mAh g^{-1} (0.1 A g^{-1})	80.2 % / 400 cycles (0.5 A g^{-1})	Electrochemical Stability	[68]
P(ICZn-AAM)	2 M ZnSO$_4$	2.15 mS cm^{-1}	322.3 mAh g^{-1} (0.5 C)	81.9 % / 500 cycles (5 C)	Electrochemical Stability	[69]

			260 mAh g^{-1}	94 % / 1000		
SA	NaCl ZnSO$_4$	-	(1 A g^{-1})	cycles (10 A g^{-1})	Electrochemical Stability	[96]
ZIS-PVA	1 M Zn(CF$_3$SO$_3$)$_2$	10.3 mS cm^{-1}	151.2 mAh g^{-1} (0.1 A g^{-1})	87.5 % / 600 cycles (5 A g^{-1})	Electrochemical Stability	[97]
Alginate	1 M Zn(Ac)$_2$	32.8 mS cm^{-1}	188 mAh g^{-1} (0.2 A g^{-1})	66.8 % / 2000 cycles (2 A g^{-1})	Electrochemical Stability	[83]
Zn-Alginate/PAM	2 M ZnSO$_4$ 0.1 M MnSO$_4$	16.3 mS cm^{-1}	272 mAh g^{-1} (0.1 A g^{-1})	81 % / 500 cycles (1.6 A g^{-1})	Multi-functional	[150]
PAMPS/PAM	2 M ZnCl$_2$ 3 M NH$_4$Cl	1.62 mS cm^{-1} (-30 ℃)	122.1 mAh g^{-1} (5 A g^{-1})	85 % / 4000 cycles (5 A g^{-1})	Multi-functional	[151]
Alginate-Zn	2 M ZnSO$_4$ 0.2 M MnSO$_4$	18.3 mS cm^{-1}	300 mAh g^{-1} (0.2 A g^{-1})	~ 56.5 % / 200 cycles (0.5 A g^{-1})	Multi-functional	[152]
PAM	2 M ZnSO$_4$ 0.1 M MnSO$_4$	17.3 mS cm^{-1}	302.1 mAh g^{-1} (60 mA g^{-1})	98.5 % / 500 cycles (2 A g^{-1})	Multi-functional	[77]
PAM	6 M KOH 0.2 M Zn(Ac)$_2$	-	148 mAh g^{-1} (1 A g^{-1})	90.1 % / 1200 cycles (2 A g^{-1})	Multi-functional	[153]
XG-PAM/CNF	2 M ZnSO$_4$ 0.1 M MnSO$_4$	28.8 mS cm^{-1}	237 mAh g^{-1} (1 C)	86.2 % / 1000 cycles (4 C)	Multi-functional	[82]
CT3G30 (Cellulose framework)	0.45 M ZnSO$_4$ 0.045 M MnSO$_4$	32.3 mS cm^{-1}	277.3 mAh g^{-1} (0.2 A g^{-1})	99.2 % / 2000 cycles (3 A g^{-1})	Multi-functional	[91]
CNF/PAM	1 M Zn(CF$_3$SO$_3$)$_2$	6.8 mS cm^{-1}	216 mAh g^{-1} (5 A g^{-1})	98.6 % / 2000 cycles (5 A g^{-1})	Multi-functional	[154]
PVA/LiCl-ZnCl$_2$-MnSO$_4$	3 M LiCl 2 M ZnCl$_2$ 0.4 M MnSO$_4$	-	3.57 mAh cm^{-2} (3.93 mA cm^{-2})	108.48 % / 3000 cycles (47.16 mA cm^{-2})	Multi-functional	[103]
Gelatin-g-PAM/PAN	2 M ZnSO$_4$ 0.1 M MnSO$_4$	17.6 mS cm^{-1}	306 mAh g^{-1} (61.6 mA g^{-1})	97 % / 1000 cycles (2772 mA g^{-1})	Multi-functional	[76]

PVA	1 M KOH 0.02 M Zn(Ac)$_2$ 0.005 M LiOH 0.005 M Ca(OH)$_2$	-	147.2 mAh g^{-1} (0.25 A g^{-1})	87.2 % / 1000 cycles (2.5 A g^{-1})	Multi-functional	[102]
PEO53-PPO34-PEO53	0.25 M ZnSO$_4$ 0.25 M Li$_2$SO$_4$	6.33 mS cm^{-1}	70 mAh g^{-1} (20 mA g^{-1})	83 % / 300 cycles (0.5 C)	Multi-functional	[155]
PSBMA	2 M ZnSO$_4$	32 mS cm^{-1}	125 mAh g^{-1} (0.5 A g^{-1})	~ 70 % / 100 cycles (0.5 A g^{-1})	Multi-functional	[156]
P(AMPSZn-AAZn)/ZnCl$_2$	0.025 M ZnCl$_2$ 0.016 M FeCl$_3$	0.66 mS cm^{-1}	458.7 F g^{-1} (1 A g^{-1})	81.2 % / 1000 cycles (10 A g^{-1})	Multi-functional	[157]
PAM	7.5 M ZnCl$_2$	71.4 mS cm^{-1}	319.4 F g^{-1} (0.5 A g^{-1})	95.1 % / 100000 cycles (5 A g^{-1})	Multi-functional	[158]

Table 3 Summary of ZIBs based on multifunctional HEs

Hydrogel matrix	Mechanical Endurance			Electrochemical Stability		Temperature Adaptability		Ref.
	Self healing	Super tough	Sewable & Tailorable	Highly adhesive	Dendrite free	Anti freezing	Wide Temperature range	
Zn-Alginate/PAM	-	○	-	-	-	○	○	[150]
PAMPS/PAM	-	○	-	-	○	○	○	[151]
Alginate-Zn	-	-	-	-	○	-	○	[152]
PAM	-	○	○	-	-	-	-	[77]
PAM	-	○	-	-	-	-	-	[153]
XG-PAM/CNF	-	○	-	○	○	-	-	[82]
CT3G30 (Cellulose framework)	○	-	-	○	○	○	○	[91]
CNF/PAM	-	○	-	-	-	○	○	[154]
PVA/LiCl-ZnCl$_2$-MnSO$_4$	-	○	-	-	-	○	○	[103]
Gelatin-g-PAM/PAN	-	○	○	-	-	-	-	[76]
PVA	-	-	○	-	○	-	-	[102]
PEO53-PPO34-PEO53	○	○	-	-	-	-	-	[155]
PSBMA	○	○	-	-	○	○	-	[156]
P(AMPSZn-AAZn)/ZnCl$_2$	○	-	-	-	○	○	-	[157]
PAM	-	-	-	-	○	○	-	[158]
DMAPS	○	○	-	-	○	-	-	[133]

The space colored with light yellow represents the highlight functions that those hydrogel electrolytes bring to the involved ZIBs.

Chapter 2. PAM-based Hydrogel Electrolytes for Zinc-ion Supercapacitors

2.1 Introduction

Combining advantages of battery anode and capacitor cathode, aqueous zinc ion hybrid capacitors (ZICs) are regarded as one powerful energy storage device for electric vehicles and smart grids. The charge-storage mechanism of ZICs is based on the electric double-layer capacitor (EDLC) and surface pseudo capacitance on the cathode together with Zn plating and stripping on the anode.[160, 161] Generally, as a hybrid energy storage device with electrochemical performance combining traditional supercapacitor and rechargeable batteries, ZIC composed of porous carbon-based cathode and zinc metal anode exhibits decent voltages and power densities, ultralong cycle life as well as advantages of low-cost, high safety, and large-scale application potential.[161-163] Although the carbon-based cathodes have long life, the Zn metal anodes suffer from dendritic growth and side reactions like corrosion and hydrogen evolution in aqueous electrolyte, which can considerably shorten the lifespan of ZICs. As such, hydrogel electrolytes were developed to effectively address the cycling issues of aqueous electrolytes *via* suppressing dendrite growth and side reactions on zinc anode. Apart from that, hydrogel electrolytes endow the devices with flexibility and wearability, features necessary for next-generation energy storage devices. Thus, the making of flexible and durable ZICs based on hydrogel electrolytes holds great potential for applications. Among all hydrogel candidates and compared with hydrogels with physical crosslinking, such as PVA-based hydrogels, gelatin, alginate, kappa-carrageenan, xanthan gum, etc., PAM stands out due to its higher mechanical property from its chemical covalent-crosslinking network.[57, 58] After polymerization, PAM can form a free-standing hydrogel film with aqueous electrolytes contained within its network due to the existence of abundant hydrophilic groups and its high water capacity can further guarantee its reliable ionic conductivity and

electrochemical performance.[59] Moreover, its thickness and porosity were controllable by modifying the amount and ratio of monomer, crosslinker and initiator. Bearing above points in mind, here my first research project involves the preparation of PAM-based hydrogel for activated carbon-based flexible ZICs. Initially, two different PAM samples were prepared through different preparation methods. They were structurally characterized and corresponding ZICs were electrochemically tested, and the optimal ZICs was obtained, and relevant hydrogel preparation approach was selected for next chapters. Then, a double-crosslinked Zn-Alginate/PAM hydrogel electrolyte with better electrochemical performance was introduced, together with its synthesis process, structural characterizations, water absorption and mechanical strength tests and electrochemical performances. Specifically, a soft-packaged ZIC pouch cell was assembled for the first time with the aforementioned hydrogel electrolytes, and the bending test was carried out to signify its flexibility brought by the Zn-Alginate/PAM hydrogel electrolyte.

2.2 Single-network PAM hydrogel

2.2.1 Introduction

Based on previously reported literature, there have been two methods for preparing PAM hydrogel electrolytes: one is the synthesis of pure PAM first followed by soaking in the zinc electrolyte solutions; the other is the direct polymerization of PAM in zinc electrolyte solutions. In this section, based on above two methods, two PAM samples were synthesized to figure out the better method for making PAM hydrogel electrolyte and future ZICs construction. SEM images of two PAM and their corresponding electrochemical performance of ZICs were obtained and compared with each other. It is found that the first method enables better performance due probably to the higher water content. Moreover, due to the existence of 3D crosslinked PAM chains and regulated ion transfer, the cycle life of both samples were

significantly improved over 10 times in comparison to ZICs based on aqueous 2M ZnSO$_4$. Despite the improved cycle life, the capacity of ZIC based on hydrogel electrolytes is lower than the counterpart based on aqueous electrolyte, mainly resulting from the large thickness and low ionic conductivity of hydrogel electrolytes. Therefore, further modification of pure PAM hydrogel electrolyte is still urgently needed.

2.2.2 Experimental Section

2.2.2.1 Materials and reagents

Reagent's name	Manufacturer	Purity
Acrylamide	Sigma-Aldrich	analytical grade
N, N'-methylenebisacrylamide (MBAA)	Sigma-Aldrich	analytical grade
Potassium persulfate (KPS)	Sigma-Aldrich	analytical grade
Commercial activated carbon (AC, TF-B520)	MTI corporation	analytical grade
Sodium alginate (SA)	Sigma-Aldrich	analytical grade
Zinc sulfate heptahydrate (ZnSO$_4$·7H$_2$O)	Sigma-Aldrich	analytical grade

All chemicals were used without further purification.

Technical parameters of commercial activated carbon (AC, TF-B520)

Technical parameters	Values
Density (g/cc)	0.32-0.40 (g/cc)
Particle size (μm)	5 (±) (μm)
Ash (%)	< 0.07 %
PH	6.0-7.0
Surface area (m^2/g)	2000 (±100) (m^2/g)
Pore volume (cm^3/g)	1.0-1.2 (cm^3/g)
Pore size (mm)	2.0-2.2 (mm)
Iodine absorption (mg/g)	2000 (±100) (mg/g)
Carbon content (%)	> 95 %
Metal ions (ppm)	< 1000 (ppm)

Organic capacitance (per unit weight) (F/g)	> 130 (F/g)
Organic capacitance (per unit volume) (F/cc)	> 60 (F/cc)
Inorganic capacitance (per unit weight) (F/g)	> 240 (F/g)
Inorganic capacitance (per unit volume) (F/cc)	> 120 (F/cc)

2.2.2.2 Preparation of pure PAM hydrogel electrolyte

Firstly, 2.5 g of acrylamide monomer was dissolved in 10 mL of water under vigorous stirring. After the solution became transparent, 0.5 mg of MBAA crosslinker and 12.5 mg of KPS initiator were added to the mixture under stirring under stirring in ice bath with the protection of Argon for 15 min, in order to prevent unevenly polymerization under room temperature and remove air bubbles. Next, the above liquid was injected into a glass Petri dish and then was put in vacuum oven at 70 °C for 30 minutes for polymerization to obtain the pure PAM hydrogel electrolyte. Then, the attained PAM film was soaked in 2 M $ZnSO_4$ solution for 1 hour at room temperature.

For the preparation of PAM hydrogel without soaking, the synthesis process was the same with above, except changing 10 mL DI water to 10 mL 2 M $ZnSO_4$ solution and directly used as hydrogel electrolyte after completing polymerization in vacuum oven.

2.2.2.3 Preparation of activated carbon (AC) slurry

Firstly, the aqueous binder was obtained by dissolving sodium alginate (SA) into DI water with a concentration of 10 mg/mL, following by stirring for 24 hours. Then the AC slurry was prepared by mixing activated carbon, super P and SA binder with a mass ratio of 8:1:1 and stirred for 24 hours before use.

2.2.2.4 Preparation of activated carbon (AC) electrode

Stainless steel mesh (SSM, #304 with a mesh size of 500) was used as current collector of the electrode with average size of 1.13 cm^2 and weight of 28.7 mg. The abovementioned slurry was coated onto SSM as AC electrode by controlling its loading between 1.3~1.8 mg cm^{-2} and drying under infrared light radiation till completely solidified.

2.2.2.5 Assembly of Zn//AC supercapacitor based on aqueous electrolyte

CR2032-type coin cell Zn//AC supercapacitor was assembled by using AC electrode as working electrode, Zn plate as reference/counter electrode and glassy fiber membrane (Whatman Grade A) as separator and 2 M $ZnSO_4$ as aqueous electrolyte.

2.2.2.6 Assembly of Zn//AC supercapacitor based on PAM hydrogel electrolytes

The assembly of CR2032-type coin cell Zn//AC supercapacitor based on series of PAM hydrogels was directly putting PAM hydrogel electrolyte sample between AC electrode (working electrode) and Zn plate (reference/counter electrode) without adding separator nor aqueous electrolyte.

2.2.2.7 Electrochemical test

Electrochemical test including galvanostatic charging/discharging (GCD), rate capacity and cycling performance were tested using Neware battery cycler system. For all the above tests, the applied voltages were 0.15 V-1.8 V.

2.2.2.8 Materials characterization

The surface morphology of PAM samples via two different synthesis methods and different ratio of monomer and crosslinker were examined on the field-emission scanning electron microscope (Zeiss Sigma FESEM). To confirm the successful synthesis of PAM, Fourier transform infrared spectra (FTIR) were tested on ATR

mode with the range of wavenumber from 400-4000 cm^{-1}. All hydrogel samples were freeze-dried before the above tests.

2.2.2.9 Statistical methods

To address the statistical reliability, average values (denoted as A) and standard deviation values (denoted as S) of particular parameters were provided by the following equations among 3 or more repeated samples:

$$A = \frac{1}{n}\sum_{i=1}^{n} x_i = \frac{1}{n}(x_1 + \cdots + x_n)$$

$$S = \sqrt{\frac{1}{n}\sum_{i-1}^{n}(x_i - A)^2}$$

where $\{x_1, x_2, \cdots, x_n\}$ are the observed values of the sample items, and A is the average value of these observations, while the denominator n stands for the size of the sample.

For the reported format of capacities, take 118 ± 2 mAh g^{-1} as an example, where 118 refers to the average value A, and error 2 refers to the 2 standard deviation S, which have been rounded without decimal digits.

2.2.3 Results and discussion
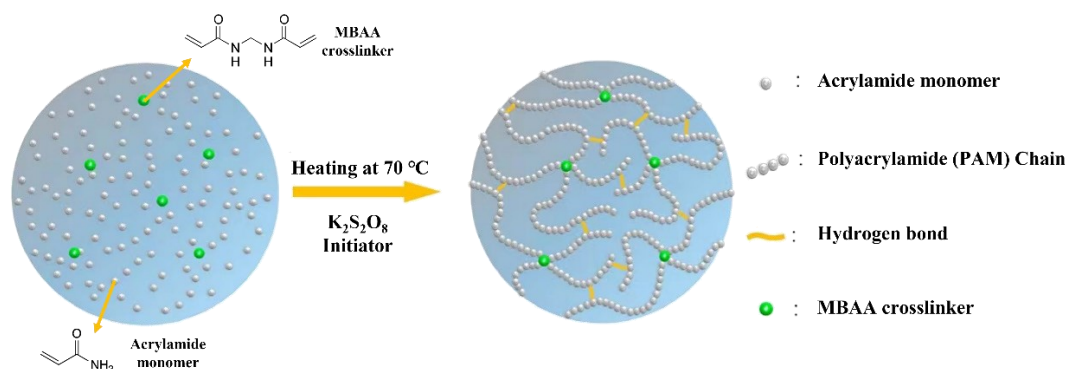
Scheme 2. Formation of chemically crosslinked PAM hydrogel. Reproduced with permission.[77] Copyright 2018, American Chemical Society.

Scheme 2 shows the making of PAM hydrogel. Chemically crosslinked network of PAM was constructed via free radical polymerization between acrylamide monomers and MBAA crosslinker in the presence of an initiator. The polymerization process was carried out at 70 °C and degassed in the vacuum oven. Of note, the default PAM indicates the PAM synthesized directly in 2 M $ZnSO_4$, while PAM-soaking denotes the making of PAM first followed by soaking in 2 M $ZnSO_4$.

Possessing abundant $-NH_2$ group with polar and hydrophilic features in the polymer chain, PAM samples exhibited high water absorbency, guaranteeing its ionic conductivity. Additionally, abundant hydrogen bonds were formed among amino groups, further strengthening the mechanical durability of PAM samples. After soaking in 2 M $ZnSO_4$ solution, the PAM-soaking hydrogels became soft and can be intimately attached with electrodes, acting as reliable quasi-solid electrolyte without the need of separator, while the PAM sample without the soaking process was much harder and stronger but with less water contained.
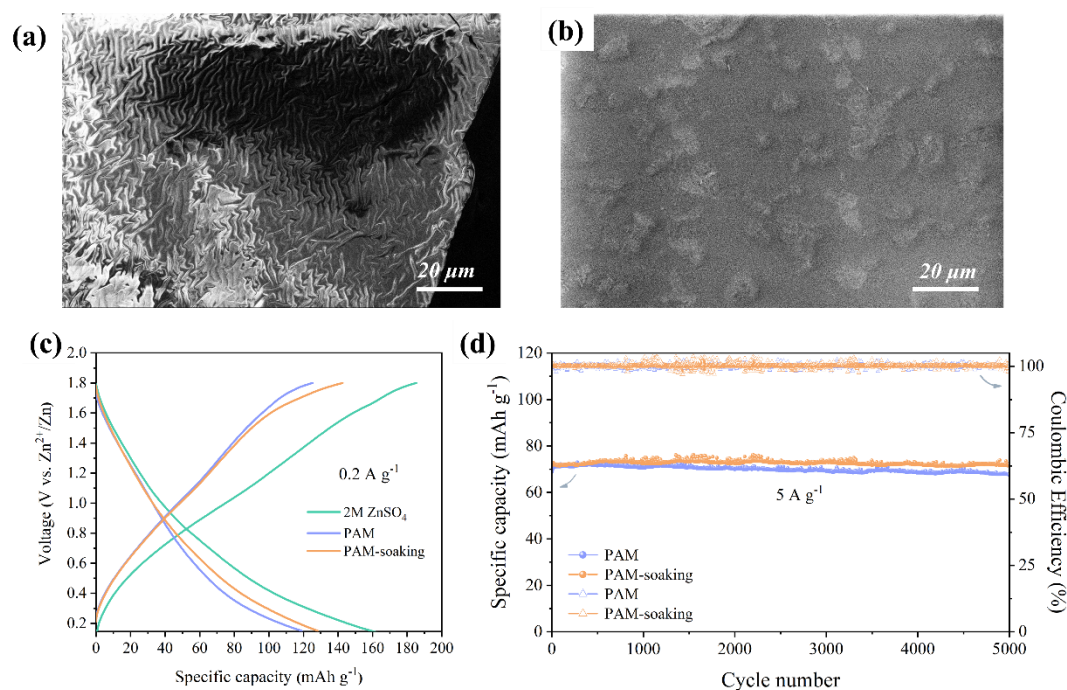
Figure 14. SEM images of a) PAM-soaking hydrogel and b) pure PAM polymerized in 2 M ZnSO₄ solution. Electrochemical performance of Zn//AC supercapacitor based on different electrolytes. c) Charge-discharge curve of supercapacitors based on PAM and PAM-soaking hydrogel electrolyte as well as aqueous 2 M ZnSO₄ electrolyte at a current density of 0.2 A g⁻¹. d) Cycling performance of supercapacitor based on PAM and PAM-soaking hydrogel electrolytes at 5.0 A g⁻¹.

Microstructure morphology investigation of PAM and PAM-soaking were carried out by FESEM and both samples were freeze-dried before test. The SEM image of PAM-soaking hydrogel (**Figure 14a**) showed its surface morphology is evenly distributed with wrinkled patterns, which is favorable for uniform transfer and deposition of Zn ions. The formation of wrinkled patterns should be the result of rapid water loss and network shrinkage during the freeze-drying process, further suggesting the water retentivity of PAM-soaking sample was good. For comparison, the SEM image of PAM (**Figure 14b**) was highly dense and smooth without wrinkles, reflecting its poor water-holding capacity.

Next, to evaluate the electrochemical performance of hydrogels, coin-cell ZICs based

on two PAM hydrogels were fabricated. As shown in **Figure 14c**, at a current density of 0.2 A g^{-1}, the specific capacity of PAM-based ZIC was 118 ± 2 mAh g^{-1}, which is lower than the value of 127 ± 2 mAh g^{-1} in PAM-soaking electrolyte-based ZIC. Cycling tests (**Figure 14d**) show that both PAM samples ran stably for over 5000 cycles, with capacity retention of 98.3 % (PAM) and 100.4 % (PAM-soaking) at 5.0 A g^{-1}, respectively. As such, the advantage of PAM hydrogel as electrolyte to protect Zn metal anodes from side reactions and dendrites from inhomogeneous ion transfer and excessive water solution was confirmed, which can be ascribed to its uniform structure, intimate electrode-electrolyte contact due to the intrinsic mechanical elasticity and adhesion property of PAM hydrogels. Moreover, PAM-soaking electrolyte showed higher capacity than PAM electrolyte due to its better adhesion and interfacial stability caused by higher water content after soaking. However, compared with traditional 2 M ZnSO$_4$ aqueous electrolyte with a higher capacity value of 160 ± 1 mAh g^{-1}, both PAM hydrogel electrolytes await further improvement.

2.2.4 Conclusion

Based on above experimental results and analysis, firstly, from SEM images, the highly wrinkled surface of PAM-samples synthesized with soaking method was confirmed, while the PAM directly polymerized in ZnSO$_4$ solution only showed dense and smooth structure unfavorable for ion transfer. In the following electrochemical tests, both PAM samples showed decent cycling stability, confirming the utilization of PAM hydrogel electrolyte can guarantee a long cycle life. Moreover, PAM with soaking method stands out for its better electrochemical performance, suggesting the crucial role of water contained in hydrogel network. However, the capacity of ZICs based on both single-network PAM hydrogels was still lower than that based on aqueous electrolyte, due probably to its large resistance from thick hydrogel film and low ionic conductivity. Thus, further modification on its intrinsic structure is still urgently needed.

2.3 Double-network PAM hydrogel

2.3.1 Introduction

Compared to single-network hydrogels, double-network (DN) hydrogels combine benefits of both its parent hydrogel, thus can achieve ionic conductivity and mechanical strength at the same time. Therefore, herein, to further enhance the electrochemical performance of hydrogel-based ZICs, a DN Zn-Alginate/PAM was introduced, and the corresponding soft-packaged ZIC pouch cell was assembled.

(a)

(b)
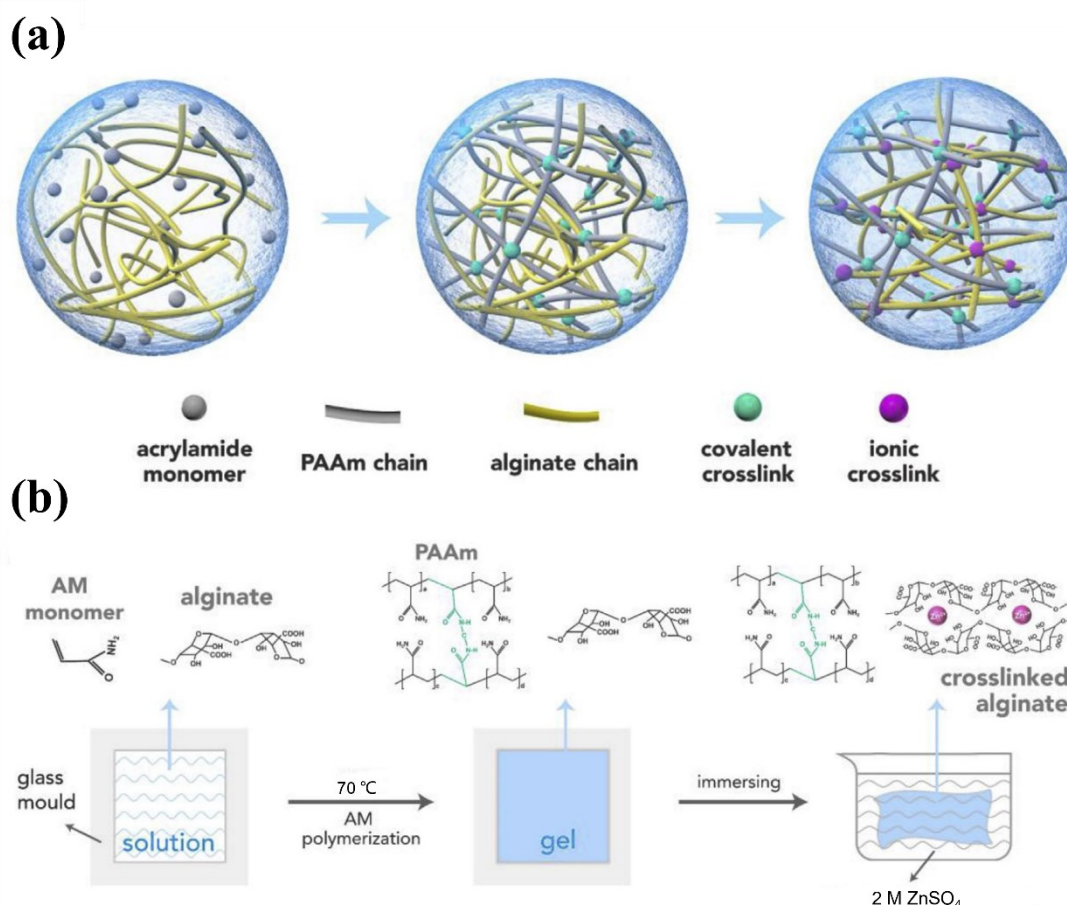
Scheme 3. a) Schematic showing the evolution of hydrogel structure. Grey lines and yellow lines represent PAM chains and alginate chains, respectively. Cyan and rosy dots represent covalent crosslinks and ionic crosslinks, respectively. b) Illustration of

the synthetic process of the double-crosslinked hydrogel electrolyte. Reproduced with permission.[85] Copyright 2019, Elsevier.

As **Scheme 3** demonstrated, there are two types of hydrogel network in DN Zn-Alginate/PAM hydrogel, in which the irreversible covalently crosslinked PAM network was firstly generated via free radical polymerization, as mentioned in the above section. On the other hand, alginate is a naturally abundant hydrophilic polysaccharide containing β-D-mannuronic acid and α-Lguluronic acid, in which the later part forms classical "egg-box" structure through ionic interaction with metal ions (eg. Ca^{2+}, Zn^{2+}, etc.), and thus the corresponding physically crosslinked metal-ion alginate hydrogel network was fabricated.[164, 165] During the formation of DN Zn-Alginate/PAM hydrogel, the first PAM network loosely interconnected with soft and formless bulk appearance. After soaking in 2 M $ZnSO_4$ solution, the alginate segments containing carboxylic acid groups cross-linked with zinc ions, forming ionically crosslinked network with dense and rigid nature. Consequently, the double-crosslinked interpenetrating polymer network of Zn-Alginate/PAM hydrogel was constructed with much improved mechanical property and ionic conductivity.[165]

SEM results show the highly uniform morphology of the above hydrogel, while its ionic conductivity of 0.22 mS cm^{-1} was then calculated from the EIS curve. FTIR characterizations confirmed the structure of Zn-Alginate/PAM hydrogel. Water content of the above hydrogel sample was determined by the weights before and after soaking in related zinc salt solutions. To evaluate its intrinsic flexibility and mechanical endurance, bending, folding, twisting and stretching test towards the as-prepared hydrogel sample were also carried out. During electrochemical tests, the involved ZIC exhibited comparable cycling stability, but much better electrochemical performance compared to single-network PAM electrolytes mentioned in the former section. Finally, the soft-package ZIC pouch cell was then assembled and showed only negligible capacity loss under different bending angles, suggesting its flexibility thanks to the use of the Zn-Alginate/PAM hydrogel electrolyte. For clarification, pure PAM sample soaked in 2 M $ZnSO_4$ solution was denoted as PAM-2M $ZnSO_4$, and the

prepared Zn-Alginate/PAM sample was denoted as Zn-Alg/PAM-2M ZnSO$_4$.

2.3.2 Experimental Section

2.3.2.1 Materials and reagents

Reagents name	Manufacturer	Purity
Commercial activated carbon (AC, TF-B520)	MTI corporation	analytical grade
Acrylamide (AM)	Sigma-Aldrich	analytical grade
N, N'-methylenebisacrylamide (MBAA)	Sigma-Aldrich	analytical grade
Ammonium persulfate (APS)	Thermo Fisher Scientific	analytical grade
Commercial activated carbon (AC, TF-B520)	MTI corporation	analytical grade
Sodium alginate (SA)	Sigma-Aldrich	analytical grade
Zinc sulfate heptahydrate (ZnSO$_4$·7H$_2$O)	Sigma-Aldrich	analytical grade

All chemicals were used without further purification.

The technical parameters commercial activated carbon (AC, TF-B520) have been provided in **2.2.2.1**.

2.3.2.2 Preparation of Zn-Alginate/PAM hydrogel electrolyte

The synthetic procedure is based on a published paper.[85] Typically, 1.45 g AM monomer, 0.88 mg MBAA crosslinker and 7.15 mg APS initiator were added to 10 mL DI water subsequently under stirring. Till the above solution became transparent, 0.18 g SA power was added under strong stirring for complete dissolution and uniform dispersion. Thereafter, the mixed solution was ultrasonicated for 20 min, and the resulting light-yellow solution with high fluidity was obtained for storage and further polymerization. To gain the Alginate/PAM hydrogel film, the former solution was injected into a glass Petri dish and then moved to the vacuum oven at 70 °C for 30 min to allow both degassing and polymerization, thus the first covalent chemical-network of PAM was formed. To generate Zn-Alginate/PAM containing the second

noncovalent ionic network among alginate and zinc ions, the as prepared Alginate/PAM hydrogel film was soaked in 3 mL 2 M ZnSO$_4$ solution for 1 hour. Therefore, the Zn-Alginate/PAM hydrogel film was successfully synthesized. For comparison, pure PAM containing 2 M ZnSO$_4$ based on APS initiator was prepared following the same steps without adding SA.

The preparation of activated carbon (AC) slurry, preparation of activated carbon (AC) electrode, assembly of aqueous coin cell Zn//AC supercapacitor and assembly of coin cell Zn//AC supercapacitor based on Zn-Alginate/PAM hydrogel was the same as previous sections (**2.2.2.3**, **2.2.2.4**, **2.2.2.5**, **2.2.2.6)**, except replacing pure PAM to Zn-Alginate PAM hydrogel.

2.3.2.3 Assembly of soft-packaged Zn//AC hybrid supercapacitor pouch cell based on Zn-Alginate/PAM hydrogel

Soft-packaged Zn//AC hybrid supercapacitor pouch cell was fabricated by sandwiching the Zn-alginate/PAM hydrogel electrolyte between zinc foil and AC electrode and sealed in an Al-plastic package under vacuum treatment. Specifically, the ultrathin Zn foil with thickness of 30 μm was applied as reference/counter electrode, while AC coated on SSM with mass loading of 1.8-2.0 mg cm^{-2} acting as working electrode. In the meanwhile, the hydrogel electrolyte, Zn foil and AC electrodes were all tailored into 24 mm × 36 mm rectangle shape for pouch cell fabrication, and the protrude electrode outside of the Al-plastic bag were wrapped with Cu foil tape for guaranteed electrical conductivity.

2.3.2.4 Electrochemical test

Electrochemical test including galvanostatic charging/discharging (GCD), rate capacity and cycling performance were tested using Neware battery cycler system with applied voltages from 0.15 V - 1.8 V, while cyclic voltammogram curve and electrochemical impedance spectroscopy (EIS) were performed on the electrochemical workstation (VMP-3, Biologic) with frequency range of 0.01 - 10^5 Hz

and magnitude of 5.0 mV at open circuit voltage based on coin cell Zn//AC supercapacitor with Zn-Alginate/PAM hydrogel electrolyte. For linear sweep voltammetry (LSV) test, stainless-steel foil and Zn foil were respectively applied as working electrode and counter/reference electrode at scan rate of 1.0 mV s^{-1} with voltage range from -0.3 V to 2.8 V.

2.3.2.5 Materials characterization

For characterizations toward both the as-prepared Zn-Alginate/PAM hydrogel and activated carbon samples, field-emission scanning electron microscope (Zeiss Sigma FESEM) was applied to characterize their surface micro morphologies. To confirm the successful synthesis of PAM, Fourier transform infrared spectra (FTIR) were tested on ATR mode with the range of wavenumber from 650 - 4000 cm^{-1}. For the flexibility test, the assembled Zn-Alginate/PAM hydrogel film was cut into 3 cm × 1 cm bar followed by stretching, bending, twisting and folding treatment.

2.3.2.6 Calculation of ionic conductivity

Derived from electrochemical impedance spectra curve, the ionic conductivity σ (mS cm^{-1}) can be calculated with the following equation:

$$\sigma = L/(R_b \times S) \times 1000$$

In which L (cm) is the thickness of the hydrogel electrolyte, R_b (Ω) is the bulk resistance (intercept at Z' axis of EIS curve), and S is the contact area (cm^2) between hydrogel electrolyte and electrode.

2.3.2.7 Calculation of mass ratio of water absorbency for hydrogel sample.

For evaluating its water absorbency ability, the empty glass Petri dish (W_0), glass Petri

dish containing as-prepared Zn-Alginate/PAM hydrogel (W_1) and glass Petri dish containing as-prepared Zn-Alginate/PAM hydrogel after soaking in 3 mL 2M ZnSO$_4$ solution for 1 h (W_s) were weighted consecutively. The mass ratio of water absorbency (R_{ab}) was calculated based on the following equation:

$$R_{ab} = \frac{(W_s - W_{gel}) \times 100\%}{W_{gel}} = \frac{[W_s - (W_1 - W_0)] \times 100\%}{(W_1 - W_0)}$$

Where R_{ab} is the water absorbency ratio, W_s is the weight of the hydrogel sample after soaking in 3 mL 2 M ZnSO$_4$ solution for 1 h, W_{gel} is the weight of the as prepared hydrogel without soaking in water, which is equal to the weight of Petri dish containing the polymerized hydrogel sample (W_1) minus the weight of empty glassy Petri dish (W_0).

2.3.2.8 Statistical methods

To address the statistical reliability, average values (denoted as A) and standard deviation values (denoted as S) of particular parameters were provided by the following equations among 3 or more repeated samples:

$$A = \frac{1}{n}\sum_{i=1}^{n} x_i = \frac{1}{n}(x_1 + \cdots + x_n)$$

$$S = \sqrt{\frac{1}{n}\sum_{i-1}^{n}(x_i - A)^2}$$

where $\{x_1, x_2, \cdots, x_n\}$ are the observed values of the sample items, and A is the average value of these observations, while the denominator n stands for the size of the sample.

For the reported format of capacities, take 118 ± 2 mAh g^{-1} as an example, where 118 refers to the average value A, and error 2 refers to the 2 standard deviation S, which have been rounded without decimal digits.

2.3.3 Results and discussion

Herein, the photo of the prepared Zn-Alginate/PAM hydrogel was provided in **Figure 15a**. This light-yellow film after soaking in 2 M ZnSO$_4$ was transparent, highly flexible and elastic, which was suitable for assembling flexible pouch cells. Notably, its thickness was comparable to typical glass-fiber separators, and significantly thinner than the former pure PAM hydrogel electrolyte, which may be resulted from the denser and strengthened double-crosslink network of covalent-crosslinked PAM and ionic-crosslinked Zn-Alginate.
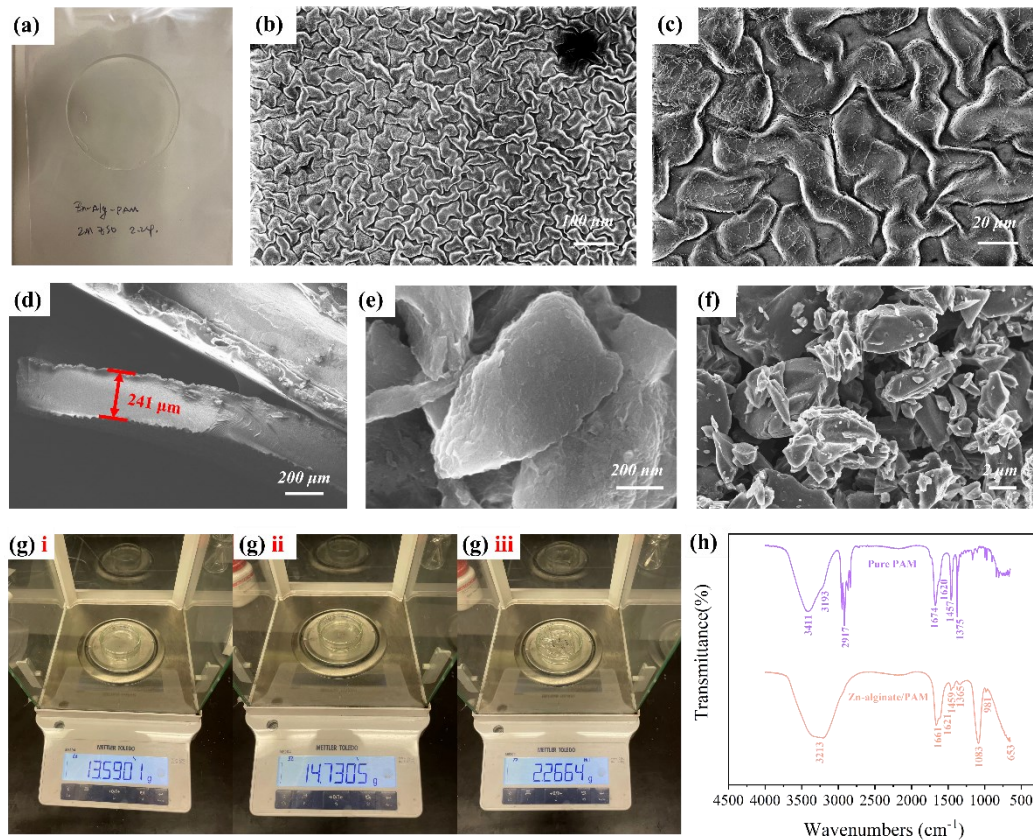
Figure 15. a) Digital photo of as-prepared Zn-Alginate/PAM hydrogel film. b)-c) SEM images of Zn-Alginate/PAM hydrogel film after freeze-drying. d) Cross-section SEM images of Zn-Alginate/PAM hydrogel film after freeze-drying. e)-f) SEM images of AC. g) Water content evaluation toward the above hydrogel electrolyte, including i) weight of empty glass Petri dish, ii) weight of glass Petri dish containing as-prepared Zn-Alginate/PAM hydrogel and iii) glass Petri dish containing as-prepared Zn-Alginate/PAM hydrogel after soaking in 3 mL 2 M $ZnSO_4$ solution for 1h (the weight of the empty Petri dish has been peeled). h) FTIR spectra of the obtained Zn-Alginate/PAM hydrogel.

As shown in **Figure 15b** and **15c**, SEM images reveal the surface morphology of hydrogels, compared to pure PAM hydrogel sample, the prepared Zn-Alginate/PAM hydrogel exhibited a dense, intertwined and homogeneous morphology appeared as distributed wavelike wrinkles with a size of 20 μm. Such highly uniform structure favored its regulated ion transfer and homogeneous zinc stripping/deposition, further guaranteeing electrochemical performance and elongated cycle life. Moreover, the cross-sectiontional SEM image (**Figure 15d**) shows that the thickness of the Zn-Alginate/PAM hydrogel was only 250 μm, which guarantees an improved ionic conductivity, and the dense structure can be a proof of its high mechanical endurance. SEM images of AC electrode (**Figure 15e** and **15f)** showed its bulky structure with size ranging from 1 μm to 20 μm.

To calculate the water content of the abovementioned hydrogel electrolyte, the weights of empty Petri dish and Petri dish loaded with Alginate/PAM hydrogel were measured in **Figure 15g i)- ii)**, and the weight of bare hydrogel was calculated to be 1.14 g. After soaking in 3 mL 2 M $ZnSO_4$ for 1 h (**Figure 15g iii)**, the weight of water content in the hydrogel is measured to be 1.13 g. In other words, the water absorbency ratio (R_{ab}) of the as-prepared Alginate/PAM hydrogel was 98.9 %. The result suggested the decent water content of the prepared hydrogel film from its abundant hydrophilic groups, which acted as the prerequisite for effective ion transport and reasonable ionic conductivity when applied as electrolyte.

The FTIR spectra in **Figure 15h** confirmed the successful synthesis of pure PAM hydrogel and Zn-Alginate/PAM hydrogel. Specifically, in the upper purple spectra of pure PAM sample, the peak at 3412 cm^{-1} was assigned to N-H stretching, while the broad bands at 3200-3500 cm^{-1} was due to O-H stretching. Strong peaks found from 3000-2840 cm^{-1} were attributed to C-H stretching. The peaks at 1674 cm^{-1} and 1620 cm^{-1} were bands of amide I (C=O stretching) and amide II (N-H deformation). The peak at 1457 cm^{-1} was assigned to -CH$_2$- in-plane scissoring and the strong peak at 1375 cm^{-1} was attributed to C-H deformation. The various bands at around 1250-1020 cm^{-1} were related to C-N stretching. After introducing Zn-Alginate network, as displayed in the bottom pink spectra, besides peaks belonging to PAM, the broad bands around 3213 cm^{-1} indicated N$\cdots$H stretching within intermolecular HN$\cdots$HO bonds generated among lone pair electrons on the -N atom of PAM and the -H atom of alginate, effectively suggesting the successful formation of Zn-Alginate/PAM double crosslink network. Moreover, the extra strong peak around 1083 cm^{-1} was attributed to SO$_4^{2-}$ triply degenerate vibrations and SO$_4^{2-}$ triply degenerate symmetric stretching mode due to the absorbance of ZnSO$_4$ solution. The peak at 981 cm^{-1} was generated form SO$_4^{2-}$ non-degenerate mode, and strong and broad peaks around 750-650 cm^{-1} were resulted from O-H out-of-plane deformation of adding alginate.[85, 164, 166]
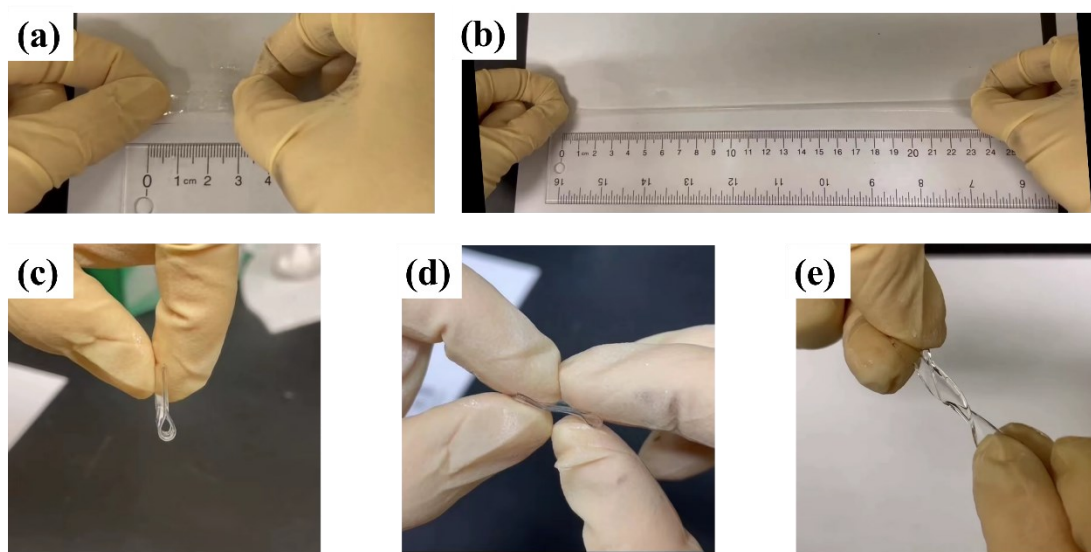
Figure 16. External force treatment including a) Original and b) stretched state of the as-prepared Zn-Alginate/PAM hydrogel film, showing good stretchability of 770 % strain. c) bending, d) folding and e) twisting test to confirm its intrinsic flexibility.

Thereafter, several mechanical tests were carried out to confirm its intrinsic flexibility and mechanical endurance. From Figure **16a** to **16b**, the as-prepared Zn-Alginate/PAM hydrogel bar with original length of 3 cm was stretched to 23 cm without fracture, exhibiting excellent elasticity of 770 % strain. From Figure **16c** to **16e**, the same hydrogel bar can be freely bent, fold and twist without any injury, and can be recovered after those above outer force treatments, showing satisfied mechanical endurance for applied as quasi-solid electrolyte.
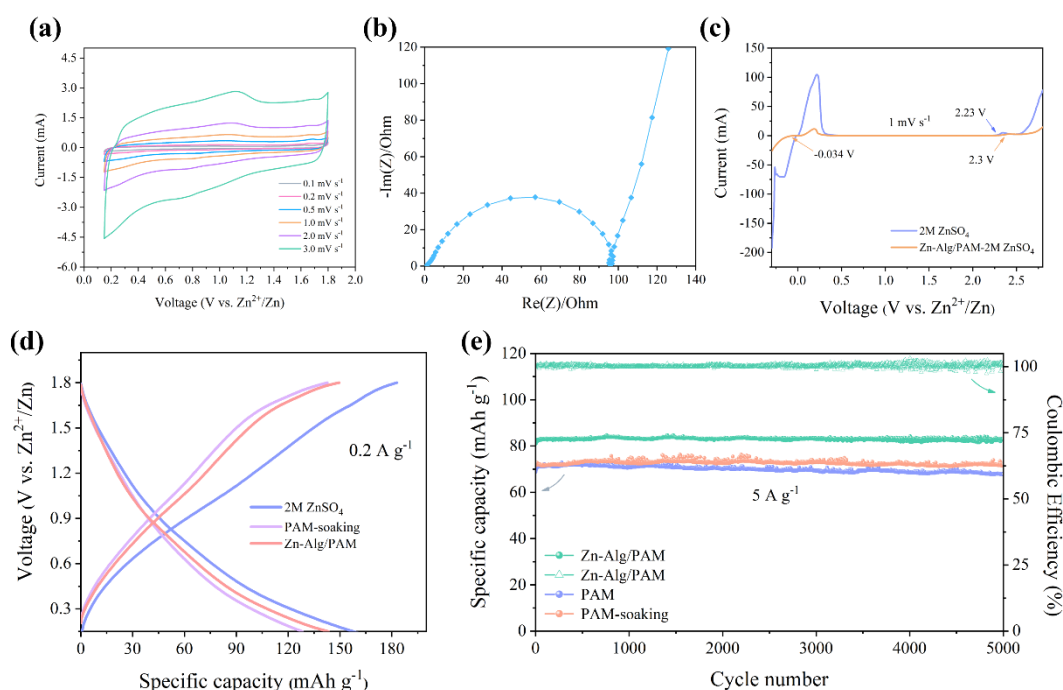
**Figure 17.** a) CV curves of Zn//AC supercapacitor based on 2 M ZnSO$_4$ aqueous electrolyte at scan rates from 0.1 mV s^{-1} to 5.0 mV s^{-1}. Electrochemical tests for coin cell Zn//AC supercapacitor based on Zn-Alginate/PAM hydrogel, including b) Electrochemical impedance spectra of as-prepared Zn-Alginate/PAM hydrogel containing 2 M ZnSO$_4$. c) Comparison of linear sweep voltammetry curve between

aqueous 2 M ZnSO$_4$ electrolyte and Zn-Alginate/PAM hydrogel containing 2 M ZnSO$_4$ at scan rate of 1.0 mV s^{-1}. d) Specific capacity comparison among ZIC with 2 M ZnSO$_4$ aqueous electrolyte, pure PAM hydrogel electrolyte and Zn-Alginate/PAM hydrogel electrolyte, at current density of 0.2 A g^{-1}. e) cycling performance comparison among ZIC Zn-Alginate/PAM hydrogel electrolyte containing 2 M ZnSO$_4$, pure PAM-2 M ZnSO$_4$ hydrogel electrolyte, pure PAM-2 M ZnSO$_4$ hydrogel electrolyte with soaking method, at current density of 5.0 A g^{-1}.

Firstly, in **Figure 17a**, CV curve of the involved AC electrode was presented as attached in Figure with the scan rate from 0.1 to 5.0 mV s^{-1} and voltage range from 0.15 to 1.8 V (vs. Zn^{2+}/Zn), from which the typical O1/R1 and O2/R2 peaks were found at 1.1 V/0.8 V and 1.5 V/1.2 V, suggesting Faradic surface reactions happened on AC electrode surface, a typical presentation of supercapacitor behavior. Electrochemical impedance spectroscopy (EIS) curve was shown **Figure 17b**. Based on the equation provided in experimental section, the ionic conductivity was calculated to be 0.22 mS cm^{-1}, which can be attributed to its densely double-crosslinked structure and limited water taken amount. Such decreased ionic conductivity compared to aqueous electrolyte can indicate the sacrificed capacity when applied hydrogel electrolyte. To quantify the working voltage window of Zn-Alginate/PAM-2 M ZnSO$_4$ hydrogel electrolyte, linear sweep voltammetry (LSV) curves were performed from -0.3 V to 2.8 V at 1 mV s^{-1}, with comparison of aqueous 2 M ZnSO$_4$ electrolyte. As shown in **Figure 17c**, when applied Zn-alginate/PAM-2 M ZnSO$_4$ hydrogel electrolyte, Zn plating and oxygen evolution reactions were found at -0.034 V and ~ 2.3 V respectively, which exhibited a wider voltage window of ~ 2.334 V as aqueous 2 M ZnSO$_4$ electrolyte (~ 2.23 V), and it was wide enough to assemble with AC electrode for ZIC fabrication. The decreased current and wider voltage window may be due to the increased resistance of hydrogel matrix, stabilized water molecules and zinc ions by hydrogen bonding with polymer chains and ionic interactions with alginate chains, respectively.

To address the improved capacity of Zn-Alginate/PAM hydrogel electrolyte than pure

PAM hydrogel, as **Figure 17d** demonstrates, at current density of 0.2 A g^{-1}, although the capacity of both of them were still lower than supercapacitor with 2 M ZnSO$_4$ aqueous solution (with specific capacity of 175 mAh g^{-1}), Zn-Alginate/PAM hydrogel electrolyte performance better than the pure PAM hydrogel with specific capacity of 141 ± 4 mAh g^{-1} compared to 127 ± 2 mAh g^{-1}, due to its lower thickness and resulted higher ionic conductivity. Moreover, in **Figure 17e**, at 5.0 A g^{-1}, the Zn-Alginate/PAM hydrogel electrolyte based ZIC showed much higher specific capacity of 83 mAh g^{-1} as pure PAM hydrogel electrolyte, and excellent cyclability with 100.3 % capacity retention after 5000 cycles was also achieved with almost 100 % Coulombic Efficiency, suggesting its improved ionic conductivity with reduced thickness, confirming the feasibility for the prepared Zn-Alginate/PAM hydrogel electrolyte utilized in ZIC operated in high current density and long cycling life.
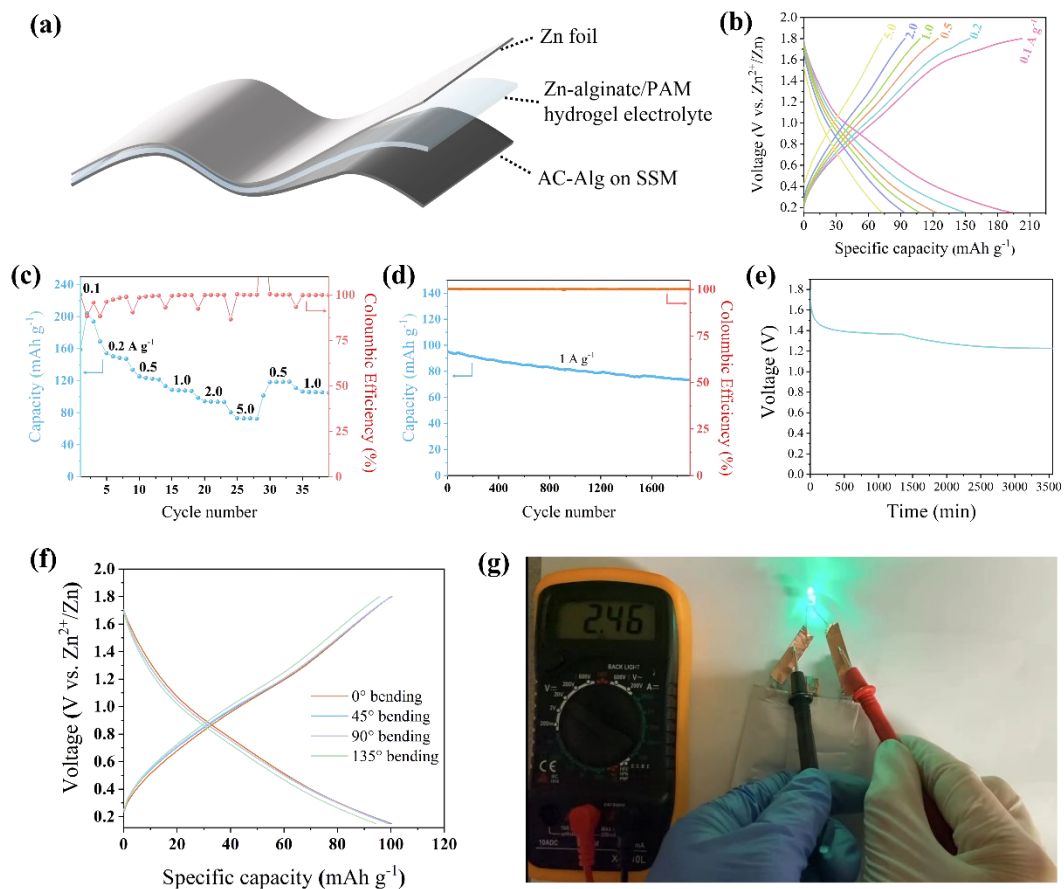
Figure 18. a) Schematic illustration of soft-packaged Zn//AC hybrid supercapacitor

pouch cell based on Zn-Alginate/PAM hydrogel. Electrochemical results of Zn//AC hybrid supercapacitor pouch cell based on Zn-Alginate/PAM hydrogel: b) galvanostatic discharge and charge curves at current density of 0.1, 0.2, 0.5, 1.0, 2.0, 5.0 A g^{-1}, c) rate performance, and d) cycling performance at 1.0 A g^{-1}. e) Open-circuit voltage change with time. f) galvanostatic discharge and charge curves under different bending angles from 0° to 135° at 1.0 A g^{-1}. g) Digital photo of one cyan LED powered by two series of ZIC pouch cell.

As **Figure 18a** demonstrated, by sandwiching the prepared Zn-Alginate/PAM hydrogel foil between Zn foil and AC coated SSM followed by sealed in aluminum plastic bag, the flexible soft-packaged Zn//AC hybrid supercapacitor pouch cell was assembled. From **Figure 18b** and **18c**, the pouch cell showed high specific capacity of 193 ± 2 mAh g^{-1} at 0.1 A g^{-1}, and 150 mAh g^{-1}, 124 mAh g^{-1}, 108 mAh g^{-1}, 94 mAh g^{-1}, 73 mAh g^{-1} at 0.2 A g^{-1}, 0.5 A g^{-1}, 1.0 A g^{-1}, 2.0 A g^{-1}, 5.0 A g^{-1}, respectively. Its specific capacity recovered to 106 mAh g^{-1} when current density changed from 5.0 A g^{-1} to 1.0 A g^{-1}. For the cycling test in **Figure 18d,** after 1900 cycles, the pouch cell retained 77.0 % of its specific capacity at current density of 1.0 A g^{-1} with almost 100 % Coulombic efficiency unchanged. Moreover, after resting for 3556 min, 68.6 % open-circuit voltage was preserved (**Figure 18e**), exhibiting a low self-discharge rate of 9.45 mV h^{-1} (0.53 % h^{-1}), which indicated reasonable stability of the hydrogel contained Zn//AC hybrid supercapacitor. For the flexibility test in **Figure 18f**, there was no obvious capacity decay with the pouch cell being bent at 45° and 90°, while only 5.8 % capacity loss was found at bending angle of 135°, suggesting the equipment of flexible hydrogel electrolyte can endow the Zn//AC hybrid supercapacitor with reliable flexibility and potential wearability. Furthermore, in **Figure 18g**, a LED bulb with cyan light can be enlightened by the prepared Zn//AC pouch cell in two series, so the pouch cell possessed great potential in flexible and portable energy storage devices.

2.3.4 Conclusion

To summarize, in Chapter 2, a series of simple comparison experiments between two synthesis methods toward PAM hydrogel synthesis were carried out to figure out a better synthesis way for hydrogel electrolytes preparation and were regarded as optimization for further hydrogel electrolyte developments. For the electrochemical results, firstly, ZIC equipped with all hydrogel electrolyte samples exhibited excellent cycling life at high current densities, confirming those PAM-based hydrogels were suitable electrolyte candidates for assembling high-performance ZICs. Moreover, compared to the PAM hydrogel directly polymerized in 2 M $ZnSO_4$ solution, the PAM-soaking sample prepared with method of preparing the pure PAM first and soaking it in 2 M $ZnSO_4$ solution showed both better capacity (128 mAh g^{-1} at 0.2 A g^{-1}) and cyclability (100.4% capacity retention after 5000 cycles at 5.0 A g^{-1}) when assembled in ZIC coin cell, showing the superiority of choosing soaking method in further hydrogel electrolyte preparation. However, the capacity of ZIC with pure PAM hydrogel electrolytes still not reach the expectation, mainly due to their large thickness and resulted low ionic conductivity.

Based on this demand, a double-network Zn-Alginate/PAM hydrogel was developed with chemical-crosslinked PAM network and ionic-crosslinked Zn-Alginate network, showing a highly dense pattern and homogeneous structure from two tightly intertwined networks and thickness of 241.0 μm, which was even thinner than glassy fiber membrane separator (260.0 nm). The FTIR spectra further supported the successful synthesis of Zn-Alginate/PAM double crosslink network, and reasonable intrinsic flexibility of withstanding 770 % stretching stress and freely recovering under outer deformations were further achieved. Based on high water storage of 98.9 % of its own original weight, the involved ZIC also reached reasonable ionic conductivity (0.22 mS cm^{-1}), suitable operation voltage window as electrolyte for ZICs, together with improved electrochemical results compared to former pure PAM hydrogel electrolytes. Then, a soft-packaged Zn//AC hybrid supercapacitor pouch cell based on Zn-Alginate/PAM hydrogel was fabricated with high specific capacity of

194 mAh g^{-1} at 0.1 A g^{-1}, 77.0 % capacity retention after 1900 cycles at 1.0 A g^{-1}, low self-discharge rate of 9.45 mV h^{-1} and excellent flexibility of only 5.8 % capacity decay under 135° bending, which were brought by the excellent intrinsic flexibility of the double crosslinked Zn-Alginate/PAM hydrogel electrolyte. Together with successfully enlightening LED bulbs, the hydrogel based ZIC holds bright potential in future application in long-cycling, flexible and wearable energy storage devices, and the involved paper has been published in 2022.[126]

Chapter 3. Zn-Alginate/PAM Hydrogel Electrolyte for Rocking-chair Zinc-ion Batteries

3.1 Introduction

Zn metal anodes suffer from dendritic growth and side reactions in aqueous electrolyte. Despite the progress on host construction, electrolyte engineering, and electrode-electrolyte interface regulation, it remains challenging to achieve dendrite-free and highly reversible Zn anodes. An alternative strategy is the development of Zn-free anode and the construction of rocking-chair type ZIBs following zinc ions (de)intercalation into the anode rather than the Zn metal plating/stripping mechanism. Among all potential anode materials, molybdenum-based materials have gained much attention due to their low discharge potential vs. Zn^{2+}/Zn, rich redox sites, high capacities, reliable layered or tunnel structure, which result from various valence of Mo and stable octahedral structures generated between Mo and oxygen.[167, 168] Till now, MoS_2, MoO_3 and Mo_6S_8 with a variety of structures has been reported as promising electrodes for ZIBs.

Among them, hexagonal molybdenum oxide (h-MoO_3) was reported to be a promising zinc-free anode because its hexagonal tunnel structure can be easily lubricated by H_2O in aqueous batteries, and this hexagonal structure possessed better mechanical stability than the traditional double-layer structure. Moreover, based on the existence of mobile ions and H_2O molecules, highly effective charge storage mechanisms within h-MoO_3 can be achieved by main (de)intercalation of Zn^{2+} and H_2O, some extent of (de)intercalation of SO_4^{2-}.[168-170] However, the cycling stability of h-MoO_3 still awaits further improvement..

As such, in this chapter, we aim to apply h-MoO_3 as the zinc-free anode for rocking-chair type ZIBs and pair it with hydrogel electrolytes to improve its cycling stability. The resultant h-MoO_3 exhibited low redox peaks at 0.21 V/0.43 V and high specific capacity of 128 mAh g^{-1} at 0.1 A g^{-1}. When this anode was coupled with

ZnMn$_2$O$_4$/Carbon (ZMC) composite cathode, it showed a capacity of 107 mAh g^{-1} at 0.1 A g^{-1} in the full cell. As expected, in aqueous electrolyte, this h-MoO$_3$ anode exhibited short cycle life of only 150 cycles in the half cell and 43 cycles in the full cell, which certainly cannot meet the needs of practical applications. After applying the hydrogel electrolyte (Zn-Alginate/PAM containing 3M ZnSO$_4$), greatly improved cycling performances of Zn//h-MoO$_3$ half-cell (63.6 % after 220 cycles) and h-MoO$_3$//ZMC full cell (91.2 % after 200 cycles) were achieved. Simultaneously, capacities of 129 mAh g^{-1} and 102 mAh g^{-1} were observed in both half-cell and full-cell, comparable with those capacities based on aqueous electrolytes. The results further confirmed the advantage of hydrogel electrolytes for elongating cycle life in rocking-chair type ZIBs.

3.2 Experimental Section

3.2.1 Materials and methods

Reagents	Manufacturer	Purity
Ammonium molybdate (VI) tetrahydrate	Fisher Scientific Acros	analytical grade
Ammonium sulfate	Fisher Scientific Acros	analytical grade
Sulfuric acid	Ricca Chemical Company	analytical grade
Sodium alginate (SA)	Sigma-Aldrich	analytical grade
Acrylamide (AM)	Sigma-Aldrich	analytical grade
N, N'-methylenebisacrylamide (MBAA)	Sigma-Aldrich	analytical grade
Ammonium persulfate (APS)	Thermo Fisher Scientific	analytical grade
Zinc sulfate heptahydrate	Sigma-Aldrich	analytical grade
Manganese (II) nitrate tetrahydrate	Sigma-Aldrich	analytical grade
Zinc (II) nitrate hexahydrate	Thermo Fisher Scientific	analytical grade

3.2.2 Preparation of h-MoO$_3$

The synthesis of h-MoO$_3$ was based on a previously reported paper.[171] Typically, 1.35 g of (NH$_4$)$_6$Mo$_7$O$_{24}$·4H$_2$O was firstly dissolved in 50 mL of DI water, followed by the addition of 3 M H$_2$SO$_4$ till pH=1. Then, 1 g of (NH$_4$)$_2$SO$_4$ was added to the above solution under stirring. Later, the solution was transferred to a 100 mL Teflon-lined autoclave and the hydrothermal reaction was conducted at 120 °C for 24 hours. Next, the resulting product was collected by vacuum filtration, washed by DI water and ethanol for several times, and dried in the vacuum oven at 70 °C for 24 hours.

3.2.3 Preparation of ZnMn$_2$O$_4$/Carbon (ZMO/C) composite

The preparation of ZMO/C composite is based on a previous paper.[172] Typically, 10 mL of 0.2 M Mn(NO$_3$)$_2$·4H$_2$O, 5 mL of 0.2 M Zn(NO$_3$)$_2$·6H$_2$O and 160 mg Super P carbon was mixed in a beaker, followed by the drop addition of 9 mL of 25 wt.% aqueous ammonia solution under stirring in 1 h. Then this mixture was evaporated at 100 °C under stirring and the solid was thermally treated in a tubular furnace at 180 °C for 3 h, leading to the formation of ZMC composite containing 60 wt % spinel and 40 wt % carbon.

3.2.4 Preparation of h-MoO$_3$ and ZMO/C slurry

Firstly, the aqueous sodium alginate (SA) binder was prepared by dissolving sodium alginate (SA) in DI water with a concentration of 10 mg/mL, followed by stirring for 24 hours. Then the h-MoO$_3$ slurry was prepared by mixing h-MoO$_3$ powder, super P and SA binder with a mass ratio of 7:2:1 and stirred for 24 hours. For the making of ZMO/C slurry, the ZMO/C powder was mixed with Super P and 10mg/mL PVDF-NMP (polyvinyl difluoride- N-methyl-2-pyrrolidone) binder in a mass ratio of 7:2:1 and stirred for 24 hours.

3.2.5 Preparation of h-MoO₃, and ZMO/C electrodes

Stainless steel mesh (SSM, #304 with a mesh size of 500 with an average area of 1.13 cm^2 was used as the current collector for electrodes fabrication. The abovementioned slurry was drop coated onto SSM via digital pipette and dried under infrared light radiation in minutes to make h-MoO₃ or ZMO/C electrode. The loading mass of active materials was controlled in the range of 1.3~1.8 mg cm^{-2}

3.2.6 Preparation of Zn-Alginate/PAM hydrogel electrolyte

The preparation procedure was the same as aforementioned section **2.3.2.2.** For comparison, another Zn-Alginate/PAM hydrogel was prepared by soaking hydrogel in 3 M $ZnSO_4$ solution for 1 hour.

3.2.7 Calculation of mass ratio of water absorbency for hydrogel sample

The method of water absorbency mass ratio is the same as mentioned in **2.3.2.7**, excepting replacing 2 M $ZnSO_4$ to 3 M $ZnSO_4$.

3.2.8 Assembly of half cells and full cells using liquid electrolyte

CR2032-type coin cells were assembled for both half-cell and full-cell tests. For half cells, Zn foil was used as the counter/reference electrode and the h-MoO₃ or ZMO/C electrode was applied as the working electrode with glassy fiber membrane (Whatman Grade A) as separator and 100 μL of 3 M $ZnSO_4$ as the aqueous electrolyte. For full cells, h-MoO₃ was used as the anode, ZMO/C was used as the cathode and the N/P ratio of electrode materials was controlled to be 1:1. The electrolyte is 100 μL of 3 M $ZnSO_4$ in water.

3.2.9 Assembly of cells using hydrogel electrolyte

The assembly strategy was the same as mentioned in section **3.2.8**, except that the glassy fiber membrane was replaced by the Zn-Alginate hydrogel electrolyte and no liquid electrolyte was added.

3.2.10 Electrochemical test

Electrochemical tests including galvanostatic charging/discharging (GCD), rate capacity and cycling performance were tested using Neware battery cycler system, while cyclic voltammogram curves were performed on the electrochemical workstation (VMP-3, Biologic). For all the above tests, the applied voltages of Zn//h-MoO_3 half-cell was 0.2-1.0 V, and Zn//$ZnMn_2O_4$ half-cell was 0.8 - 1.9 V. For full cell test, the voltage applied to h-MoO_3//$ZnMn_2O_4$ was set from 0.1 V to 1.8 V. For LSV test, stainless-steel foil and Zn foil were applied as working electrode and counter/reference electrode at scan rate of 1.0 mV s^{-1} with voltage range from -0.3 V to 2.8 V.

3.2.11 Materials characterization

Field-emission scanning electron microscope (Zeiss Sigma FESEM) (Oxford AZtecSynergy) were applied to characterize the microstructure morphologies of samples. X-ray diffraction (XRD) test was conducted on Rigaku XRD Ultima IV X-ray diffractometer with Cu target (wavelength: 1.5406 Å) to characterize the crystal structure of samples.

3.2.12 Statistical methods

To address the statistical reliability, average values (denoted as A) and standard deviation values (denoted as S) of particular parameters were provided by the

following equations among 3 or more repeated samples:

$$A = \frac{1}{n}\sum_{i=1}^{n} x_i = \frac{1}{n}(x_1 + \cdots + x_n)$$

$$S = \sqrt{\frac{1}{n}\sum_{i-1}^{n}(x_i - A)^2}$$

where $\{x_1, x_2, \cdots, x_n\}$ are the observed values of the sample items, and A is the average value of these observations, while the denominator n stands for the size of the sample.

For the reported format of capacities, take 118 ± 2 mAh g^{-1} as an example, where 118 refers to the average value A, and error 2 refers to the 2 standard deviation S, which have been rounded without decimal digits.

3.3 Results and discussion
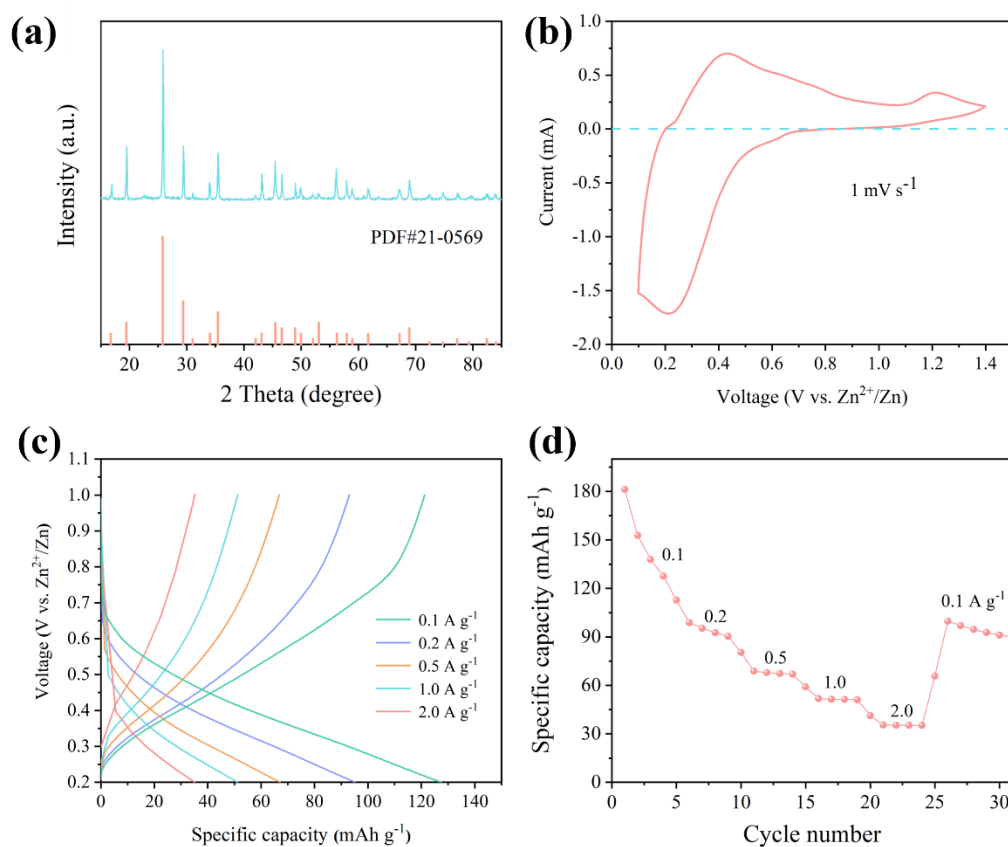
Figure 19. a) XRD pattern of as-prepared h-MoO₃ sample. b) CV curve performed at scan rete of 1 mV s⁻¹ from 0.1 to 1.4 V. Electrochemical test of Zn//h-MoO₃ half-cell. c) Galvanostatic discharge and charge curves and d) rate performance at current density of 0.1, 0.2, 0.5, 1.0, 2.0 A g⁻¹ from 0.2 to 1.0 V.

Firstly, h-MoO₃ was synthesized by a hydrothermal method. Its successful preparation was confirmed by XRD pattern (Figure **19a**), with all peaks belonging to standard h-MoO₃ card (JCPDS no. 21-0569) without impurities. Then, its electrochemical performance was tested in Zn//h-MoO₃ half cells with 100 μL 3 M ZnSO₄ aqueous solution as the electrolyte. CV in **Figure 19b** shows redox peaks at 0.21 V and 0.43 V, suggesting the reduction and oxidization of Mo during charge and discharge process. Moreover, the low redox voltages indicate the potential of h-MoO₃ as anode materials for ZIBs. Next, Zn//h-MoO₃ half cells were tested by the battery cycler with voltage range from 0.2 V to 1.0 V. The galvanostatic discharge and charge curves (**Figure 19c**)

showed redox plateau at 0.21 V/0.43 V, matching well with CV results. The rate performance was displayed in **Figure 19d**, exhibiting high specific capacity of 126 ± 3 mAh g^{-1} at 0.1 A g^{-1}, and 95, 67, 51, 35 mAh g^{-1} at current density of 0.2, 0.5, 1.0, 2.0 A g^{-1}, respectively. It retained 100 mAh g^{-1} when the current density was recovered to 0.1 A g^{-1}. However, its cycling performance was poor, which died after only 152 cycles mainly due to side reactions and dendrite growth. Therefore, investigating solution for its cyclability improvements has become an urgency.
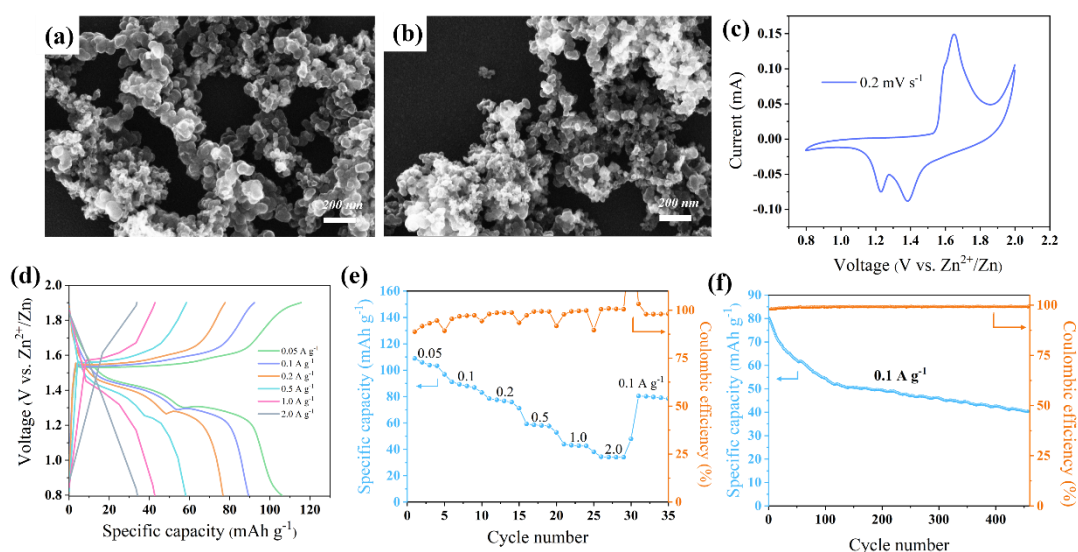
Figure 20. a) – b) SEM images of as-prepared ZnMn$_2$O$_4$/Carbon composite sample. Electrochemical results of assembled Zn//ZMC coin cell, including c) CV curve performed at scan rete of 0.2 mV s^{-1} from 0.8 to 2.0 V, d) galvanostatic discharge and charge curves at current density of 0.05, 0.1, 0.2, 0.5, 1.0, 2.0 A g^{-1} from 0.8 V to 1.9 V, e) rate performance and f) cycling performance at 0.1 A g^{-1}.

To pair with abovementioned h-MoO$_3$ anode and make a full cell, ZnMn$_2$O$_4$/Carbon (denoted as ZMC) composite was chosen as the cathode material. ZMC was prepared based on a reported paper with some modifications and characterized by SEM.[172] SEM images (**Figure 20a** and **20b**) showcase the nanoparticle morphology of the prepared ZMC with an average size of 50 nm. For electrochemical tests, the Zn//ZMC

was assembled with 100 uL 3 M $ZnSO_4$ aqueous electrolyte. The CV curve (**Figure 20c**) shows obvious anodic peaks at 1.58/1.65 V and cathodic peaks at 1.23/1.38 V, suggesting the (de)intercalation of zinc ion (from)into the structure of ZMC. The plateaus in galvanostatic discharge and charge curves corresponds well with the peaks from CV curve (**Figure 20d**). At a current density of 0.05 A g^{-1}, the ZMC shows highest specific capacity of 104 ± 2 mAh g^{-1}, and specific capacify of 89, 77, 58, 43, 34 mAh g^{-1} were found at current density of 0.1, 0.2, 0.5, 1.0, 2.0 A g^{-1}, respectively. When the current density was set back to 0.1 A g^{-1}, the specific capacity of 80 mAh g^{-1} can still be retained, indicating the excellent reversibility of ZMC (**Figure 20e**). **Figure 20f** shows the cycling performance of ZMC with a capacity retention of 51.0 % after 460 cycles at 0.1 A g^{-1}. Above results indicated ZMC is good cathode for pairing with h-MoO_3 to make full cells.
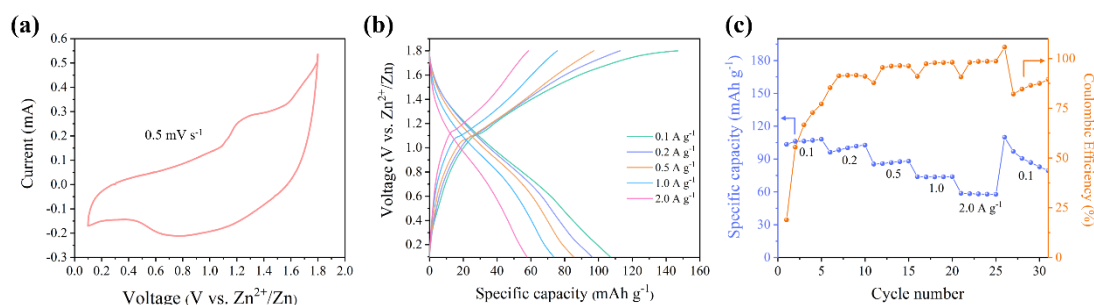
Figure 21. Electrochemical performance of the h-MoO_3//ZMC full cell, including a) CV curve performed at scan rete of 0.5 mV s^{-1} from 0.1 to 1.8 V, b) galvanostatic discharge and charge curves at current density of 0.1, 0.2, 0.5, 1.0, 2.0 A g^{-1} from 0.1 V to 1.8 V, c) rate performance from 0.1 A g^{-1} to 2.0 A g^{-1}.

Following above results, the rocking-chair-type full cell was assembled by using the h-MoO_3 as the zinc-free anode, ZMC as the cathode and 100 μL of 3 M $ZnSO_4$ as the aqueous electrolyte. The N/P ratio was controlled as 1:1. CV curve tested at 0.5 mV s^{-1} was shown in **Figure 21a**, from which the anodic peak at 1.28 V and cathodic peak at 0.79 V were found and indicated reversible redox reactions among Zn ion and

active materials. The plateaus in galvanostatic discharge and charge curves in **Figure 21b** from 0.1 to 1.8 V further confirmed the results in CV curve. From the rate performance shown in Figure **21c**, at 0.1 A g^{-1}, the highest specific capacity was found to be 107 ± 1 mAh g^{-1}, and the specific capacity was 96, 85, 74, 58 mAh g^{-1} at the current density of 0.2, 0.5, 1.0, 2.0 A g^{-1}, respectively. However, the h-MoO$_3$//ZMC full cell stopped working after only 43 cycles at 0.1 A g^{-1}, which may result from severe electrolyte consumption by side reactions, including cathode materials dissolution and formation of insoluble zinc salts with the use of ZnSO$_4$ mild acid solution as aqueous electrolyte. Thus, a solution for mitigating side reactions and enhancing the cycling performance is urgently needed.
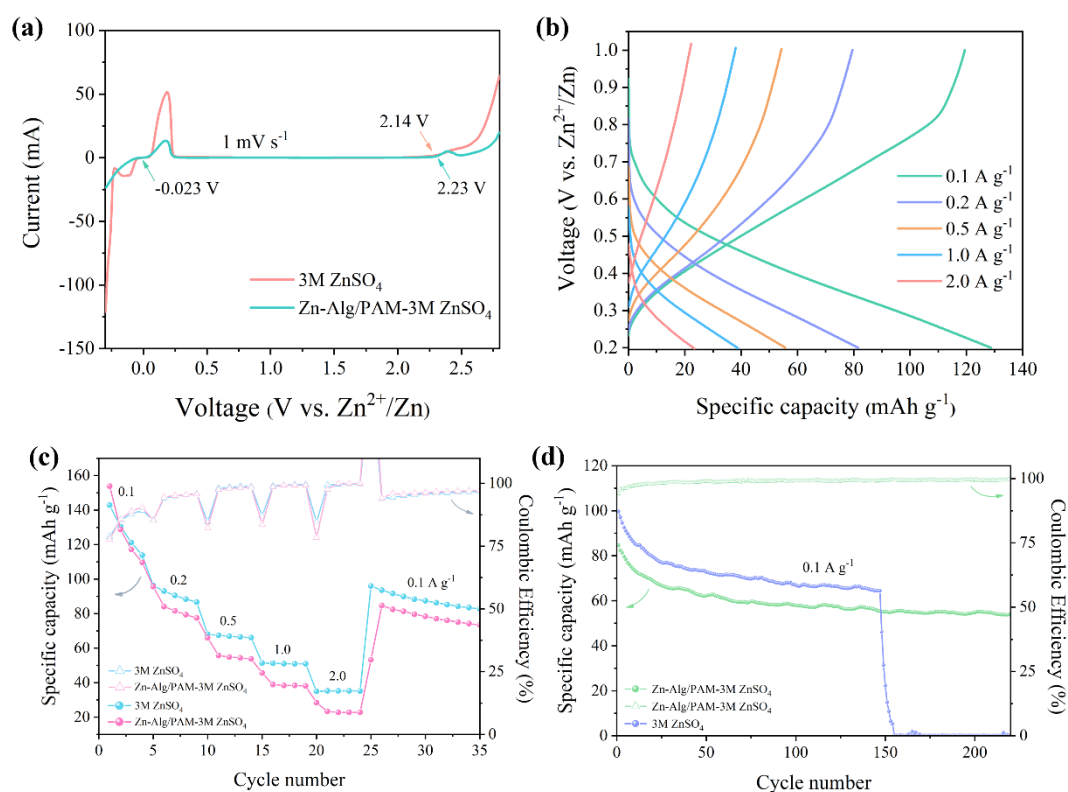
Figure 22. a) Comparison of linear sweep voltammetry curve at 1.0 mV s^{-1} between aqueous 3 M ZnSO$_4$ electrolyte and Zn-Alginate/PAM hydrogel containing 3 M ZnSO$_4$. Electrochemical performance of the Zn//h-MoO$_3$ half-cell equipped with Zn-Alginate/PAM hydrogel electrolyte containing 3 M ZnSO$_4$ (denoted as Zn-Alg/PAM-

3M ZnSO$_4$), including b) galvanostatic discharge and charge curves at current density of 0.1, 0.2, 0.5, 1.0, 2.0 A g^{-1} within 0.2 V to 1.0 V, c) comparison of rate performance from 0.1 A g^{-1} to 2.0 A g^{-1} and d) cycling performance at 0.1 A g^{-1} between Zn//h-MoO$_3$ half-cells based on aqueous 3 M ZnSO$_4$ electrolyte and Zn-Alg/PAM-3 M ZnSO$_4$ hydrogel electrolyte.

To improve the cycling performance of the h-MoO$_3$ anodes and h-MoO$_3$/ZMC full cells, Zn-Alginate/PAM hydrogel was applied as the electrolyte, given the advantages of hydrogel electrolytes, including proper water content for limiting side reactions, stable electrode-electrolyte interface with its excellent adhesion behavior as well as interactions among alginate chains and water molecules through H-bonds, functional groups along its polymer chain to regulate ion transfer through ionic interaction, homogeneous 3D polymer network for uniform ion transfer and intrinsic decent mechanical robustness for physically suppressing dendrite growth, etc.[96] Firstly, LSV curves were performed to evaluate the voltage window of the Zn-Alginate/PAM-3 M ZnSO$_4$ (denoted as Zn-Alg/PAM-3M ZnSO$_4$) hydrogel electrolyte as well as that of aqueous 3 M ZnSO$_4$ electrolyte. From **Figure 22a**, for Zn-Alginate/PAM-3 M ZnSO$_4$, Zn plating and oxygen evolution reactions were observed at -0.023 V and ~ 2.23 V, respectively, leading to a voltage window of ~ 2.25 V. By contrast, aqueous 3 M ZnSO$_4$ electrolyte displays a narrower voltage window of 2.14 V, suggesting the advantage of hydrogel electrolyte.

The hydrogel electrolyte was firstly applied in Zn//h-MoO$_3$ half-cells. Galvanostatic discharge and charge curves and rate performance are shown in **Figure 22b** and **22c** with its capacity of 127 ± 2 mAh g^{-1}, 82, 56, 39, and 23 mAh g^{-1} at the current density of 0.2, 0.5, 1.0, 2.0 A g^{-1}, respectively. Although the specific capacity of hydrogel electrolyte-based battery is lower than that of aqueous electrolyte-based battery (**Figure 22c**), the cycle life can be dramatically extended using hydrogel electrolytes with a capacity retention of 63.6 % and high Coulombic Efficiency of > 95 % after 220 cycles at 0.1 A g^{-1}, surpassing the short life of only 152 cycles in aqueous electrolyte (3 M ZnSO$_4$).
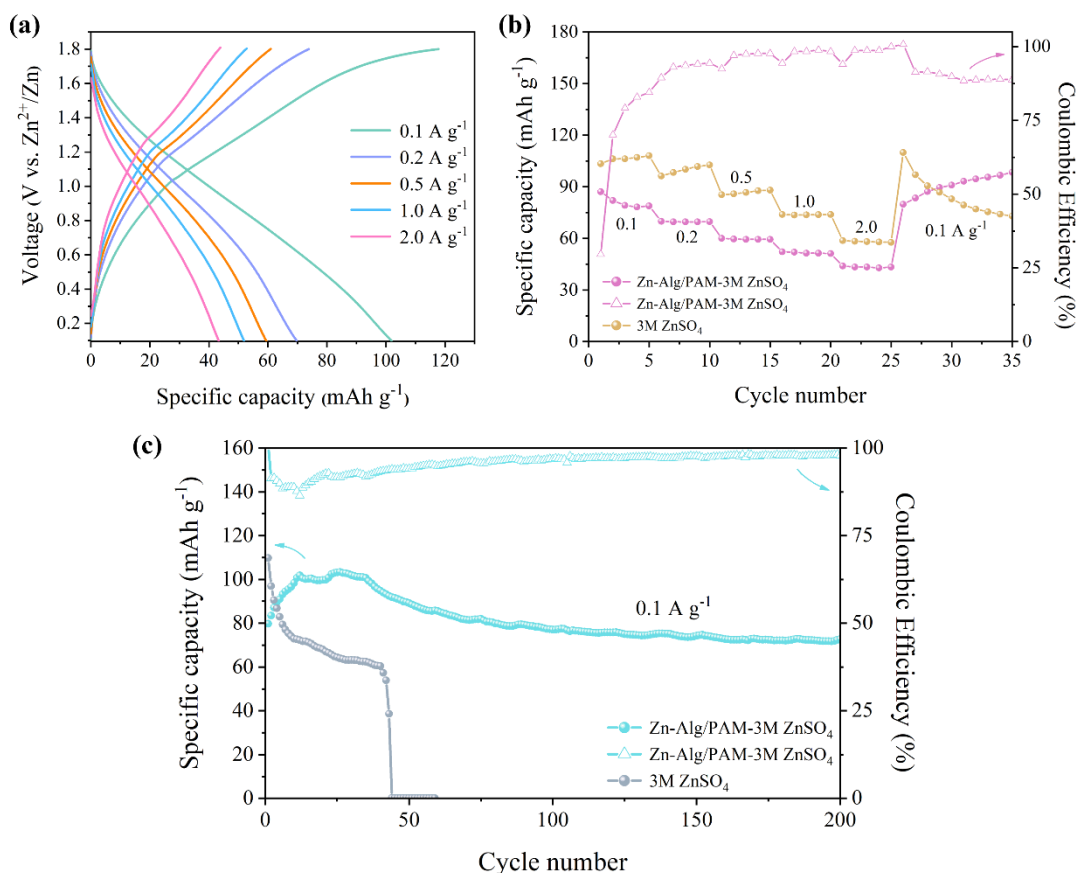
Figure 23. Electrochemical performance of the h-MoO₃//ZMC full cell based on Zn-Alginate/PAM-3M ZnSO₄ hydrogel electrolyte, including a) galvanostatic discharge and charge curves of h-MoO₃//ZMC full cell based on Zn-Alg/PAM-3 M ZnSO₄ at current density of 0.1, 0.2, 0.5, 1.0, 2.0 A g⁻¹ from 0.1 V to 1.8 V, b) Comparison of rate performance from 0.1 A g⁻¹ to 2.0 A g⁻¹ and c) cycling performance at 0.1 A g⁻¹ among h-MoO₃//ZMC full cells based on Zn-Alg/PAM-3M ZnSO₄ and aqueous 3 M ZnSO₄ electrolyte, respectively.

Encouraged by half-cell results, the hydrogel electrolyte was further applied in h-MoO₃//ZMC full cells to improve its cycling performance. **Figure 23a** shows the voltage-capacity curves, after optimizing the concentrations of contained ZnSO₄ solution, the h-MoO₃//ZMC battery with Zn-Alginate/PAM hydrogel electrolyte containing 3 M ZnSO₄ with water absorbency ratio of 80.4 % reached a high specific

capacity of 101 ± 2 mAh g^{-1} at 0.1 A g^{-1}, which was comparable to h-MoO$_3$//ZMC battery using 3 M ZnSO$_4$. In **Figure 23b**, the hydrogel-based battery showed specific capacities of 70, 60, 52, 43 mAh g^{-1} at current densities of 0.2, 0.5, 1.0, 2.0 A g^{-1}, respectively. After the current density was revered backed to 0.1 A g^{-1}, hydrogel electrolyte-based ZIB shows a gradually increasing capacity in stark contrast to the continuously decreasing capacity in aqueous electrolyte-based ZIB. The cycling performance was shown in **Figure 23c**, at the current density of 0.1 A g^{-1}, the h-MoO$_3$//ZMC full cell based on aqueous electrolyte failed to work after only 43 cycles whereas the cycle life is extended to be more than 200 cycles in the hydrogel electrolyte-based full cell with a high-capacity retention of 91.2 % and high Coulombic efficiency. Moreover, the capacity increase in the first 50 cycles may relate to the stabilization and lubrication of hydrogel and electrodes interface, together with less consumption of Zn^{2+} by suppressed side reactions due to the existence of hydrogel electrolyte, such excellent cycling performance was achieved. The results further confirmed the superiority of hydrogel electrolyte with homogeneous and highly regulated ion transfer, improved interfacial stability and intrinsic mechanical robustness, thus side reactions were suppressed and cycling life was elongated.

3.4 Conclusion

In summary, hydrogel electrolytes were employed to extend rocking-chair type zinc ion batteries in both half cells and full cells. First, h-MoO$_3$ was successfully synthesized and applied as zinc-free anode for aqueous ZIBs with redox peaks at 0.21 V/0.43 V and high specific capacity of 128 mAh g^{-1}. However, its cycling performances were poor, which died only after 150 cycles in half-cell test and 43 cycles in h-MoO$_3$//ZMC full cell test. Therefore, to lessen electrolyte consumption by severe side reactions and enhance its cycling stability, Zn-Alginate/PAM hydrogel electrolyte containing 3 M ZnSO$_4$ was applied to this rocking chair ZIB system with wider voltage window, fast ion transfer, stabilized interface and mechanical strength

mitigated side reactions. When applied in Zn//h-MoO$_3$ half-cell, it showed much better cyclability of with 63.6 % after 220 cycles without dying, while utilized in h-MoO$_3$//ZMC full cell, rather than stopping after only 43 cycles based on aqueous electrolyte, h-MoO$_3$//ZMC full cell based on Zn-alginate/PAM-3M ZnSO$_4$ exhibited better cycling stability with 91.2 % capacity retention after 200 cycles and high Coulombic Efficiency of 86.5 % ~ 98.2 %. Therefore, all the results indicated the cycling performance of h-MoO$_3$ were greatly enhanced with a few capacities sacrifice, which was benefited by the involved Zn-Alginate/PAM hydrogel electrolyte. Moreover, the advantages of utilizing Zn-Alginate/PAM hydrogel as quasi-solid electrolyte were further confirmed in zinc-ion battery field, suggesting its great potential for fabricating zinc-ion energy storage devices with both improved cycling stability and flexibility. However, since the energy storage mechanisms within molybdenum-based zinc-free anode and how hydrogel electrolytes work for stabilizing its performance are still needed to be further investigated, more mechanism investigations and calculations are important for advancing research toward both developments for MoO$_3$ anode and involved hydrogel electrolytes.

Chapter 4. Summary and Prospective

To conquer the existing challenges getting in the way of aqueous ZIBs development, especially the short cycle life caused by dendrite growth and side reactions, there has been many solutions proposed and investigated. Among all potential solutions, hydrogel electrolytes with uniform 3D polymer network and designable functional groups can regulate zinc ion transfer and homogenize zinc ion deposition on electrode, together with its intimate adhesion to electrodes as well as elastic nature, dendrite growth and side reactions can be further suppressed in both macro and micro scale. Thus, in the three chapters of the thesis, a literature review and a series of experiments were carried out to reveal and highlight the essential role of hydrogel electrolytes.

To meet the ever-increasing demand toward next-generation energy storage devices to be used in various and extreme conditions, more than the greatly improved cycling stability, flexibility and other environmental-adaptive functions (such as self-healing, super-tough, tailorable, anti-freezing, thermal-gated, etc.) can be achieved by choosing different hydrogel with different nature and designing different hydrogel network with different types of hydrogel polymer chains. Therefore, in Chapter 1, a literature review was prepared from the above aspects with hydrogel electrolytes being classified with various functions they can bring to the involved ZIBs.

In Chapter 2, a series of optimization experiments was carried out to identify the best way for hydrogel preparation, and a flexible Zn//AC supercapacitor was assembled with the utilization of the double-crosslink Zn-Alginate/PAM hydrogel electrolyte. The above pouch cell exhibits nice flexibility with negligible capacity loss under different bending angles due to the existence of the elastic and quasi-solid Zn-Alginate/PAM hydrogel electrolyte. In the other hand, it also exhibited excellent specific capacity of 194 mAh g^{-1} at 0.1 A g^{-1} and stable cycling performance with 77.0 % capacity retention after 1900 cycles at 1.0 A g^{-1}. Those results can further support the important roles the hydrogel electrolytes played in flexible and other environmental-adaptive ZIBs, which were mentioned in Chapter 1.

In chapter 3, the benefits, especially the superior cycling stability of Zn-Alginate/PAM hydrogel electrolyte were further confirmed in rocking-chair type ZIBs with h-MoO$_3$ as zinc-free anode material. With low redox potential of 0.21 V/0.43 V and high specific capacity of 128 mAh g^{-1} at current density of 0.1 A g^{-1}, h-MoO$_3$ was regarded as a promising zinc-free anode materials, excepting its large average capacity loss per cycle. Nevertheless, its cyclability was greatly improved by the utilization of Zn-Alginate/PAM hydrogel electrolyte with comparable capacity as aqueous electrolyte, which further solidate the merits of Zn-Alginate/PAM hydrogel electrolyte in both zinc-ion supercapacitor and zinc-ion battery.

For the existing challenges and prospects toward hydrogel electrolytes, first, compared to aqueous electrolyte, hydrogel electrolyte still possessed much lower ionic conductivity due to its quasi-solid state, resulting in obvious capacity sacrifice. Thus, how to balance capacity sacrifice and other embedded functions can be a vital topic in future hydrogel electrolyte research. For example, other methods can also be combined to realize "1+1>2" goal, such as the application of "water-in-gel" strategy and ionic liquid or adding other inorganic or organic additives or fillers to enhance its electrochemical performance. Moreover, when applied in wearable electronic devices, the mechanical strength, water maintaining ability and range of working temperatures of hydrogel electrolytes still have space to be improved, and these will arise larger interests of the future research toward advance hydrogel electrolytes and functional energy storage devices.

.

References

1.   Kim, J.,Kumar, R.,Bandodkar, A. J.: Wang, J.: Advanced Materials for Printed Wearable Electrochemical Devices: A Review. Advanced Electronic Materials. (2016). https://doi.org/10.1002/aelm.201600260

2.   Trung, T. Q.: Lee, N. E.: Flexible and Stretchable Physical Sensor Integrated Platforms for Wearable Human-Activity Monitoringand Personal Healthcare. Adv Mater. (2016). https://doi.org/10.1002/adma.201504244

3.   Guo, R.,Chen, J.,Yang, B.,Liu, L.,Su, L.,Shen, B.: Yan, X.: In-Plane Micro-Supercapacitors for an Integrated Device on One Piece of Paper. Adv. Funct. Mater. (2017). https://doi.org/10.1002/adfm.201702394

4.   Zhang, Q.,Xu, W.,Sun, J.,Pan, Z.,Zhao, J.,Wang, X.,Zhang, J.,Man, P.,Guo, J.,Zhou, Z.,He, B.,Zhang, Z.,Li, Q.,Zhang, Y.,Xu, L.: Yao, Y.: Constructing Ultrahigh-Capacity Zinc–Nickel–Cobalt Oxide@Ni(OH)2 Core–Shell Nanowire Arrays for High-Performance Coaxial Fiber-Shaped Asymmetric Supercapacitors. Nano Letters. (2017). https://doi.org/10.1021/acs.nanolett.7b03507

5.   Lee, H. E.,Park, J. H.,Kim, T. J.,Im, D.,Shin, J. H.,Kim, D. H.,Mohammad, B.,Kang, I.-S.: Lee, K. J.: Novel Electronics for Flexible and Neuromorphic Computing. Adv. Funct. Mater. (2018). https://doi.org/10.1002/adfm.201801690

6.   Fan, X.,Liu, B.,Ding, J.,Deng, Y.,Han, X.,Hu, W.: Zhong, C.: Flexible and Wearable Power Sources for Next-Generation Wearable Electronics. Batteries & Supercaps. (2020). https://doi.org/10.1002/batt.202000115

7.   Lu, T. C.,Fu, C. M.,Ma, M. H.,Fang, C. C.: Turner, A. M.: Healthcare Applications of Smart Watches. A Systematic Review. Appl Clin Inform. (2016). https://doi.org/10.4338/ACI-2016-03-R-0042

8.   Reeder, B.: David, A.: Health at hand: A systematic review of smart watch uses for health and wellness. J Biomed Inform. (2016). https://doi.org/10.1016/j.jbi.2016.09.001

9.   Williams, A. J.: Pence, H. E.: Smart Phones, a Powerful Tool in the Chemistry Classroom. Journal of Chemical Education. (2011). https://doi.org/10.1021/ed200029p

10. Cima, M. J.: Next-generation wearable electronics. Nat Biotechnol. (2014).

https://doi.org/10.1038/nbt.2952

11.   Liu, Z.,Yang, Q.,Wang, D.,Liang, G.,Zhu, Y.,Mo, F.,Huang, Z.,Li, X.,Ma, L.,Tang, T.,Lu, Z.: Zhi, C.: A Flexible Solid-State Aqueous Zinc Hybrid Battery with Flat and High-Voltage Discharge Plateau. Adv. Energy Mater. (2019). https://doi.org/10.1002/aenm.201902473

12.   Li, K.,Zhang, Q.,Wang, H.: Li, Y.: Red, green, blue (RGB) electrochromic fibers for the new smart color change fabrics. ACS Appl. Mater. Interfaces. (2014). https://doi.org/10.1021/am502929p

13.   Li, M.,Meng, J.,Li, Q.,Huang, M.,Liu, X.,Owusu, K. A.,Liu, Z.: Mai, L.: Finely Crafted 3D Electrodes for Dendrite-Free and High-Performance Flexible Fiber-Shaped Zn-Co Batteries. Adv. Funct. Mater. (2018). https://doi.org/10.1002/adfm.201802016

14.   Liu, Y.,Wang, X.,Qi, K.: Xin, J. H.: Functionalization of cotton with carbon nanotubes. Journal of Materials Chemistry. (2008). https://doi.org/10.1039/b801849a

15.   Macharia, D. K.,Ahmed, S.,Zhu, B.,Liu, Z.,Wang, Z.,Mwasiagi, J. I.,Chen, Z.: Zhu, M.: UV/NIR-Light-Triggered Rapid and Reversible Color Switching for Rewritable Smart Fabrics. ACS Appl. Mater. Interfaces. (2019). https://doi.org/10.1021/acsami.8b22443

16.   Zhou, Y.,Fang, J.,Wang, H.,Zhou, H.,Yan, G.,Zhao, Y.,Dai, L.: Lin, T.: Multicolor Electrochromic Fibers with Helix-Patterned Electrodes. Advanced Electronic Materials. (2018). https://doi.org/10.1002/aelm.201800104

17.   Di, J.,Zhang, X.,Yong, Z.,Zhang, Y.,Li, D.,Li, R.: Li, Q.: Carbon-Nanotube Fibers for Wearable Devices and Smart Textiles. Adv Mater. (2016). https://doi.org/10.1002/adma.201601186

18.   Ge, F.,Fei, L.,Zhang, J.: Wang, C.: The Electrical-Triggered High Contrast and Reversible Color-Changing Janus Fabric Based on Double Side Coating. ACS Appl. Mater. Interfaces. (2020). https://doi.org/10.1021/acsami.0c03194

19.   Shi, Q.,Sun, J.,Hou, C.,Li, Y.,Zhang, Q.: Wang, H.: Advanced Functional Fiber and Smart Textile. Advanced Fiber Materials. (2019). https://doi.org/10.1007/s42765-019-0002-z

20.   Weng, W.,Chen, P.,He, S.,Sun, X.: Peng, H.: Smart Electronic Textiles. Angew. Chem. Int. Ed. Engl. (2016). https://doi.org/10.1002/anie.201507333

21.   Hammock, M. L.,Chortos, A.,Tee, B. C.,Tok, J. B.: Bao, Z.: 25th anniversary article: The evolution of electronic skin (e-skin): a brief history, design considerations, and recent progress. Adv Mater. (2013). https://doi.org/10.1002/adma.201302240

22.   Lin, L.,Ning, H.,Song, S.,Xu, C.: Hu, N.: Flexible electrochemical energy storage: The role of

composite materials. Composites Science and Technology. (2020). https://doi.org/10.1016/j.compscitech.2020.108102

23. Kwak, S.,Kang, J.,Nam, I.: Yi, J.: Free-Form and Deformable Energy Storage as a Forerunner to Next-Generation Smart Electronics. Micromachines (Basel). (2020). https://doi.org/10.3390/mi11040347

24. Liu, W.,Song, M. S.,Kong, B.: Cui, Y.: Flexible and Stretchable Energy Storage: Recent Advances and Future Perspectives. Adv Mater. (2017). https://doi.org/10.1002/adma.201603436

25. Meng, F.,Li, Q.: Zheng, L.: Flexible fiber-shaped supercapacitors: Design, fabrication, and multi-functionalities. Energy Storage Mater. (2017). https://doi.org/10.1016/j.ensm.2017.05.002

26. Pan, Z.,Yang, J.,Yang, J.,Zhang, Q.,Zhang, H.,Li, X.,Kou, Z.,Zhang, Y.,Chen, H.,Yan, C.: Wang, J.: Stitching of Zn3(OH)2V2O7.2H2O 2D Nanosheets by 1D Carbon Nanotubes Boosts Ultrahigh Rate for Wearable Quasi-Solid-State Zinc-Ion Batteries. ACS Nano. (2020). https://doi.org/10.1021/acsnano.9b07956

27. Long, B.,Luo, L.,Yang, H.,Balogun, M.-S.,Song, S.: Tong, Y.: Promoting Alternative Flexible Substrate for Electrode Materials to Achieve Enhanced Lithium Storage Properties. ChemistrySelect. (2018). https://doi.org/10.1002/slct.201801000

28. Liu, Z.,Li, H.,Zhu, M.,Huang, Y.,Tang, Z.,Pei, Z.,Wang, Z.,Shi, Z.,Liu, J.,Huang, Y.: Zhi, C.: Towards wearable electronic devices: A quasi-solid-state aqueous lithium-ion battery with outstanding stability, flexibility, safety and breathability. Nano Energy. (2018). https://doi.org/10.1016/j.nanoen.2017.12.006

29. Mackanic, D. G.,Chang, T. H.,Huang, Z.,Cui, Y.: Bao, Z.: Stretchable electrochemical energy storage devices. Chem Soc Rev. (2020). https://doi.org/10.1039/d0cs00035c

30. Wu, Z.,Wang, Y.,Liu, X.,Lv, C.,Li, Y.,Wei, D.: Liu, Z.: Carbon-Nanomaterial-Based Flexible Batteries for Wearable Electronics. Adv Mater. (2019). https://doi.org/10.1002/adma.201800716

31. Wang, F.,Wu, X.,Li, C.,Zhu, Y.,Fu, L.,Wu, Y.: Liu, X.: Nanostructured positive electrode materials for post-lithium ion batteries. Energy Environ. Sci. (2016). https://doi.org/10.1039/c6ee02070d

32. Li, S.,Zhang, S.,Sun, C.,Zhao, W.,Zhao, T.,Zhang, M.,Wang, H.: Ma, Y.: Honeycomb Inspired Lithiophilic Scaffold for Ultra-Stable, High-Areal-Capacity Metallic Deposition. Energy Storage Mater. (2021). https://doi.org/10.1016/j.ensm.2020.11.024

33. Kim, H.,Hong, J.,Park, K. Y.,Kim, H.,Kim, S. W.: Kang, K.: Aqueous rechargeable Li and Na ion

batteries. Chem Rev. (2014). https://doi.org/10.1021/cr500232y

34. Li, H.,Ma, L.,Han, C.,Wang, Z.,Liu, Z.,Tang, Z.: Zhi, C.: Advanced rechargeable zinc-based batteries: Recent progress and future perspectives. Nano Energy. (2019). https://doi.org/10.1016/j.nanoen.2019.05.059

35. Shan, L.,Zhou, J.,Han, M.,Fang, G.,Cao, X.,Wu, X.: Liang, S.: Reversible Zn-driven reduction displacement reaction in aqueous zinc-ion battery. J. Mater. Chem. A. (2019). https://doi.org/10.1039/c9ta00125e

36. Wang, F.,Borodin, O.,Gao, T.,Fan, X.,Sun, W.,Han, F.,Faraone, A.,Dura, J. A.,Xu, K.: Wang, C.: Highly reversible zinc metal anode for aqueous batteries. Nat Mater. (2018). https://doi.org/10.1038/s41563-018-0063-z

37. Xiong, T.,Zhang, Y.,Wang, Y.,Lee, W. S. V.: Xue, J.: Hexagonal MoO3 as a zinc intercalation anode towards zinc metal-free zinc-ion batteries. J. Mater. Chem. A. (2020). https://doi.org/10.1039/d0ta02236e

38. Hao, J.,Li, B.,Li, X.,Zeng, X.,Zhang, S.,Yang, F.,Liu, S.,Li, D.,Wu, C.: Guo, Z.: An In-Depth Study of Zn Metal Surface Chemistry for Advanced Aqueous Zn-Ion Batteries. Adv Mater. (2020). https://doi.org/10.1002/adma.202003021

39. Ma, L.,Schroeder, M. A.,Borodin, O.,Pollard, T. P.,Ding, M. S.,Wang, C.: Xu, K.: Realizing high zinc reversibility in rechargeable batteries. Nature Energy. (2020). https://doi.org/10.1038/s41560-020-0674-x

40. Shi, H. Y.,Ye, Y. J.,Liu, K.,Song, Y.: Sun, X.: A Long-Cycle-Life Self-Doped Polyaniline Cathode for Rechargeable Aqueous Zinc Batteries. Angew. Chem. Int. Ed. Engl. (2018). https://doi.org/10.1002/anie.201808886

41. Wu, K.,Huang, J.,Yi, J.,Liu, X.,Liu, Y.,Wang, Y.,Zhang, J.: Xia, Y.: Recent Advances in Polymer Electrolytes for Zinc Ion Batteries: Mechanisms, Properties, and Perspectives. Adv. Energy Mater. (2020). https://doi.org/10.1002/aenm.201903977

42. Liu, Y.: Wu, X.: Review of vanadium-based electrode materials for rechargeable aqueous zinc ion batteries. Journal of Energy Chemistry. (2021). https://doi.org/10.1016/j.jechem.2020.08.016

43. Wang, R.: Yang, Z.: Synthesis and high cycle performance of Zn–Al–In-hydrotalcite as anode materials for Ni–Zn secondary batteries. RSC Adv. (2013). https://doi.org/10.1039/c3ra43045f

44. Chao, D.,Zhu, C. R.,Song, M.,Liang, P.,Zhang, X.,Tiep, N. H.,Zhao, H.,Wang, J.,Wang, R.,Zhang,

H.: Fan, H. J.: A High-Rate and Stable Quasi-Solid-State Zinc-Ion Battery with Novel 2D Layered Zinc Orthovanadate Array. Adv Mater. (2018). https://doi.org/10.1002/adma.201803181

45. Kang, L.,Cui, M.,Jiang, F.,Gao, Y.,Luo, H.,Liu, J.,Liang, W.: Zhi, C.: Nanoporous CaCO3 Coatings Enabled Uniform Zn Stripping/Plating for Long-Life Zinc Rechargeable Aqueous Batteries. Adv. Energy Mater. (2018). https://doi.org/10.1002/aenm.201801090

46. Wan, F.,Zhang, L.,Dai, X.,Wang, X.,Niu, Z.: Chen, J.: Aqueous rechargeable zinc/sodium vanadate batteries with enhanced performance from simultaneous insertion of dual carriers. Nat Commun. (2018). https://doi.org/10.1038/s41467-018-04060-8

47. Wang, Z.,Wu, Z.,Bramnik, N.: Mitra, S.: Fabrication of high-performance flexible alkaline batteries by implementing multiwalled carbon nanotubes and copolymer separator. Adv Mater. (2014). https://doi.org/10.1002/adma.201304020

48. Fang, G.,Zhou, J.,Pan, A.: Liang, S.: Recent Advances in Aqueous Zinc-Ion Batteries. ACS Energy Letters. (2018). https://doi.org/10.1021/acsenergylett.8b01426

49. Lorca, S.,Santos, F.: Fernandez Romero, A. J.: A Review of the Use of GPEs in Zinc-Based Batteries. A Step Closer to Wearable Electronic Gadgets and Smart Textiles. Polymers (Basel). (2020). https://doi.org/10.3390/polym12122812

50. Liu, K.,Zang, S.,Xue, R.,Yang, J.,Wang, L.,Huang, J.: Yan, Y.: Coordination-Triggered Hierarchical Folate/Zinc Supramolecular Hydrogels Leading to Printable Biomaterials. ACS Appl. Mater. Interfaces. (2018). https://doi.org/10.1021/acsami.7b18155

51. Guo, W.,Lu, C. H.,Orbach, R.,Wang, F.,Qi, X. J.,Cecconello, A.,Seliktar, D.: Willner, I.: pH-stimulated DNA hydrogels exhibiting shape-memory properties. Adv Mater. (2015). https://doi.org/10.1002/adma.201403702

52. Chen, Y. N.,Peng, L.,Liu, T.,Wang, Y.,Shi, S.: Wang, H.: Poly(vinyl alcohol)-Tannic Acid Hydrogels with Excellent Mechanical Properties and Shape Memory Behaviors. ACS Appl. Mater. Interfaces. (2016). https://doi.org/10.1021/acsami.6b08374

53. Tam, A. Y.: Yam, V. W.: Recent advances in metallogels. Chem Soc Rev. (2013). https://doi.org/10.1039/c2cs35354g

54. Shang, J.,Le, X.,Zhang, J.,Chen, T.: Theato, P.: Trends in polymeric shape memory hydrogels and hydrogel actuators. Polymer Chemistry. (2019). https://doi.org/10.1039/c8py01286e

55. Zakharchenko, S.,Puretskiy, N.,Stoychev, G.,Stamm, M.: Ionov, L.: Temperature controlled

encapsulation and release using partially biodegradable thermo-magneto-sensitive self-rolling tubes. Soft Matter. (2010). https://doi.org/10.1039/c0sm00088d

56.   Xue, H.,Hu, L.,Xiong, Y.,Zhu, X.,Wei, C.,Cao, F.,Zhou, W.,Sun, Y.,Endo, Y.,Liu, M.,Liu, Y.,Liu, J.,Abududilibaier, A.,Chen, L.,Yan, C.,Mi, B.: Liu, G.: Quaternized chitosan-Matrigel-polyacrylamide hydrogels as wound dressing for wound repair and regeneration. Carbohydr Polym. (2019). https://doi.org/10.1016/j.carbpol.2019.115302

57.   Yi, F. L.,Guo, F. L.,Li, Y. Q.,Wang, D. Y.,Huang, P.: Fu, S. Y.: Polyacrylamide Hydrogel Composite E-skin Fully Mimicking Human Skin. ACS Appl. Mater. Interfaces. (2021). https://doi.org/10.1021/acsami.1c05661

58.   Zheng, K.,Tong, Y.,Zhang, S.,He, R.,Xiao, L.,Iqbal, Z.,Zhang, Y.,Gao, J.,Zhang, L.,Jiang, L.: Li, Y.: Flexible Bicolorimetric Polyacrylamide/Chitosan Hydrogels for Smart Real-Time Monitoring and Promotion of Wound Healing. Adv. Funct. Mater. (2021). https://doi.org/10.1002/adfm.202102599

59.   Chen, W.-H.,Liao, W.-C.,Sohn, Y. S.,Fadeev, M.,Cecconello, A.,Nechushtai, R.: Willner, I.: Stimuli-Responsive Nucleic Acid-Based Polyacrylamide Hydrogel-Coated Metal-Organic Framework Nanoparticles for Controlled Drug Release. Adv. Funct. Mater. (2018). https://doi.org/10.1002/adfm.201705137

60.   Sharifzadeh, G.,Hezaveh, H.,Muhamad, II,Hashim, S.: Khairuddin, N.: Montmorillonite-based polyacrylamide hydrogel rings for controlled vaginal drug delivery. Mater Sci Eng C Mater Biol Appl. (2020). https://doi.org/10.1016/j.msec.2019.110609

61.   Zhang, C.,Dai, Y.,Wu, Y.,Lu, G.,Cao, Z.,Cheng, J.,Wang, K.,Yang, H.,Xia, Y.,Wen, X.,Ma, W.,Liu, C.: Wang, Z.: Facile preparation of polyacrylamide/chitosan/Fe3O4 composite hydrogels for effective removal of methylene blue from aqueous solution. Carbohydr Polym. (2020). https://doi.org/10.1016/j.carbpol.2020.115882

62.   da Silva, R. C.,de Aguiar, S. B.,da Cunha, P. L. R.,de Paula, R. C. M.: Feitosa, J. P. A.: Effect of microwave on the synthesis of polyacrylamide-g-chitosan gel for azo dye removal. Reactive and Functional Polymers. (2020). https://doi.org/10.1016/j.reactfunctpolym.2020.104491

63.   Li, Y.,Fu, J.,Zhong, C.,Wu, T.,Chen, Z.,Hu, W.,Amine, K.: Lu, J.: Recent Advances in Flexible Zinc-Based Rechargeable Batteries. Adv. Energy Mater. (2018). https://doi.org/10.1002/aenm.201802605

64.   Hu, X.,Li, Z.: Chen, J.: Flexible Li-CO2 Batteries with Liquid-Free Electrolyte. Angew. Chem. Int.

Ed. Engl. (2017). https://doi.org/10.1002/anie.201701928

65. Huang, S.,Wan, F.,Bi, S.,Zhu, J.,Niu, Z.: Chen, J.: A Self-Healing Integrated All-in-One Zinc-Ion Battery. Angew. Chem. Int. Ed. Engl. (2019). https://doi.org/10.1002/anie.201814653

66. Cui, H.,Mi, H.,Ji, C.,Guo, F.,Chen, Y.,Wu, D.,Qiu, J.: Xie, H.: A durable MXene-based zinc ion hybrid supercapacitor with sulfated polysaccharide reinforced hydrogel/electrolyte. J. Mater. Chem. A. (2021). https://doi.org/10.1039/d1ta06974h

67. Duan, J.,Xie, W.,Yang, P.,Li, J.,Xue, G.,Chen, Q.,Yu, B.,Liu, R.: Zhou, J.: Tough hydrogel diodes with tunable interfacial adhesion for safe and durable wearable batteries. Nano Energy. (2018). https://doi.org/10.1016/j.nanoen.2018.04.014

68. Cong, J.,Shen, X.,Wen, Z.,Wang, X.,Peng, L.,Zeng, J.: Zhao, J.: Ultra-stable and highly reversible aqueous zinc metal anodes with high preferred orientation deposition achieved by a polyanionic hydrogel electrolyte. Energy Storage Mater. (2021). https://doi.org/10.1016/j.ensm.2020.11.041

69. Chan, C. Y.,Wang, Z.,Li, Y.,Yu, H.,Fei, B.: Xin, J. H.: Single-Ion Conducting Double-Network Hydrogel Electrolytes for Long Cycling Zinc-Ion Batteries. ACS Appl. Mater. Interfaces. (2021). https://doi.org/10.1021/acsami.1c05941

70. Dueramae, I.,Okhawilai, M.,Kasemsiri, P.,Uyama, H.: Kita, R.: Properties enhancement of carboxymethyl cellulose with thermo-responsive polymer as solid polymer electrolyte for zinc ion battery. Sci. Rep. (2020). https://doi.org/10.1038/s41598-020-69521-x

71. Rudhziah, S.,Ahmad, A.,Ahmad, I.: Mohamed, N. S.: Biopolymer electrolytes based on blend of kappa-carrageenan and cellulose derivatives for potential application in dye sensitized solar cell. Electrochim. Acta. (2015). https://doi.org/10.1016/j.electacta.2015.02.153

72. Nan, J.,Zhang, G.,Zhu, T.,Wang, Z.,Wang, L.,Wang, H.,Chu, F.,Wang, C.: Tang, C.: A Highly Elastic and Fatigue-Resistant Natural Protein-Reinforced Hydrogel Electrolyte for Reversible-Compressible Quasi-Solid-State Supercapacitors. Adv Sci (Weinh). (2020). https://doi.org/10.1002/advs.202000587

73. Wang, K.,Zhang, X.,Li, C.,Sun, X.,Meng, Q.,Ma, Y.: Wei, Z.: Chemically Crosslinked Hydrogel Film Leads to Integrated Flexible Supercapacitors with Superior Performance. Adv Mater. (2015). https://doi.org/10.1002/adma.201503543

74. Chen, M.,Chen, J.,Zhou, W.,Xu, J.: Wong, C.-P.: High-performance flexible and self-healable quasi-solid-state zinc-ion hybrid supercapacitor based on borax-crosslinked polyvinyl

alcohol/nanocellulose hydrogel electrolyte. J. Mater. Chem. A. (2019). https://doi.org/10.1039/c9ta10944g

75. Subramania, A.,Kalyanasundaram, N.: Sukumar, N.: Development of PVA based micro-porous polymer electrolyte by a novel preferential polymer dissolution process. J. Power Sources. (2005). https://doi.org/10.1016/j.jpowsour.2004.09.001

76. Li, H.,Han, C.,Huang, Y.,Huang, Y.,Zhu, M.,Pei, Z.,Xue, Q.,Wang, Z.,Liu, Z.,Tang, Z.,Wang, Y.,Kang, F.,Li, B.: Zhi, C.: An extremely safe and wearable solid-state zinc ion battery based on a hierarchical structured polymer electrolyte. Energy Environ. Sci. (2018). https://doi.org/10.1039/c7ee03232c

77. Li, H.,Liu, Z.,Liang, G.,Huang, Y.,Huang, Y.,Zhu, M.,Pei, Z.,Xue, Q.,Tang, Z.,Wang, Y.,Li, B.: Zhi, C.: Waterproof and Tailorable Elastic Rechargeable Yarn Zinc Ion Batteries by a Cross-Linked Polyacrylamide Electrolyte. ACS Nano. (2018). https://doi.org/10.1021/acsnano.7b09003

78. Wang, X.,Wang, F.,Wang, L.,Li, M.,Wang, Y.,Chen, B.,Zhu, Y.,Fu, L.,Zha, L.,Zhang, L.,Wu, Y.: Huang, W.: An Aqueous Rechargeable Zn//Co3 O4 Battery with High Energy Density and Good Cycling Behavior. Adv Mater. (2016). https://doi.org/10.1002/adma.201505370

79. Liu, J.,Hu, M.,Wang, J.,Nie, N.,Wang, Y.,Wang, Y.,Zhang, J.: Huang, Y.: An intrinsically 400% stretchable and 50% compressible NiCo//Zn battery. Nano Energy. (2019). https://doi.org/10.1016/j.nanoen.2019.01.028

80. Ibrahim, S. M.: El Salmawi, K. M.: Preparation and Properties of Carboxymethyl Cellulose (CMC)/Sodium alginate (SA) Blends Induced by Gamma Irradiation. Journal of Polymers and the Environment. (2012). https://doi.org/10.1007/s10924-012-0464-z

81. Zhong, H.,He, A.,Lu, J.,Sun, M.,He, J.: Zhang, L.: Carboxymethyl chitosan/conducting polymer as water-soluble composite binder for LiFePO4 cathode in lithium ion batteries. J. Power Sources. (2016). https://doi.org/10.1016/j.jpowsour.2016.10.041

82. Wang, B.,Li, J.,Hou, C.,Zhang, Q.,Li, Y.: Wang, H.: Stable Hydrogel Electrolytes for Flexible and Submarine-Use Zn-Ion Batteries. ACS Appl. Mater. Interfaces. (2020). https://doi.org/10.1021/acsami.0c12313

83. Shang, W.,Zhu, J.,Liu, Y.,Kang, L.,Liu, S.,Huang, B.,Song, J.,Li, X.,Jiang, F.,Du, W.,Gao, Y.: Luo, H.: Establishing High-Performance Quasi-Solid Zn/I2 Batteries with Alginate-Based Hydrogel Electrolytes. ACS Appl. Mater. Interfaces. (2021). https://doi.org/10.1021/acsami.1c03804

84. Li, J.,Yu, P.,Zhang, S.,Wen, Z.,Wen, Y.,Zhou, W.,Dong, X.,Liu, Y.: Liang, Y.: Mild synthesis of superadhesive hydrogel electrolyte with low interfacial resistance and enhanced ionic conductivity for flexible zinc ion battery. J. Colloid Interface Sci. (2021). https://doi.org/10.1016/j.jcis.2021.05.023

85. Liu, Z.,Wang, D.,Tang, Z.,Liang, G.,Yang, Q.,Li, H.,Ma, L.,Mo, F.: Zhi, C.: A mechanically durable and device-level tough Zn-MnO2 battery with high flexibility. Energy Storage Mater. (2019). https://doi.org/10.1016/j.ensm.2019.03.007

86. Wang, D.,Li, H.,Liu, Z.,Tang, Z.,Liang, G.,Mo, F.,Yang, Q.,Ma, L.: Zhi, C.: A Nanofibrillated Cellulose/Polyacrylamide Electrolyte-Based Flexible and Sewable High-Performance Zn-MnO2 Battery with Superior Shear Resistance. Small. (2018). https://doi.org/10.1002/smll.201803978

87. Li, M.,Li, Z.,Ye, X.,Zhang, X.,Qu, L.: Tian, M.: Tendril-Inspired 900% Ultrastretching Fiber-Based Zn-Ion Batteries for Wearable Energy Textiles. ACS Appl. Mater. Interfaces. (2021). https://doi.org/10.1021/acsami.1c02329

88. Wan, F.,Zhang, L.,Wang, X.,Bi, S.,Niu, Z.: Chen, J.: An Aqueous Rechargeable Zinc-Organic Battery with Hybrid Mechanism. Adv. Funct. Mater. (2018). https://doi.org/10.1002/adfm.201804975

89. Zhu, J.,Yao, M.,Huang, S.,Tian, J.: Niu, Z.: Thermal-Gated Polymer Electrolytes for Smart Zinc-Ion Batteries. Angew. Chem. Int. Ed. Engl. (2020). https://doi.org/10.1002/anie.202007274

90. Mo, F.,Liang, G.,Meng, Q.,Liu, Z.,Li, H.,Fan, J.: Zhi, C.: A flexible rechargeable aqueous zinc manganese-dioxide battery working at −20 °C. Energy Environ. Sci. (2019). https://doi.org/10.1039/c8ee02892c

91. Chen, M.,Chen, J.,Zhou, W.,Han, X.,Yao, Y.: Wong, C. P.: Realizing an All-Round Hydrogel Electrolyte toward Environmentally Adaptive Dendrite-Free Aqueous Zn-MnO2 Batteries. Adv Mater. (2021). https://doi.org/10.1002/adma.202007559

92. Sonigara, K. K.,Zhao, J.,Machhi, H. K.,Cui, G.: Soni, S. S.: Self-Assembled Solid-State Gel Catholyte Combating Iodide Diffusion and Self-Discharge for a Stable Flexible Aqueous Zn–I

2

Battery. Adv. Energy Mater. (2020). https://doi.org/10.1002/aenm.202001997

93. Huang, J.,Dong, X.,Guo, Z.: Wang, Y.: Progress of Organic Electrodes in Aqueous Electrolyte for Energy Storage and Conversion. Angew. Chem. Int. Ed. Engl. (2020). https://doi.org/10.1002/anie.202003198

94. Tang, X.,Wang, P.,Bai, M.,Wang, Z.,Wang, H.,Zhang, M.: Ma, Y.: Unveiling the Reversibility and

Stability Origin of the Aqueous V2 O5 -Zn Batteries with a ZnCl2 "Water-in-Salt" Electrolyte. Adv Sci (Weinh). (2021). https://doi.org/10.1002/advs.202102053

95. Shen, Y.,Liu, B.,Liu, X.,Liu, J.,Ding, J.,Zhong, C.: Hu, W.: Water-in-salt electrolyte for safe and high-energy aqueous battery. Energy Storage Mater. (2021). https://doi.org/10.1016/j.ensm.2020.10.011

96. Pan, W.,Wang, Y.,Zhao, X.,Zhao, Y.,Liu, X.,Xuan, J.,Wang, H.: Leung, D. Y. C.: High-Performance Aqueous Na–Zn Hybrid Ion Battery Boosted by "Water-In-Gel" Electrolyte. Adv. Funct. Mater. (2021). https://doi.org/10.1002/adfm.202008783

97. Li, L.,Zhang, L.,Guo, W.,Chang, C.,Wang, J.,Cong, Z.: Pu, X.: High-performance dual-ion Zn batteries enabled by a polyzwitterionic hydrogel electrolyte with regulated anion/cation transport and suppressed Zn dendrite growth. J. Mater. Chem. A. (2021). https://doi.org/10.1039/d1ta08127f

98. Dong, H.,Li, J.,Guo, J.,Lai, F.,Zhao, F.,Jiao, Y.,Brett, D. J. L.,Liu, T.,He, G.: Parkin, I. P.: Insights on Flexible Zinc-Ion Batteries from Lab Research to Commercialization. Adv Mater. (2021). https://doi.org/10.1002/adma.202007548

99. Park, J.,Park, M.,Nam, G.,Lee, J. S.: Cho, J.: All-solid-state cable-type flexible zinc-air battery. Adv Mater. (2015). https://doi.org/10.1002/adma.201404639

100. Huang, S.,Zhu, J.,Tian, J.: Niu, Z.: Recent Progress in the Electrolytes of Aqueous Zinc-Ion Batteries. Chemistry. (2019). https://doi.org/10.1002/chem.201902660

101. Samsudin, A. S.,Lai, H. M.: Isa, M. I. N.: Biopolymer Materials Based Carboxymethyl Cellulose as a Proton Conducting Biopolymer Electrolyte for Application in Rechargeable Proton Battery. Electrochim. Acta. (2014). https://doi.org/10.1016/j.electacta.2014.02.074

102. Liu, M.,Pu, X.,Cong, Z.,Liu, Z.,Liu, T.,Chen, Y.,Fu, J.,Hu, W.: Wang, Z. L.: Resist-Dyed Textile Alkaline Zn Microbatteries with Significantly Suppressed Zn Dendrite Growth. ACS Appl. Mater. Interfaces. (2019). https://doi.org/10.1021/acsami.8b19825

103. Zhao, J.,Xu, Z.,Zhou, Z.,Xi, S.,Xia, Y.,Zhang, Q.,Huang, L.,Mei, L.,Jiang, Y.,Gao, J.,Zeng, Z.: Tan, C.: A Safe Flexible Self-Powered Wristband System by Integrating Defective MnO2-x Nanosheet-Based Zinc-Ion Batteries with Perovskite Solar Cells. ACS Nano. (2021). https://doi.org/10.1021/acsnano.1c03341

104. Guo, L.,Ma, W.-B.,Wang, Y.,Song, X.-Z.,Ma, J.,Han, X.-D.,Tao, X.-Y.,Guo, L.-T.,Fan, H.-L.,Liu, Z.-S.,Zhu, Y.-B.: Wei, X.-Y.: A chemically crosslinked hydrogel electrolyte based all-in-one flexible supercapacitor with superior performance. Journal of Alloys and Compounds. (2020).

https://doi.org/10.1016/j.jallcom.2020.155895

105. Lu, K.,Song, B.,Zhang, Y.,Ma, H.: Zhang, J.: Encapsulation of zinc hexacyanoferrate nanocubes with manganese oxide nanosheets for high-performance rechargeable zinc ion batteries. J. Mater. Chem. A. (2017). https://doi.org/10.1039/c7ta07834j

106. Li, S.,Liu, Y.,Zhao, X.,Cui, K.,Shen, Q.,Li, P.,Qu, X.: Jiao, L.: Molecular Engineering on MoS2 Enables Large Interlayers and Unlocked Basal Planes for High-Performance Aqueous Zn-Ion Storage. Angew. Chem. Int. Ed. Engl. (2021). https://doi.org/10.1002/anie.202108317

107. Huang, Y.,Ip, W. S.,Lau, Y. Y.,Sun, J.,Zeng, J.,Yeung, N. S. S.,Ng, W. S.,Li, H.,Pei, Z.,Xue, Q.,Wang, Y.,Yu, J.,Hu, H.: Zhi, C.: Weavable, Conductive Yarn-Based NiCo//Zn Textile Battery with High Energy Density and Rate Capability. ACS Nano. (2017). https://doi.org/10.1021/acsnano.7b03322

108. Li, C.,Zhang, Q.,E, S.,Li, T.,Zhu, Z.,He, B.,Zhou, Z.,Man, P.,Li, Q.: Yao, Y.: An ultra-high endurance and high-performance quasi-solid-state fiber-shaped Zn–Ag2O battery to harvest wind energy. J. Mater. Chem. A. (2019). https://doi.org/10.1039/c8ta10807b

109. He, B.,Zhang, Q.,Li, L.,Sun, J.,Man, P.,Zhou, Z.,Li, Q.,Guo, J.,Xie, L.,Li, C.,Wang, X.,Zhao, J.,Zhang, T.: Yao, Y.: High-performance flexible all-solid-state aqueous rechargeable Zn–MnO2 microbatteries integrated with wearable pressure sensors. J. Mater. Chem. A. (2018). https://doi.org/10.1039/c8ta05862h

110. Guo, J.,Zhang, R.,Zhang, L.: Cao, X.: 4D Printing of Robust Hydrogels Consisted of Agarose Nanofibers and Polyacrylamide. ACS Macro Letters. (2018). https://doi.org/10.1021/acsmacrolett.7b00957

111. Huang, Y.,Zhong, M.,Shi, F.,Liu, X.,Tang, Z.,Wang, Y.,Huang, Y.,Hou, H.,Xie, X.: Zhi, C.: An Intrinsically Stretchable and Compressible Supercapacitor Containing a Polyacrylamide Hydrogel Electrolyte. Angew. Chem. Int. Ed. Engl. (2017). https://doi.org/10.1002/anie.201705212

112. Xiao, X.,Liu, W.,Wang, K.,Li, C.,Sun, X.,Zhang, X.,Liu, W.: Ma, Y.: High-performance solid-state Zn batteries based on a free-standing organic cathode and metal Zn anode with an ordered nano-architecture. Nanoscale Adv. (2020). https://doi.org/10.1039/c9na00562e

113. Ma, L.,Chen, S.,Li, H.,Ruan, Z.,Tang, Z.,Liu, Z.,Wang, Z.,Huang, Y.,Pei, Z.,Zapien, J. A.: Zhi, C.: Initiating a mild aqueous electrolyte Co3O4/Zn battery with 2.2 V-high voltage and 5000-cycle lifespan by a Co(iii) rich-electrode. Energy Environ. Sci. (2018). https://doi.org/10.1039/c8ee01415a

114. Shim, G.,Tran, M. X.,Liu, G.,Byun, D.: Lee, J. K.: Flexible, fiber-shaped, quasi-solid-state Zn-

polyaniline batteries with methanesulfonic acid-doped aqueous gel electrolyte. Energy Storage Mater. (2021). https://doi.org/10.1016/j.ensm.2020.12.009

115. Ma, L.,Chen, S.,Li, N.,Liu, Z.,Tang, Z.,Zapien, J. A.,Chen, S.,Fan, J.: Zhi, C.: Hydrogen-Free and Dendrite-Free All-Solid-State Zn-Ion Batteries. Adv Mater. (2020). https://doi.org/10.1002/adma.201908121

116. Lu, Y.,Zhu, T.,Xu, N.: Huang, K.: A Semisolid Electrolyte for Flexible Zn-Ion Batteries. ACS Appl. Energy Mater. (2019). https://doi.org/10.1021/acsaem.9b01415

117. Hu, Y.,Shen, P.,Zeng, N.,Wang, L.,Yan, D.,Cui, L.,Yang, K.: Zhai, C.: Hybrid Hydrogel Electrolyte Based on Metal-Organic Supermolecular Self-Assembly and Polymer Chemical Cross-Linking for Rechargeable Aqueous Zn-MnO2 Batteries. ACS Appl. Mater. Interfaces. (2020). https://doi.org/10.1021/acsami.0c10321

118. Li, H.,Yang, Q.,Mo, F.,Liang, G.,Liu, Z.,Tang, Z.,Ma, L.,Liu, J.,Shi, Z.: Zhi, C.: MoS2 nanosheets with expanded interlayer spacing for rechargeable aqueous Zn-ion batteries. Energy Storage Mater. (2019). https://doi.org/10.1016/j.ensm.2018.10.005

119. Xu, W.,Liu, C.,Ren, S.,Lee, D.,Gwon, J.,Flake, J. C.,Lei, T.,Baisakh, N.: Wu, Q.: A cellulose nanofiber–polyacrylamide hydrogel based on a co-electrolyte system for solid-state zinc ion batteries to operate at extremely cold temperatures. J. Mater. Chem. A. (2021). https://doi.org/10.1039/d1ta08023g

120. Liu, Z.,Liang, G.,Zhan, Y.,Li, H.,Wang, Z.,Ma, L.,Wang, Y.,Niu, X.: Zhi, C.: A soft yet device-level dynamically super-tough supercapacitor enabled by an energy-dissipative dual-crosslinked hydrogel electrolyte. Nano Energy. (2019). https://doi.org/10.1016/j.nanoen.2019.01.087

121. Huang, Y.,Liu, J.,Zhang, J.,Jin, S.,Jiang, Y.,Zhang, S.,Li, Z.,Zhi, C.,Du, G.: Zhou, H.: Flexible quasi-solid-state zinc ion batteries enabled by highly conductive carrageenan bio-polymer electrolyte. RSC Adv. (2019). https://doi.org/10.1039/c9ra01120j

122. Liu, C.,Xu, W.,Mei, C.,Li, M.,Chen, W.,Hong, S.,Kim, W. Y.,Lee, S. y.: Wu, Q.: A Chemically Self-Charging Flexible Solid-State Zinc-Ion Battery Based on VO

2

Cathode and Polyacrylamide–Chitin Nanofiber Hydrogel Electrolyte. Adv. Energy Mater. (2021). https://doi.org/10.1002/aenm.202003902

123. Hsu, H.-L.,Tien, C.-F.,Yang, Y.-T.: Leu, J.: Dye-sensitized solar cells based on agarose gel electrolytes using allylimidazolium iodides and environmentally benign solvents. Electrochim. Acta.

(2013). https://doi.org/10.1016/j.electacta.2012.12.133

124. Wang, Y.: Chen, Y.: A flexible zinc-ion battery based on the optimized concentrated hydrogel electrolyte for enhanced performance at subzero temperature. Electrochim. Acta. (2021). https://doi.org/10.1016/j.electacta.2021.139178

125. Sun, J.,Zhang, Y.,Liu, Y.,Jiang, H.,Dong, X.,Hu, T.: Meng, C.: Hydrated vanadium pentoxide/reduced graphene oxide-polyvinyl alcohol (V2O5nH2O/rGO-PVA) film as a binder-free electrode for solid-state Zn-ion batteries. J. Colloid Interface Sci. (2021). https://doi.org/10.1016/j.jcis.2020.10.148

126. Xu, Z.,Ma, R.: Wang, X.: Ultrafast, long-life, high-loading, and wide-temperature zinc ion supercapacitors. Energy Storage Mater. (2022). https://doi.org/10.1016/j.ensm.2022.01.011

127. Jiang, D.,Lu, N.,Li, L.,Zhang, H.,Luan, J.: Wang, G.: A highly compressible hydrogel electrolyte for flexible Zn-MnO2 battery. J. Colloid Interface Sci. (2022). https://doi.org/10.1016/j.jcis.2021.10.121

128. Lin, T.,Shi, M.,Huang, F.,Peng, J.,Bai, Q.,Li, J.: Zhai, M.: One-Pot Synthesis of a Double-Network Hydrogel Electrolyte with Extraordinarily Excellent Mechanical Properties for a Highly Compressible and Bendable Flexible Supercapacitor. ACS Appl. Mater. Interfaces. (2018). https://doi.org/10.1021/acsami.8b11377

129. Wang, Z.,Mo, F.,Ma, L.,Yang, Q.,Liang, G.,Liu, Z.,Li, H.,Li, N.,Zhang, H.: Zhi, C.: Highly Compressible Cross-Linked Polyacrylamide Hydrogel-Enabled Compressible Zn-MnO2 Battery and a Flexible Battery-Sensor System. ACS Appl. Mater. Interfaces. (2018). https://doi.org/10.1021/acsami.8b17607

130. Xu, P.,Wang, C.,Zhao, B.,Zhou, Y.: Cheng, H.: A high-strength and ultra-stable halloysite nanotubes-crosslinked polyacrylamide hydrogel electrolyte for flexible zinc-ion batteries. J. Power Sources. (2021). https://doi.org/10.1016/j.jpowsour.2021.230196

131. Jiang, Z.,Diggle, B.,Shackleford, I. C. G.: Connal, L. A.: Tough, Self-Healing Hydrogels Capable of Ultrafast Shape Changing. Adv Mater. (2019). https://doi.org/10.1002/adma.201904956

132. Liu, J.,Long, J.,Shen, Z.,Jin, X.,Han, T.,Si, T.: Zhang, H.: A Self-Healing Flexible Quasi-Solid Zinc-Ion Battery Using All-In-One Electrodes. Adv Sci (Weinh). (2021). https://doi.org/10.1002/advs.202004689

133. Qiu, M.,Liu, H.,Tawiah, B.,Jia, H.: Fu, S.: Zwitterionic triple-network hydrogel electrolyte for

advanced flexible zinc ion batteries. Compos.Commun. (2021). https://doi.org/10.1016/j.coco.2021.100942

134. Han, L.,Huang, H.,Fu, X.,Li, J.,Yang, Z.,Liu, X.,Pan, L.: Xu, M.: A flexible, high-voltage and safe zwitterionic natural polymer hydrogel electrolyte for high-energy-density zinc-ion hybrid supercapacitor. Chemical Engineering Journal. (2020). https://doi.org/10.1016/j.cej.2019.123733

135. Mo, F.,Chen, Z.,Liang, G.,Wang, D.,Zhao, Y.,Li, H.,Dong, B.: Zhi, C.: Zwitterionic Sulfobetaine Hydrogel Electrolyte Building Separated Positive/Negative Ion Migration Channels for Aqueous Zn-MnO

2

Batteries with Superior Rate Capabilities. Adv. Energy Mater. (2020). https://doi.org/10.1002/aenm.202000035

136. Zhao, S.,Zuo, Y.,Liu, T.,Zhai, S.,Dai, Y.,Guo, Z.,Wang, Y.,He, Q.,Xia, L.,Zhi, C.,Bae, J.,Wang, K.: Ni, M.: Multi-Functional Hydrogels for Flexible Zinc-Based Batteries Working under Extreme Conditions. Adv. Energy Mater. (2021). https://doi.org/10.1002/aenm.202101749

137. Li, Z.,Chen, D.,An, Y.,Chen, C.,Wu, L.,Chen, Z.,Sun, Y.: Zhang, X.: Flexible and anti-freezing quasi-solid-state zinc ion hybrid supercapacitors based on pencil shavings derived porous carbon. Energy Storage Mater. (2020). https://doi.org/10.1016/j.ensm.2020.01.028

138. Quan, Y.,Chen, M.,Zhou, W.,Tian, Q.: Chen, J.: High-Performance Anti-freezing Flexible Zn-MnO2 Battery Based on Polyacrylamide/Graphene Oxide/Ethylene Glycol Gel Electrolyte. Front Chem. (2020). https://doi.org/10.3389/fchem.2020.00603

139. Wang, J.,Huang, Y.,Liu, B.,Li, Z.,Zhang, J.,Yang, G.,Hiralal, P.,Jin, S.: Zhou, H.: Flexible and anti-freezing zinc-ion batteries using a guar-gum/sodium-alginate/ethylene-glycol hydrogel electrolyte. Energy Storage Mater. (2021). https://doi.org/10.1016/j.ensm.2021.06.034

140. Zhu, M.,Wang, X.,Tang, H.,Wang, J.,Hao, Q.,Liu, L.,Li, Y.,Zhang, K.: Schmidt, O. G.: Antifreezing Hydrogel with High Zinc Reversibility for Flexible and Durable Aqueous Batteries by Cooperative Hydrated Cations. Adv. Funct. Mater. (2019). https://doi.org/10.1002/adfm.201907218

141. Fu, Q.,Hao, S.,Meng, L.,Xu, F.: Yang, J.: Engineering Self-Adhesive Polyzwitterionic Hydrogel Electrolytes for Flexible Zinc-Ion Hybrid Capacitors with Superior Low-Temperature Adaptability. ACS Nano. (2021). https://doi.org/10.1021/acsnano.1c08193

142. Yang, L.,Song, L.,Feng, Y.,Cao, M.,Zhang, P.,Zhang, X.-F.: Yao, J.: Zinc ion trapping in a

cellulose hydrogel as a solid electrolyte for a safe and flexible supercapacitor. J. Mater. Chem. A. (2020). https://doi.org/10.1039/d0ta04360e

143. Wu, S.,Chen, Y.,Jiao, T.,Zhou, J.,Cheng, J.,Liu, B.,Yang, S.,Zhang, K.: Zhang, W.: An Aqueous Zn-Ion Hybrid Supercapacitor with High Energy Density and Ultrastability up to 80 000 Cycles. Adv. Energy Mater. (2019). https://doi.org/10.1002/aenm.201902915

144. Hansen, B. B.,Spittle, S.,Chen, B.,Poe, D.,Zhang, Y.,Klein, J. M.,Horton, A.,Adhikari, L.,Zelovich, T.,Doherty, B. W.,Gurkan, B.,Maginn, E. J.,Ragauskas, A.,Dadmun, M.,Zawodzinski, T. A.,Baker, G. A.,Tuckerman, M. E.,Savinell, R. F.: Sangoro, J. R.: Deep Eutectic Solvents: A Review of Fundamentals and Applications. Chem Rev. (2021). https://doi.org/10.1021/acs.chemrev.0c00385

145. Wu, Y.,Deng, Y.,Zhang, K.,Qiu, J.,Wu, J.: Yan, L.: Ultrahigh Conductive and Stretchable Eutectogel Electrolyte for High-Voltage Flexible Antifreeze Quasi-solid-state Zinc-Ion Hybrid Supercapacitor. ACS Appl. Energy Mater. (2022). https://doi.org/10.1021/acsaem.1c03654

146. Chan, S. Y.,Goh, S. S.,Dou, Q.,Chan, B. Q. Y.,Choo, W. S.,Young, D. J.: Loh, X. J.: Unprecedented Acid-Promoted Polymerization and Gelation of Acrylamide: A Serendipitous Discovery. Chem Asian J. (2018). https://doi.org/10.1002/asia.201800552

147. Yang, W.,Du, X.,Zhao, J.,Chen, Z.,Li, J.,Xie, J.,Zhang, Y.,Cui, Z.,Kong, Q.,Zhao, Z.,Wang, C.,Zhang, Q.: Cui, G.: Hydrated Eutectic Electrolytes with Ligand-Oriented Solvation Shells for Long-Cycling Zinc-Organic Batteries. Joule. (2020). https://doi.org/10.1016/j.joule.2020.05.018

148. Zhao, J.,Zhang, J.,Yang, W.,Chen, B.,Zhao, Z.,Qiu, H.,Dong, S.,Zhou, X.,Cui, G.: Chen, L.: "Water-in-deep eutectic solvent" electrolytes enable zinc metal anodes for rechargeable aqueous batteries. Nano Energy. (2019). https://doi.org/10.1016/j.nanoen.2018.12.086

149. Yang, P.,Feng, C.,Liu, Y.,Cheng, T.,Yang, X.,Liu, H.,Liu, K.: Fan, H. J.: Thermal Self-Protection of Zinc-Ion Batteries Enabled by Smart Hygroscopic Hydrogel Electrolytes. Adv. Energy Mater. (2020). https://doi.org/10.1002/aenm.202002898

150. Mo, F.,Liang, G.,Wang, D.,Tang, Z.,Li, H.: Zhi, C.: Biomimetic organohydrogel electrolytes for high-environmental adaptive energy storage devices. EcoMat. (2019). https://doi.org/10.1002/eom2.12008

151. Li, X.,Wang, H.,Sun, X.,Li, J.: Liu, Y.-N.: Flexible Wide-Temperature Zinc-Ion Battery Enabled by an Ethylene Glycol-Based Organohydrogel Electrolyte. ACS Appl. Energy Mater. (2021). https://doi.org/10.1021/acsaem.1c02433

152. Tang, Y.,Liu, C.,Zhu, H.,Xie, X.,Gao, J.,Deng, C.,Han, M.,Liang, S.: Zhou, J.: Ion-confinement effect enabled by gel electrolyte for highly reversible dendrite-free zinc metal anode. Energy Storage Mater. (2020). https://doi.org/10.1016/j.ensm.2020.01.023

153. Ma, L.,Chen, S.,Pei, Z.,Li, H.,Wang, Z.,Liu, Z.,Tang, Z.,Zapien, J. A.: Zhi, C.: Flexible Waterproof Rechargeable Hybrid Zinc Batteries Initiated by Multifunctional Oxygen Vacancies-Rich Cobalt Oxide. ACS Nano. (2018). https://doi.org/10.1021/acsnano.8b04317

154. Xu, W.,Liu, C.,Wu, Q.,Xie, W.,Kim, W.-Y.,Lee, S.-Y.: Gwon, J.: A stretchable solid-state zinc ion battery based on a cellulose nanofiber–polyacrylamide hydrogel electrolyte and a Mg0.23V2O5·1.0H2O cathode. J. Mater. Chem. A. (2020). https://doi.org/10.1039/d0ta06467j

155. Zhao, J.,Sonigara, K. K.,Li, J.,Zhang, J.,Chen, B.,Zhang, J.,Soni, S. S.,Zhou, X.,Cui, G.: Chen, L.: A Smart Flexible Zinc Battery with Cooling Recovery Ability. Angew. Chem. Int. Ed. Engl. (2017). https://doi.org/10.1002/anie.201704373

156. Leng, K.,Li, G.,Guo, J.,Zhang, X.,Wang, A.,Liu, X.: Luo, J.: A Safe Polyzwitterionic Hydrogel Electrolyte for Long-Life Quasi-Solid State Zinc Metal Batteries. Adv. Funct. Mater. (2020). https://doi.org/10.1002/adfm.202001317

157. Ji, G.,Hu, R.,Wang, Y.: Zheng, J.: High energy density, flexible, low temperature resistant and self-healing Zn-ion hybrid capacitors based on hydrogel electrolyte. J. Energy Storage. (2022). https://doi.org/10.1016/j.est.2021.103858

158. Wang, C.,Pei, Z.,Meng, Q.,Zhang, C.,Sui, X.,Yuan, Z.,Wang, S.: Chen, Y.: Toward Flexible Zinc-Ion Hybrid Capacitors with Superhigh Energy Density and Ultralong Cycling Life: The Pivotal Role of ZnCl2 Salt-Based Electrolytes. Angew. Chem. Int. Ed. Engl. (2021). https://doi.org/10.1002/anie.202012030

159. Zhu, X.,Ji, C.,Meng, Q.,Mi, H.,Yang, Q.,Li, Z.,Yang, N.: Qiu, J.: Freeze-Tolerant Hydrogel Electrolyte with High Strength for Stable Operation of Flexible Zinc-Ion Hybrid Supercapacitors. Small. (2022). https://doi.org/10.1002/smll.202200055

160. Wang, H.,Ye, W.,Yang, Y.,Zhong, Y.: Hu, Y.: Zn-ion hybrid supercapacitors: Achievements, challenges and future perspectives. Nano Energy. (2021). https://doi.org/10.1016/j.nanoen.2021.105942

161. Li, Z.,An, Y.,Dong, S.,Chen, C.,Wu, L.,Sun, Y.: Zhang, X.: Progress on zinc ion hybrid supercapacitors: Insights and challenges. Energy Storage Mater. (2020). https://doi.org/10.1016/j.ensm.2020.06.014

162. Shao, Y.,Shen, F.: Shao, Y.: Recent Advances in Aqueous Zinc-ion Hybrid Capacitors: A Minireview. ChemElectroChem. (2020). https://doi.org/10.1002/celc.202001322

163. Yin, J.,Zhang, W.,Alhebshi, N. A.,Salah, N.: Alshareef, H. N.: Electrochemical Zinc Ion Capacitors: Fundamentals, Materials, and Systems. Adv. Energy Mater. (2021). https://doi.org/10.1002/aenm.202100201

164. Yue, Y.,Wang, X.,Han, J.,Yu, L.,Chen, J.,Wu, Q.: Jiang, J.: Effects of nanocellulose on sodium alginate/polyacrylamide hydrogel: Mechanical properties and adsorption-desorption capacities. Carbohydr Polym. (2019). https://doi.org/10.1016/j.carbpol.2018.10.105

165. Zhao, D.,Feng, M.,Zhang, L.,He, B.,Chen, X.: Sun, J.: Facile synthesis of self-healing and layered sodium alginate/polyacrylamide hydrogel promoted by dynamic hydrogen bond. Carbohydr Polym. (2021). https://doi.org/10.1016/j.carbpol.2020.117580

166. Ghobashy, M. M.: Bassioni, G.: pH stimuli-responsive poly(acrylamide-co -sodium alginate) hydrogels prepared by γ-radiation for improved compressive strength of concrete. Advances in Polymer Technology. (2018). https://doi.org/10.1002/adv.21870

167. Zhang, L.,Zheng, S.,Wang, L.,Tang, H.,Xue, H.,Wang, G.: Pang, H.: Fabrication of Metal Molybdate Micro/Nanomaterials for Electrochemical Energy Storage. Small. (2017). https://doi.org/10.1002/smll.201700917

168. Xie, J.,Zhang, H.,Liu, Q.,Liu, X.: Lu, X.: Recent progress of molybdenum-based materials in aqueous rechargeable batteries. Materials Today Advances. (2020). https://doi.org/10.1016/j.mtadv.2020.100100

169. Chithambararaj, A.,Rajeswari Yogamalar, N.: Bose, A. C.: Hydrothermally Synthesized h-MoO3 and α-MoO3 Nanocrystals: New Findings on Crystal-Structure-Dependent Charge Transport. Crystal Growth & Design. (2016). https://doi.org/10.1021/acs.cgd.5b01571

170. Kumar, V.,Wang, X.: Lee, P. S.: Formation of hexagonal-molybdenum trioxide (h-MoO(3)) nanostructures and their pseudocapacitive behavior. Nanoscale. (2015). https://doi.org/10.1039/c5nr01505g

171. Chen, Z.,Peng, Y.,Liu, F.,Le, Z.,Zhu, J.,Shen, G.,Zhang, D.,Wen, M.,Xiao, S.,Liu, C. P.,Lu, Y.: Li, H.: Hierarchical Nanostructured WO3 with Biomimetic Proton Channels and Mixed Ionic-Electronic Conductivity for Electrochemical Energy Storage. Nano Lett. (2015). https://doi.org/10.1021/acs.nanolett.5b02642

172. Zhang, N.,Cheng, F.,Liu, Y.,Zhao, Q.,Lei, K.,Chen, C.,Liu, X.: Chen, J.: Cation-Deficient Spinel ZnMn2O4 Cathode in Zn(CF3SO3)2 Electrolyte for Rechargeable Aqueous Zn-Ion Battery. J Am Chem Soc. (2016). https://doi.org/10.1021/jacs.6b05958